CENTRAL RESEARCH LIBRARY
DOCUMENT COLLECTION

141

MARTIN MARIETTA ENERGY SYSTEMS LIBRARIES
3 4456 0134145 4

ORNL-3502
Special

THE JOINT NATIONAL INSTITUTES OF HEALTH–ATOMIC ENERGY COMMISSION ZONAL CENTRIFUGE DEVELOPMENT PROGRAM SEMIANNUAL REPORT FOR PERIOD JANUARY 1–JUNE 30, 1963

CENTRAL RESEARCH LIBRARY
DOCUMENT COLLECTION
LIBRARY LOAN COPY
DO NOT TRANSFER TO ANOTHER PERSON
If you wish someone else to see this document, send in name with document and the library will arrange a loan.

OAK RIDGE NATIONAL LABORATORY
operated by
UNION CARBIDE CORPORATION
for the
U.S. ATOMIC ENERGY COMMISSION

~~CAUTION~~

~~THE DOCUMENT IS NOT TO BE RELEASED TO THE PUBLIC OR GIVEN EXTERNAL DISTRIBUTION WITHOUT THE APPROVAL OF THE OAK RIDGE LEGAL AND INFORMATION CONTROL DEPARTMENT OF UNION CARBIDE NUCLEAR COMPANY.~~ Changed 3/20/64 per Patent Dept. through LRD

LEGAL NOTICE

This report was prepared as an account of Government sponsored work. Neither the United States, nor the Commission, nor any person acting on behalf of the Commission:

A. Makes any warranty or representation, expressed or implied, with respect to the accuracy, completeness, or usefulness of the information contained in this report, or that the use of any information, apparatus, method, or process disclosed in this report may not infringe privately owned rights; or

B. Assumes any liabilities with respect to the use of, or for damages resulting from the use of any information, apparatus, method, or process disclosed in this report.

As used in the above, "person acting on behalf of the Commission" includes any employee or contractor of the Commission, or employee of such contractor, to the extent that such employee or contractor of the Commission, or employee of such contractor prepares, disseminates, or provides access to, any information pursuant to his employment or contract with the Commission, or his employment with such contractor.

ORNL-3502

Contract No. W-7405-eng-26

BIOLOGY DIVISION

THE JOINT NATIONAL INSTITUTES OF HEALTH–ATOMIC ENERGY COMMISSION ZONAL CENTRIFUGE DEVELOPMENT PROGRAM SEMIANNUAL REPORT

For Period January 1–June 30, 1963

Prepared by
N. G. Anderson

NOTICE

This document contains information of a preliminary nature and was prepared primarily for internal use at the Oak Ridge National Laboratory. It is subject to revision or correction and, therefore, does not represent a final report. Quotations from or references to this report must not be made in open literature without written permission from the individual authors.

DATE ISSUED

OCT 11 1963

OAK RIDGE NATIONAL LABORATORY
Oak Ridge, Tennessee
operated by
UNION CARBIDE CORPORATION
for the
U. S. ATOMIC ENERGY COMMISSION

MARTIN MARIETTA ENERGY SYSTEMS LIBRARIES
3 4456 0134145 4

Summary

This report describes development work on methods of particle separation by the Biology Division of the Oak Ridge National Laboratory and the Oak Ridge Gaseous Diffusion Plant during the period January 1 to June 30, 1963, under the Joint National Institutes of Health–Atomic Energy Commission Zonal Centrifuge Development Program. The central effort has been to develop zonal centrifuge systems for the separation of cells and subcellular particles, including viruses, and biocolloids, including proteins and nucleic acids.

The development of basic new tools requires close collaboration between specialists in the biological and physical sciences. Initially it is essential to develop the (1) rotors and drive systems, (2) seals, and (3) containment systems necessary for work with virus materials. Three types of low-speed (A series) rotors have been developed. The stability problems which limited the B-II rotor to approximately 25,000 rpm are being solved, and operation at 40,000 rpm (90,800 × *g*) has been obtained with a new experimental upper damping bearing. In addition, high-speed zonal ultracentrifuges have been designed and tested by the personnel at the Oak Ridge Gaseous Diffusion Plant [C-I to C-V, 141,000 rpm (310,000 × *g*) to 40,000 rpm (91,000 × *g*)]. These rotors are in various stages of development, as noted in this report. A prototype of an ultrahigh-speed centrifugal system (D series capable of 1.2 million × *g*) has been tested to 300,000 rpm.

This work, initiated in the Biology Division at ORNL, has required the talents of various groups at the Oak Ridge Gaseous Diffusion Plant. Theoretical studies have been undertaken in many areas which bear upon the problem. These are, among others: (1) rotor stability and design, including fabrication, (2) metallurgical studies, including stress analysis and corrosion resistance, (3) instrumentation and controls, (4) chemistry of cesium chloride for reprocessing, (5) electron microscopy, (6) mathematical analyses of flow rates for continuous centrifugation, (7) containment and sterilization, and (8) data reduction.

Under the NIH-AEC Program the principles of zonal centrifugation developed in the Biology Division at ORNL have been combined with certain revolutionary advances made by the Technical Division at ORGDP in high-speed centrifugation and rotor fabrication. The aim is to perfect high-resolution fractionation methods for separating particles ranging in size from whole cells to protein molecules. Virus particles fall within this range, and to date two types of adenovirus and respiratory syncytial virus have been separated and concentrated, using the B- and C-series rotors. The biological implications of these centrifuge systems extend from determining the distribution of drugs or other materials in cells to the separating of viruses from tumors. Also under study is the possibility of using zonal centrifuges for vaccine production. These problems are discussed in detail in this report.

Ancillary studies carried out by ORGDP have included (1) pressure filtration and dialysis, (2) ultrahigh-pressure chromatography, (3) flame ionization analysis, capable of resolving 10^{-12} g of carbon, and (4) a cell synchronizer capable of continuously growing 10 to 60 liters of cells. These programs are in various stages of development, as noted in this report.

Other biological studies reported here include (1) a new method for cesium chloride banding, using angle-head rotors, (2) cell synchronization studies, (3) sugar analyzer development, (4) automated nucleotide studies, (5) separation of radionuclides from river water, (6) distribution of particulates in *Escherichia coli*, and (7) protein synthesis of ribosomes from *E. coli* and rat liver thymus.

The ultimate aim of this program is to develop methods for viewing the cell as a spectrum of

particles, each portion of which may be analyzed biochemically and biophysically. Three general areas of investigation are included in this broad program and are closely interrelated in the achievement of the final goals:

1. For studies on subcellular particles it is important to have available a population of cells which are as nearly identical in size, composition, and physiological state as possible. Studies on mass cell synchronization, therefore, will in the future occupy an increasing portion of the total effort.

2. Development of centrifugal methods for subcellular particles, which constitutes the bulk of the present effort and will continue to do so for two or three years, will eventually be decreased to a supporting effort.

3. The development of molecular separation methods, which has been a minor effort in the form of the automated nucleotide and carbohydrate analytical systems, will be gradually increased as high-pressure chromatography and new on-stream analytical systems are developed.

The biological studies undertaken in parallel with the developmental effort are (1) the isolation of virus particles from complex mixtures, (2) examination of changes in cell composition which follow virus infection, and (3) alterations in cell composition during the cell cycle. In collaboration with interested groups outside the Laboratory, studies are being undertaken on the intracellular localization of drugs, herbicides, and pesticides, since the systems described in this report are readily adaptable to such problems.

Contents

SUMMARY iii

I. INTRODUCTION 1

II. BIOMEDICAL APPLICATIONS OF ZONAL CENTRIFUGES 2

A. Isolation of Trace Amounts of Virus from Tissues 2
1. Physical Properties of Viruses 2
2. Search for Viruses in Sections by Electron Miscroscopy 4
3. Detection of Virus Particles in Gradients 4
4. Subcellular Particles with Virus-Like Sedimentation Properties 4
5. Sedimentation of Virus Added to Tissues 7
6. Isopycnic Separations of Particles Previously Isolated by Rate-Zonal Centrifugation 7
7. Further Studies 7

B. Large-Scale Virus Isolation 8
1. Types of Viruses to be Isolated 8
2. Preliminary Studies on Adenovirus 2 9

III. THEORETICAL STUDIES 11

A. Use of Zonal Centrifuges for Virus Concentration 11
1. Theoretical Approaches to Virus Concentration 11
2. Effect of Transient Times and Coriolis Forces on Sedimentation Rates (Spherical Particles) 13

IV. ROTOR DESIGN 15

A. Stability Studies 15
1. General Considerations 15
2. Stability of the Liquid 16

B. Theory of Rotor Stability and Its Application to Rotor Design 16
1. General Considerations 16
2. Critical Speed of the Rotor 16

C. Physical Properties of Materials 17
1. Design Calculations 17
2. Design Data 18
3. Filament-Wound Vessels 18

D. Metallurgical Studies 23

E. Corrosion Studies 27

F. Dye-Penetration Studies 29

V. LOW-SPEED ZONAL ROTORS 31
A. Rotor A-VIII 31
B. Rotor A-IX 31
VI. INTERMEDIATE-SPEED ZONAL ROTORS 34
A. Rotor B-II System 34
VII. HIGH-SPEED ZONAL ROTORS 38
A. General Considerations 38
B. Rotor C-II 38
C. Rotor C-III 39
D. Rotor C-IV 40
E. Rotor C-V 41
F. Future C Rotors 42
VIII. ULTRAHIGH-SPEED ROTOR SYSTEMS 43
A. Rotor D-I 43
B. Magnetic Support System 44
IX. DENSITY-GRADIENT CENTRIFUGATION IN ANGLE-HEAD ROTORS 45
X. SEAL DEVELOPMENT 47
A. Seal Design 47
B. Seal Types 47
1. A-Type Rotor Seal 47
2. B-Type Rotor Seal 48
3. C-Type Rotor Seals 48
XI. REPROCESSING OF CESIUM CHLORIDE 50
A. Introduction 50
B. Removal of Metallic Impurities 50
1. Method 50
2. Tests and Results 51
XII. CONTAINMENT AND STERILIZATION 53
A. Biohazards 53
B. Containment 53
XIII. PRESSURE ULTRAFILTRATION 55
A. Flow Rates Through Visking Dialysis Tubing 55
B. Design of Concentration Systems 56
XIV. DATA REDUCTION 57
A. Computer Program for Determining Sedimentation Coefficients Using Sucrose Gradients in the B-II Zonal Centrifuge 57
1. General Considerations 57
2. The Program 58
3. Data Preparation 59
4. Reports of Results 59

B. Calculation of Density and Viscosity of Sucrose Solutions 64
1. General Considerations 64
2. Density Relations 64
3. Viscosity Relations 66

XV. CENTRIFUGE INSTRUMENTATION 68

A. Requirements 68

B. Centrifuge Instrumentation 68

XVI. ELECTRON MICROSCOPY 70

XVII. ANCILLARY STUDIES 72

A. Studies on Synchronized Cell Division 72
1. Respiratory Activity of Synchronized Cells 72
2. Other Investigations 75

B. Automatic Carbohydrate Analyzer 75
1. General Considerations 75
2. Materials and Design 76
3. Performance 82

C. Flame Ionization Analyzer for Determining Total Carbon in Liquid Streams or Solid Samples 83
1. General Considerations 83
2. Experimental Prototype 83

D. High-Pressure Ion Exchange Chromatography 85

E. Analysis of Particulate Material from Natrual Water 86

F. Rate-Zonal Separation of Large Particulates from Bacterial Protoplasts 87

G. Protein Synthesis on Ribosomes 89
1. Problems of Ribosome Isolation 89
2. Separation of Ribosomes 89

H. Automated Nucleotide Analyzer 92

I. Introduction

N. G. Anderson

The central purpose of this program has been to develop biophysical separation methods for the separation of cells, subcellular particles, macromolecules, and low-molecular-weight cell constituents, and to apply these methods to cells in a single stage of the cell cycle. Emphasis at the outset has been on particle separation based on differences in either sedimentation rate or particle density as observed in liquid density gradients. A variety of centrifuge systems has been developed to explore these methods.[1] During this report period, efforts were directed toward centrifuge development. These will continue for the coming year. However, studies aimed at exploring biophysical separations based on ion exchange and electrophoresis, as well as those on the large-scale culture and synchronization of cells, are being carried on concurrently. We seek to integrate biophysical, biochemical, theoretical, physical, engineering, and metallurgical studies to search for specific solutions to basic biological problems. These studies are described in the Summary and are presented in detail in subsequent chapters.

At present, we wish to focus on a few carefully chosen biological problems that can be tested meaningfully with the systems under development. While the zonal centrifuge is a tool that provides a rapid method for separating cell constituents into a spectrum of particles, most cell components are very poor models for studying centrifuge performance and resolution. With a polydisperse particle suspension, such as a tissue homogenate, broadening of a zone caused by low centrifuge resolution cannot be distinguished readily from that due to particle heterogeneity. What we require is a homogeneous preparation that can be studied alone to determine resolution and its dependence on concentration. The particle also must be easily identified when added to polydisperse systems to determine if anomalous sedimentation occurs during centrifugation. Uniform particle preparations are also required for studies on continuous-flow centrifugation, which is of increasing importance as a method for obtaining large quantities of material for biochemical analyses.

Homogeneous synthetic particles in the size range required here are relatively difficult to obtain. Fortunately, many virus strains yield very uniform particle populations, and viruses are available in suitable ranges of sizes and densities. By studying viruses in fairly concentrated suspensions, we can examine the resolution of rate-zonal centrifuges. By adding very small amounts of virus to tissue breis, we may determine the resolution obtained with complex mixtures; by comparing resolution in these breis we may judge the heterogeneity of the smaller subcellular particles. Furthermore, by using very dilute virus suspensions, we may study the performance of continuous-flow centrifuges. The position of virus particles in gradients may be detected by ultraviolet absorption, by particle observation and counting in the electron microscope, by infectivity, and by monitoring for a radioactive label incorporated into the virus. The amount of virus may be determined in a wide range of concentrations by these methods. Virus particles are thus invaluable test or indicator units for developing methods aimed at eventual attempts to isolate minor cell constituents, such as centrioles or individual chromosomes.

It is of interest to consider virus particles not only from the viewpoint of resolution obtainable, but also of sensitivity. For the isolation of subcellular particles the lower limit of particle concentration of general interest is one particle per cell, and it is important to ask whether systems can be devised which are capable of this resolution and sensitivity. If such systems can be developed, it is evident that they would provide solutions for many less difficult separations.

[1] *Joint NIH-AEC Zonal Centrifuge Development Program Semiann. Rept. Dec. 31, 1962,* ORNL-3415 (Special).

II. Biomedical Applications of Zonal Centrifuges

A. ISOLATION OF TRACE AMOUNTS OF VIRUS FROM TISSUES

N. G. Anderson W. D. Fisher
C. L. Burger W. W. Harris

Subcellular particles may be considered operationally as a population that may exhibit differences in sedimentation rate or density. If these properties are plotted as a spectrum in two dimensions, the following question arises: Is there a "window" in that portion of the plot where most virus particles occur? Stated another way, are there particles in normal cells which have the same physical properties as known viruses? For a given virus, what fraction of the cell mass would have exactly the same density and sedimentation rate under a defined set of conditions? To attempt to answer these questions it is necessary to consider the sedimentation rates and densities of known virus particles, and then to examine tissues to see what fraction of the total tissue mass falls within the same size and density range. If a "window" indeed exists, then it is important to maximize the resolution of available separation methods and attack the problem of isolating very small amounts of virus which may occur in masses of normal or tumor tissue.

1. Physical Properties of Viruses

Available data on the composition and masses of viruses and the absorbance of solutions containing known amounts of particles are shown in Table II-A-1. The latter are calculated values and do not include the increased absorbance caused by scattered light. Ultimately it will be necessary to determine the absorbance of suspensions on which particle counts have been done carefully. The data are considered provisional.

As highly purified virus materials become available for investigation and medical use, it is necessary to consider the units in which concentration of virus particles are expressed, the relation between these units, and the methods used for analyzing virus suspensions. The following proposals are internally consistent and would help one to compare different viruses, to analyze given preparations, and to estimate concentration.

The basic unit is the weight of an anhydrous virus particle in grams. Fractions of a gram have been given names corresponding to 10^{-3N} g, where N is a whole number.[1] In keeping with this convention, 10^{-18} has been chosen as the weight unit, and might well be termed a "virogram." The viruses listed in Table II-A-1 range from 11 to 3500 virograms. Thus whole numbers can be used. In the past, virus concentration has often been expressed as micrograms of virus per milliliter of suspension. If a unit of virus concentration is chosen which contains 10^{12} virus particles per ml, then the μg of virus per unit concentration is found to be numerically equal to the weight of a single virus in virograms. Thus the weight of a single cowpox virus is 3500 virograms, and a solution containing 10^{12} cowpox virus particles would contain 3500 μg of virus per ml. A polio virus with a weight of 12 virograms yields a suspension with 12 μg of virus per ml at a concentration of 10^{12} physical particles/ml. In this work, we consider the *physically defined* particle (PP) and not the *infectious* one (IU). The absorbance at 260 mμ of virus suspensions at 10^{12} PP/ml spans very nicely the range of absorbancies usually measured with conventional spectrophotometers, except for the large pox viruses, where dilution by one order of magnitude (10^{11} PP/ml) is required to make reliable measurements. With these units there are simple correlations between number, particle weight, concentration, and absorbance.

[1] *Microchem. J.* 5, 1–3 (1961).

Table II-A-1. Provisional Data on the Properties and Composition of Some Viruses

Virus	Dimensions (μ)	DNA (%)	RNA (%)	Particle Weight (virograms)[a]	At 10^{12} PP/ml				10^{12} Physical Particles per Optical Density Unit
					Nucleic Acid/ml (μg)	Protein/ml (μg)	Virus/ml (μg)	Absorbance[b] at 260 mμ	
T2, T4, T6	95 × 65	40		500	200	300	500	4.2	0.24
T1, T3, T7	50 × 45	40		140	56	84	140	1.18	0.85
ϕ X 174	37 diam	25		11	2.7	8.3	11	0.055	18
Vaccinia	260 × 220 × 220	7.8		3300	257	3043	3300	7.3	0.14
Cowpox	260 × 220 × 220	7.2		3500	252	3248	3500	7.3	0.14
Adenovirus 5	70 diam	30		350	105	245	350	2.3	0.43
Rabbit papilloma	45 diam	8		150	12	138	150	0.34	2.9
Poliomyelitis	27		25	12	3	9	12	0.076	13.2
Foot and mouth	25		40	13	5.2	7.8	13	0.16	6.2
Encephalomyocarditis	27		30	12	4	8	12	0.11	9.1
Equine encephalitis	50		4.4	83	3.7	79	83	0.15	6.7
Influenza	80		0.8	500	4.0	496	500	0.45	2.2

[a]Virogram equals 10^{-18} g.

[b]At 260 mμ, 1-cm light path at a concentration of 1 μg/ml, direct readings are as follows: RNA, 0.025; protein, 0.0007; DNA, 0.02.

2. Search for Viruses in Sections by Electron Microscopy

The electron microscope has been invaluable in identifying virus particles in cells. It is important to know whether centrifuge systems can be built which will approach, or possibly surpass, the sensitivity of the electron microscope in identifying virus particles in cells. For this discussion we will consider virus concentrations at the level of one particle per cell.

An estimation of the number of photographs which must be examined to find one virus particle per cell is given by the approximation

$$N = \frac{4\pi r^3 M^2}{3TA},$$

where N is the number of photographs to be examined; r, the radius of the cell in cm; M, the electron microscope magnification; T, the thickness of the section in cm; and A, the area of the photograph in cm^2.

For a cell 15 μ in diameter, approximately six hundred 8 × 10 in. photographs at 20,000×, using 250-A sections, would be required. As the diameter of the cell or the magnification is increased, so is the number of photographs.

It is evident that a statistical study of the number of virus particles in a tissue at this level is an inordinately tedious task involving thousands of photographs (6000 for ten cells).

3. Detection of Virus Particles in Gradients

For detection of virus particles by ultraviolet (UV) absorption, the lower limit with present systems is approximately 0.1 absorbance unit. With a small virus, such as polio, this represents approximately 1.3×10^{12} PP; with a large one, such as vaccinia, the same absorbancy is produced by about 1.4×10^{10} PP. If one particle per cell is to be detected, then the number of original cells must equal the number of particles.

Using rat liver as an example, 1 g of tissue contains 2 to 4×10^8 cells. The upper limit for tissue used directly in the B-II rotor is about 10 g, giving about 3×10^9 cells. This is one order of magnitude below the UV absorption limits for vaccinia, and three below that for polio.

However, if 10^8 virus particles can be isolated from 1 g of tissue free of other contamination and in a volume of 1 ml, then their detection through conventional counting techniques by electron microscopy is fairly simple. Further, if the isopycnic separations are done in a small volume, the limit of 0.1 absorbance unit may be considerably decreased.

4. Subcellular Particles with Virus-Like Sedimentation Properties

For present purposes the osmotic properties of subcellular particles will be ignored, and the question that will be asked is: What percentage of the protein in a tissue sediments in a sucrose density gradient under a given set of conditions to a position that would also have been reached by a virus of known properties? The amount of such "contamination" will directly affect the level at which virus particles may be detected in the electron microscope.

The results of typical experiments are shown in Figs. II-A-1 and -2. The amount of protein present was determined by an automated method to be described in a subsequent report. In rat liver, from approximately 0.5 to 1.5% of the total cell protein is found in each 40-ml fraction in the area between the soluble phase and the mitochondrial peak. Most of this material is probably fragmented endoplasmic reticulum. This conclusion is supported by the findings obtained with rat spleen, shown in Fig. II-A-2. In most tumor cells, and in many cell lines used in tissue culture, the amount of endoplasmic reticulum is less than in liver. If a virus particle is restricted to only a few of the 40-ml fractions, it is evident that considerable purification is achieved in one zonal centrifuge run.

These studies do not demonstrate the full capabilities of the B-II rotor system, however. To retain the larger particulates in the rotor, a short, steep gradient was used. In practice, nuclei, cells, and mitochondria can be sedimented to the rotor wall or to a "cushion" near the rotor edge, and the virus-like particle range can be extended considerably.

It is also evident that preconcentration can be used to increase greatly the amount of virus-range

material in the rotor. Thus the large particles may be sedimented at low speed, and the virus-sized material may be sedimented at higher speed, resuspended, and then run in the zonal ultracentrifuge. As much as 100 g of tissue or cells may be processed in this manner. However, in the present work, efforts have been made to develop general methods that would not necessarily involve pelleting virus materials at any stage, so that very sensitive materials may be isolated.

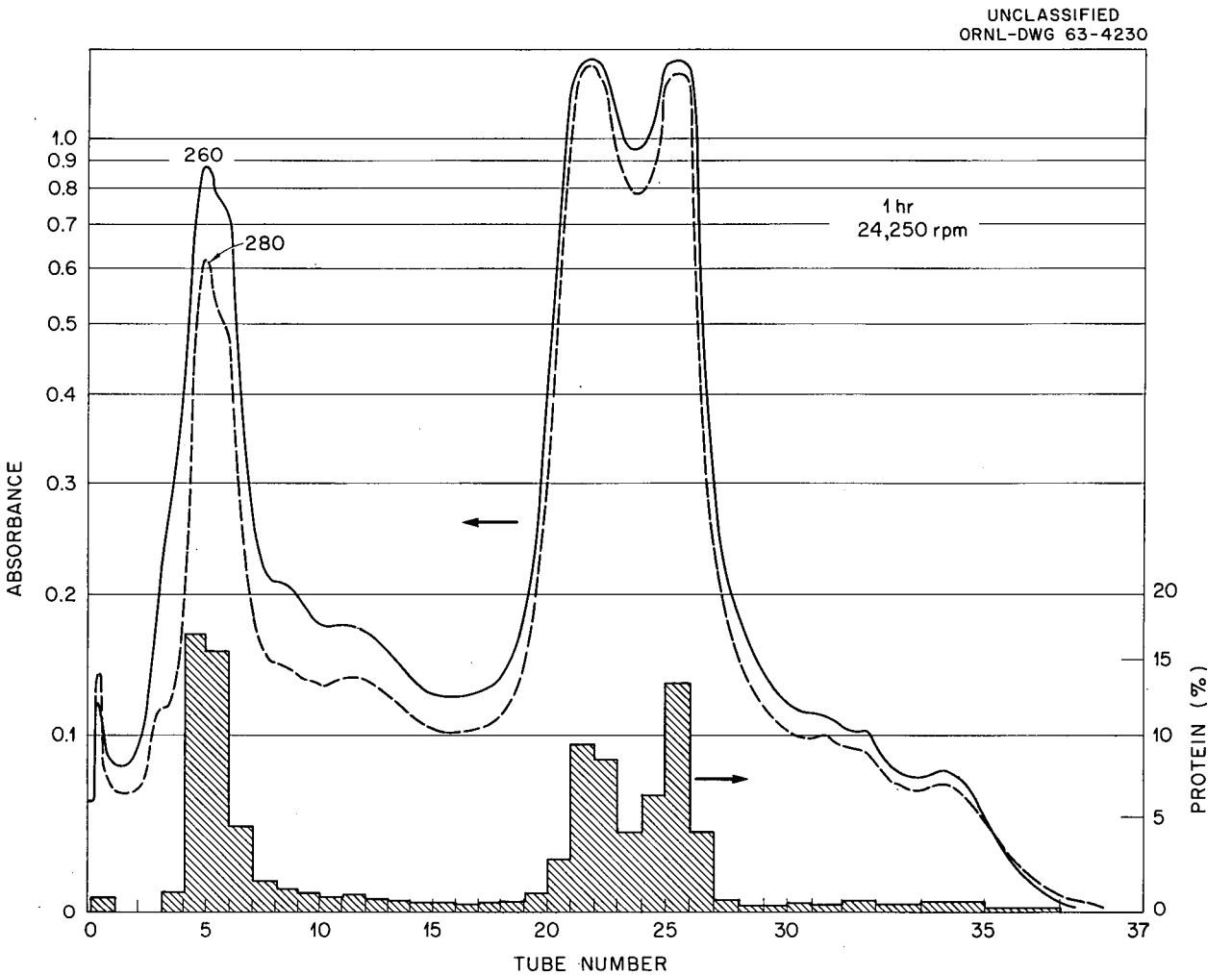

Fig. II-A-1. Distribution of Absorbance and Protein in Rat Liver Brei Centrifuged in Sucrose Density Gradient in B-II Zonal Centrifuge. A total of 12.5 ml of a 20% perfused rat liver brei was introduced centripetal to a 1200-ml 17 to 55% sucrose gradient with a cushion of 66% sucrose. This was overlayed with 216 ml of Miller Golder buffer (pH 7.5, $\mu = 0.1$), and the homogenate centrifuged 1 hr at 24,250 rpm at 5°C. Protein is shown as percent of the total sample found in each fraction collected.

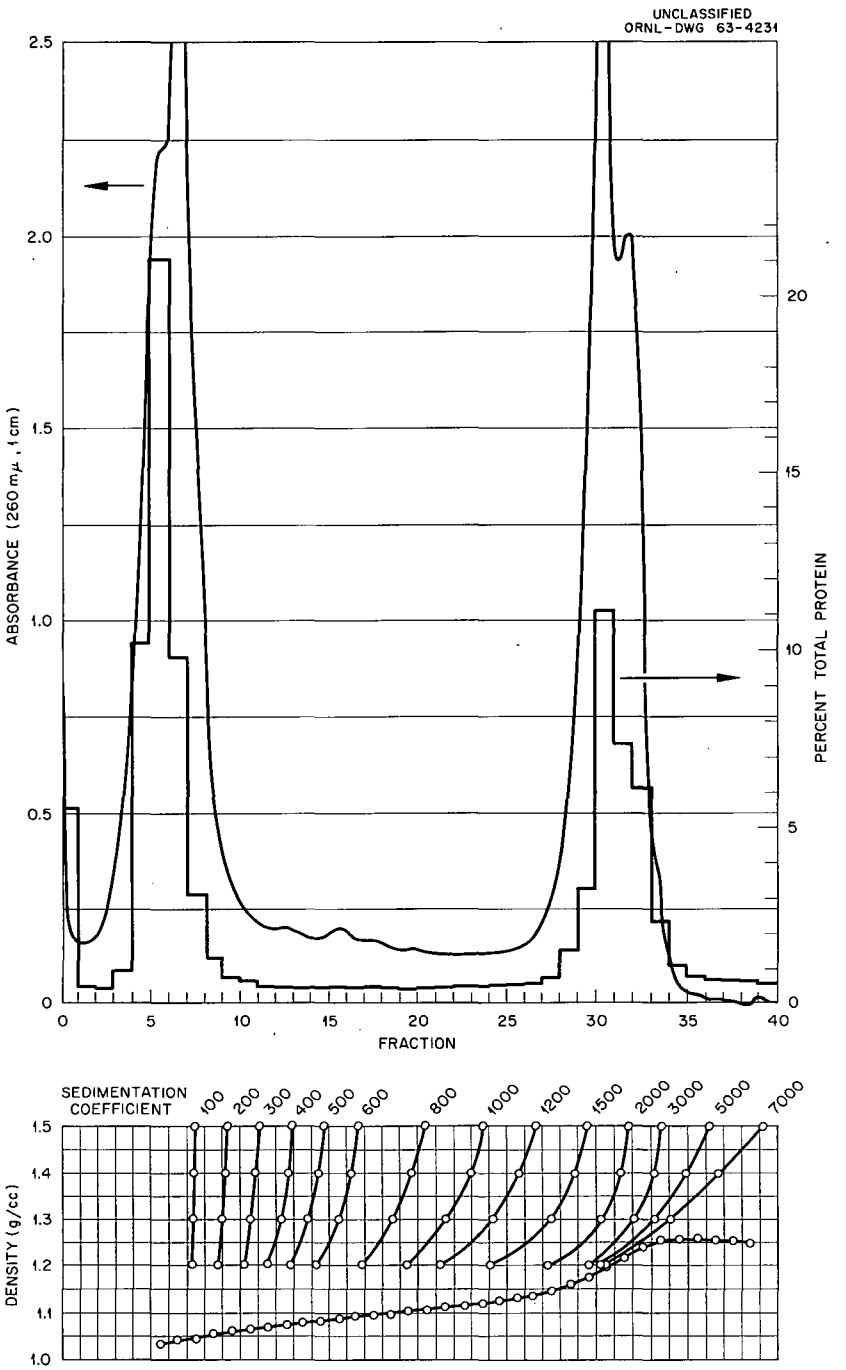

Fig. II-A-2. Fractionation of Rat Spleen Brei in B-II Zonal Centrifuge. A total of 3.42 g of spleen from four adult Sprague-Dawley rats was homogenized in 8% sucrose to give a total volume of 24 ml. One milliliter of T3 phage solution containing 4×10^{12} phage particles was added. The 1000-ml sucrose gradient varied linearly with volume from 10 to 30% sucrose, with a cushion of 55% sucrose. An overlay of 216 ml of sodium phosphate–NaCl (pH 7.5, $\mu = 0.1$) was used, and the homogenate was centrifuged 1 hr at 20,000 rpm. The value of $\omega^2 t$ at the start of unloading was $16{,}912 \times 10^6$. Protein was determined using an automated Folin-biuret method and was expressed as percent of total protein in the starting sample. Sedimentation coefficients plotted in terms of particle density are plotted below the chart.

5. Sedimentation of Virus Added to Tissues

The possibility must be considered that virus particles may not sediment as expected in the presence of large amounts of subcellular material. To examine this possibility, small amounts of phage labeled with P^{32} were added to rat liver breis, and the separated fractions counted. The results show that negligible adsorption to subcellular particles occurred. With other cells and viruses, however, adsorption may occur, and each cell-virus system must be examined for this possibility. The isolation of adenovirus 2 from infected human tissue culture cells will be discussed in a subsequent report.

6. Isopycnic Separations of Particles Previously Isolated by Rate-Zonal Centrifugation

The fractions collected from the zonal ultracentrifuge suspected of containing virus particles must now be separated on the basis of particle density by banding in cesium chloride or other dense solution. The centrifugal systems that will ultimately be used for this cannot be visualized with certainty at this time. To centrifuge particles from sucrose solutions into small-volume CsCl gradients, for example, may require specially designed tubes and rotors. At least 12 samples must be examined at one time, and preferably many more.

To complete the two-dimensional sedimentation rate-density plot of tissue constituents, it is necessary to band the particles in each of many fractions collected during the rate-zonal separations. In our initial studies the latter fractions have first been centrifuged at high speed in an angle-head rotor, followed by pellet resuspension in CsCl of appropriate density. We intend to study methods for centrifuging particles directly out of sucrose into CsCl. For equilibrium banding of many samples in CsCl, we need simple methods for centrifuging up to 12 samples at a time and automated systems for monitoring CsCl gradients for refractive index and absorbance. The status of this work is presented in Chap. IX, where the use of angle-head rotors in place of swinging-bucket rotors is discussed.

To explore rate-zonal centrifugation in the B-II rotor, followed by CsCl banding of the virus-containing fractions, T3 phage particles were added to a rat spleen brei which was then centrifuged as described in the legend of Fig. II-A-2. The virus peak is small as observed in the B-II rotor UV monitor. Presence of virus in this peak was confirmed by electron microscopy. A number of fractions were then centrifuged for 2 hr at 30,000 rpm in the Spinco 30 rotor, and the pellets resuspended in CsCl with a density of 1.5. After centrifugation for 15 hr at 24,000 rpm, the virus was recovered as shown in Fig. II-A-3. While the virus sample represents a very large number of particles (4×10^{12}), the virus mass was only 560 μg, 0.0163% of the sample mass. The phage particles were easily identified in the electron microscope, and only a small amount of contamination was observed. The T3 sample was equivalent to approximately 6000 particles per cell – a concentration yielding about ten particles per 250-A section of a cell. It is evident that the method can be scaled down by nearly a full order of magnitude using methods available now and can possibly be increased in sensitivity by two orders of magnitude using more refined methods for scanning isopycnic gradients. If the gradients were scanned with the electron microscope, a considerable additional sensitivity could be obtained.

7. Further Studies

We wish ultimately to scan human tumors and other tissues for virus particles. To properly interpret the results it will be necessary to make extensive observations on "normal" materials to discover the nature of any subcellular particles that may resemble viruses in physical properties. Preliminary results obtained with human leukemic plasma show the presence of particles having the size, morphology, and density of viruses.

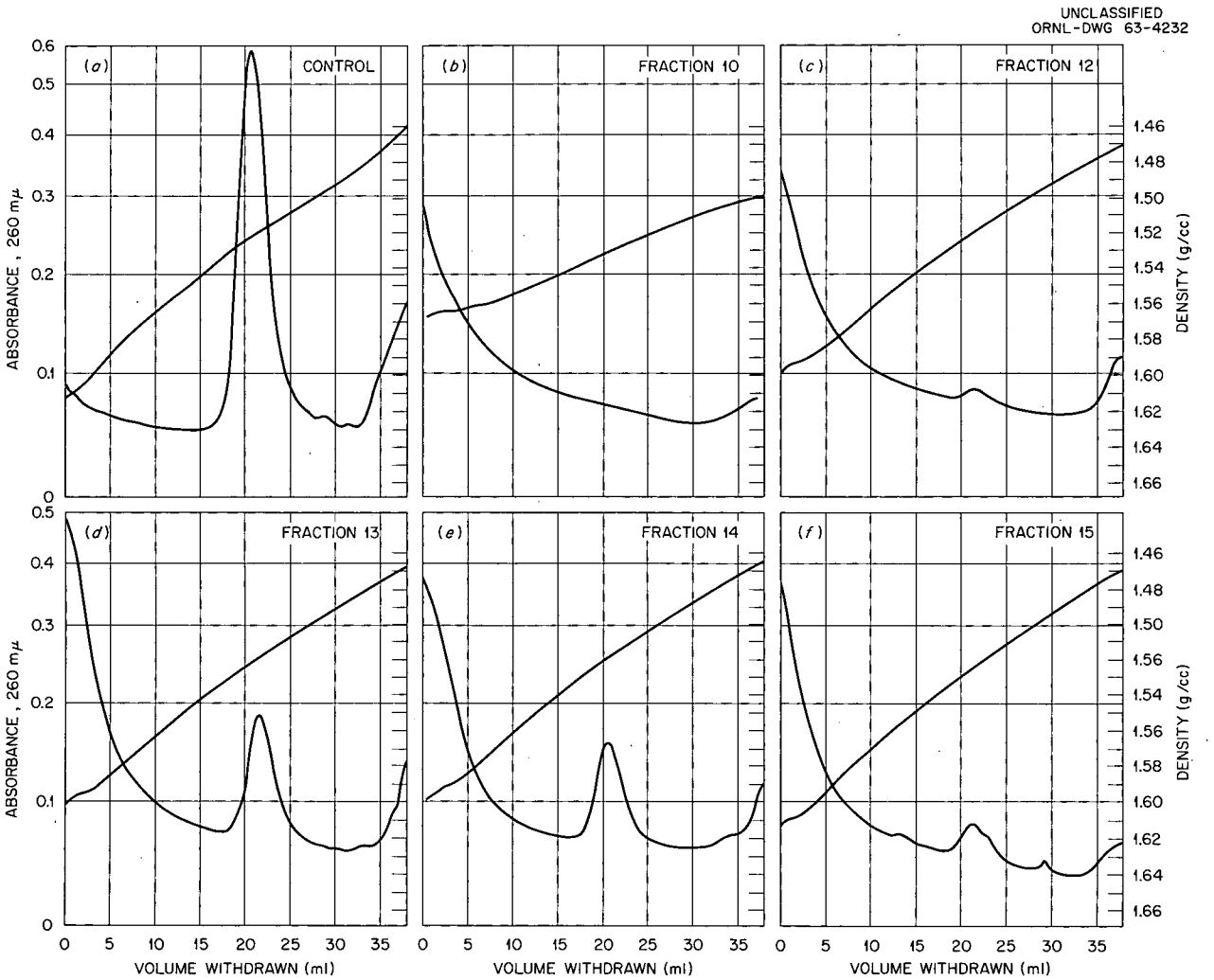

Fig. II-A-3. Banding of T3 Phage in CsCl. In (*a*), the same number of phage was added to the spleen brei described in Fig. II-A-2 and was similarly centrifuged. In (*b–f*), five fractions from the rate-zonal run shown in Fig. II-A-2 have been banded in CsCl, and the runs have been monitored using the refractive index–absorbance monitor described in a subsequent section. The majority of the T3 virus was found in fractions 13 and 14. Very little background material with the same density as T3 was found in tube 10, a result indicating the small amount of contaminating material found in this sedimentation rate region.

B. LARGE-SCALE VIRUS ISOLATION

N. G. Anderson
R. E. Canning
C. T. Rankin, Jr.
C. L. Burger

1. Types of Viruses To Be Isolated

While stable spherical viruses are excellent test objects for studying the performance of zonal centrifuges, many of the most important isolation problems involve virus particles that are unstable and do not necessarily behave ideally. It is important, therefore, to determine the applicability of zonal centrifuges to the isolation of a number of different types of viruses.

Initially, four viruses presenting quite different isolation problems have been considered. These are adenovirus 2, Echo 28, the respiratory syncytial virus, and the Rauscher mouse leukemia virus. The first is a nuclear virus that must be separated from

other subcellular particles. Echo 28 is a small virus growing to very low titer in tissue culture. The respiratory virus is a very sensitive virus that may require the development of rapid, refined concentration methods, while the Rauscher virus may serve as a prototype for the oncogenic viruses now being sought in human materials.

The basic problems are (1) concentration of the virus into a small volume, (2) separation based on sedimentation rate, and (3) sedimentation based on particle density. For some applications the B-II rotor system[2] serves all three purposes. However, for very small virus particles this rotor has not provided sufficient centrifugal force at a reasonable flow rate. Further, a number of viruses lose infectivity when sedimented against a solid surface. Alternate approaches to the concentration of virus particles, therefore, have been investigated. These include ultrafiltration (Chap. XIII) and sedimentation in a large-capacity rotor, for example C-V (Chap. VII), directly into a dense medium such as a CsCl solution. For separations based on rate, the rotors B-II and the newer modification, B-V, will probably continue to be most useful. To achieve purification by isopycnic banding, a series of rotors (C-II to C-IV) are being developed for samples of varying size (Chap. VII), while angle-head centrifugation of CsCl-suspended particles has been developed where many different individual samples are to be banded. As these methods are perfected they will be applied to the isolation of the viruses listed.

2. Preliminary Studies on Adenovirus 2

The initial studies on the isolation of adenovirus 2 were done on whole cultures (cells plus culture fluid) that had been frozen and thawed several times to release the virus particles. The fluid was passed through the B-II rotor, using it as a continuous-flow centrifuge. The sedimented virus was then displaced off the wall and banded in a CsCl density gradient. Because of instabilities observed at high speeds (Chap. VI), the rotor was operated at only 20,000 rpm, a speed insufficient to achieve complete sedimentation of the virus. While encouraging concentrations were obtained, further study on continuous-flow separation of adenoviruses has been delayed until higher speeds can be routinely achieved.

The second method investigated involved preconcentration of the culture fluid lysate by dialysis against high-molecular-weight Dextran. The concentrated material (53 ml) was then separated by rate-zonal centrifugation through a sucrose density gradient for 30 min at 20,000 rpm. The results are shown in Fig. II-B-1. The virus was found in the sharp peak at the 1.234 density level, using the electron microscope. Whether this is the isopycnic point for the virus in sucrose remains to be seen. Infectivity studies by Maurice Mufson at the Laboratory of Infectious Diseases at the National Institutes of Health indicate that the majority of the virus particles are in this peak, with a few being scattered in the lighter portions of the gradient. The peak material was banded in CsCl in an angle-head rotor, as described in Chap. IX. A photomicrograph of purified material is shown in Fig. II-B-2.

The results shown in Fig. II-B-1 are surprising because the virus sedimented much farther down the gradient than would be expected on the basis of physical dimensions of the particles. This strongly suggests that the virus particles may aggregate in solution. Preliminary studies carried out by W. W. Harris in which adenovirus 2 was

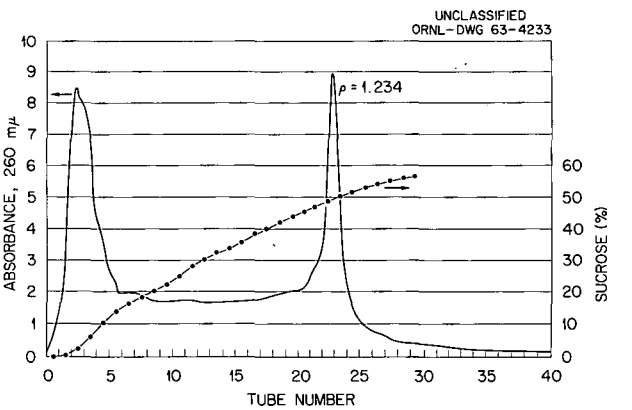

Fig. II-B-1. Separation of Soluble Material and Adenovirus 2 in Sucrose Gradient in the B-II Rotor.

[2]N. G. Anderson, *Joint NIH-AEC Zonal Centrifuge Development Program Semiann. Rept. Dec. 31, 1962*, ORNL-3415 (Special), p 39.

sedimented onto a flat surface from solutions containing varying concentrations of virus suggest that the degree of aggregation is concentration dependent. The peak observed to the right in Fig. II-B-1 may therefore represent highly aggregated material, while the small amount of infectivity observed closer to the starting zone is probably due to the presence of aggregates of smaller size.

Studies on the pH dependence of aggregation are now being done so that rate-zonal centrifugation may be used to purify adenoviruses. The results of this work will be presented in detail in the next report.

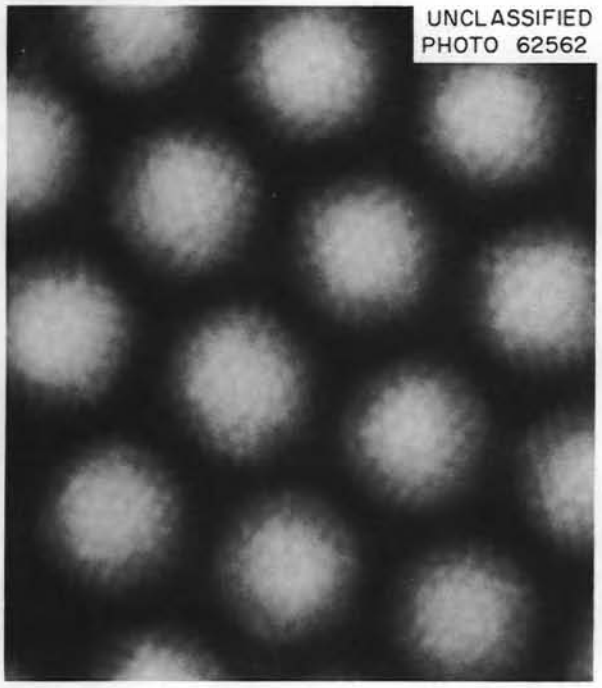

Fig. II-B-2. Photomicrograph of Purified Adenovirus 2. 320,000X.

III. Theoretical Studies

A. USE OF ZONAL CENTRIFUGES FOR VIRUS CONCENTRATION

A. S. Berman

1. Theoretical Approaches to Virus Concentration

A study was made of how B-type rotors could be used for virus concentration. Three techniques were examined: (1) the conventional batch, (2) a semibatch, and (3) a continuous-flow procedure.

In the conventional batch technique the rotor is filled with a virus suspension, and the material is centrifuged for the time required to remove a given fraction of the virus. The depleted medium is then displaced out of the spinning rotor with distilled water, which is added through the center line, and the original filling procedure is repeated. After the desired number of batches are run, the virus that has accumulated on the wall is removed by using a density-gradient banding technique or is mechanically removed after stopping the rotor.

In the semibatch process the rotor is never completely filled with the virus suspension. Instead, batches are consecutively introduced which fill the rotor to a predetermined thickness. The remainder of the rotor is filled with distilled water or other fluid that is lighter than the virus suspension. The centrifuge is then run for the time required to remove a given fraction of the virus from the layer, after which the layer is "backed out" by feeding the light displacement fluid to the center of the rotor.

With all the rotor systems used thus far, a core is used which occupies the rotor axis and defines the minimum radius of the fluid mass in the rotor. It can be shown that the *minimum* total centrifugation time required in the semibatch process is given by

$$T_m = \frac{9\eta V_t f}{V(\rho - \rho_1)D^2\omega^2}, \qquad (1)$$

where η is the viscosity of the suspending medium; V_t, the *total* volume of material to be processed; f, the fraction of virus removed; V, the volume of the rotor; ρ, the density of the virus (assumed spherical); ρ_1, the density of the suspending medium; D, the diameter of the virus particle; and ω, the angular velocity of the rotor. All quantities are expressed in cgs units. For the actual semibatch process in which the material to be processed is handled in N steps, the total centrifugation time[1] is given by

$$T_{SB} = \frac{9\eta N}{(\rho - \rho_1)D^2\omega^2} \ln\left[\frac{1}{1 - (V_t f/VN)}\right]. \qquad (2)$$

For the batch process, the time required is

$$T_B = \frac{9\eta V_t}{V(\rho - \rho_1)D^2\omega^2} \ln\left(\frac{1}{1 - f}\right). \qquad (3)$$

A convenient comparison between the batch and semibatch techniques is obtained by defining the process efficiency as

$$E = \left(\frac{T_m}{T_{actual}}\right) f. \qquad (4)$$

This efficiency is unity if all the virus is removed in the minimum time defined above. Note that this definition *does not include* the times involved in adding material to or removing it from the rotor.

[1]The total time for the process is the sum of the total centrifugation time and the time required to add material to, and to remove material from, the rotor. These latter times can be appreciable, and they are comparable to centrifugation times.

Figure III-A-1 shows the efficiency as a function of the fraction of virus removed for the semibatch and batch processes. The superiority of the semibatch process for the removal of a substantial fraction of virus is clearly seen. In addition, this efficiency improves rapidly with increasing number of steps, for a given f, and little is gained by continuing the increase in N.

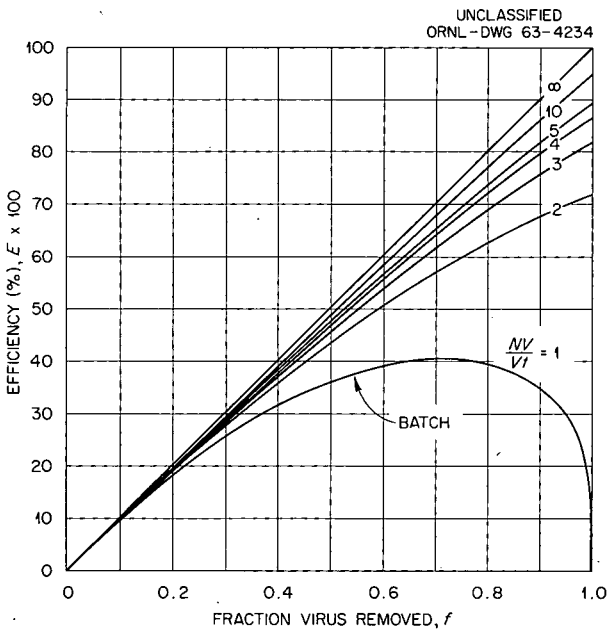

Fig. III-A-1. Efficiency of Batch and Semibatch Techniques for Virus Concentration. V_t is the volume to be processed; V, volume of centrifuge; N, number of steps. Waiting time for processing equals $(T_m F)/E$ sec with $T_m = [\alpha V_T/V(\rho - \rho_1)]f$ and $\alpha = 9\eta/\omega^2 d^2$. See text for other symbols. For example,

$\eta = 0.015188$ poise,

$\omega = (20{,}000 \text{ rpm}) \left(2\pi \frac{\text{radians}}{\text{rpm}}\right)\left(\frac{1}{60}\frac{\text{min}}{\text{sec}}\right)$,

$d = 550 \times 10^{-8}$ cm,

$\alpha = 10.3015 \times 10^2$,

$V_t = 10^4$ cm^3,

$V = 1625$ cm^3,

$T_m = 13{,}781\ f$ sec $= 3.828\ f$ hr;

$\rho = 1.51$,

$\rho_1 = 1.05$.

For 95% removal,

$f = 0.95$

$T_B = 12.070$ hr,

$T_{SB} = 4.245$ hr for $\frac{V_t}{NV} = 5$; $N \approx 31$.

Both processes were considered for use in existing B-type rotors. If a design change is permitted in the core of a B-type rotor, then a continuous flow-through technique can be considered. In this technique the core is such as to almost fill the rotor, leaving a thin annular space between the core and the rotor wall. The medium containing the virus is fed continuously to the annular space at one end of the rotor, flows along the annular space, and is removed at the opposite end of the rotor. The flow rate is adjusted so that a given fraction of the virus is removed.

A solution to this sedimentation problem has been obtained[2] which accounts for the radial variation of the centrifugal field across the annular space, and also for the radial variation in axial flow along the annular space. The solution relates a cluster of variables, G (depending on the properties of the centrifuge, the virus, and the suspending medium), to the fraction of virus to be removed and the inner and outer radii of the annular flow channel:

$$G = \frac{\pi r_2^2 \omega^2 Le}{Q} \frac{D^2(\rho - \rho_1)}{9\eta}$$

$$= \frac{2 \ln R^2}{(1 - R^2)[(1 + R^2) \ln R^2 + 2(1 - R^2)]}$$

$$\times \left\{ \ln \frac{1}{1 - (1 - R^2)f} - (1 - R^2)f + \frac{1}{2} \frac{1 - R^2}{\ln R^2} \left[\ln \frac{1}{1 - (1 - R^2)f} \right]^2 \right\}, \quad (5)$$

where Q is the volume flow rate (cm^3/sec); r^2, the outer radius of the annulus (cm); R, the ratio of the inner to outer radii of the annular flow channel; and Le, the effective length of the rotor. The remaining symbols have been defined previously. The effective rotor length, Le, approaches the length of the annular flow channel as the axial mixing caused by the feed to the rotor approaches zero.

[2]Viscosity and pressure have been assumed constant in the annular flow channel, and the virus has been assumed spherical. It has also been assumed that the virus is uniformly distributed across the annular space at the feed point.

For radius ratios greater than $R = 0.8$, G is given with a maximum error of 5% by the much simpler expression

$$G \doteq f^2(3 - 2f) - (f^2/2)(5f^2 - 8f + 2)(1 - R^2) . \quad (6)$$

These equations permit preliminary design calculations to be made readily, once the required properties of the centrifuge, the virus, and the suspending medium are known.

Figure III-A-2 gives G as a function of the radius ratio R, for three values of f, the fraction of virus removed. The figure also shows (broken line) the values of G obtained from the simple formula valid for radius ratios close to unity. A typical calculation may illustrate the use of the equations:

Centrifuge Properties

$r_2 = 5$ cm
$Le = 25$ cm
$R = (r_1/r_2) = 0.9$
Speed = 20,000 rpm or
$\omega = 2.094 \times 10^3$ radians/sec
$V = 1963$ cm^3

Particle and Medium Properties

$\rho = 1.51$ g/cm^3 (T3 phage)
$D = 5.5 \times 10^{-6}$ cm (T3 phage)
$\rho_1 = 1.05$ g/cm^3
$\eta = 0.015188$ poise

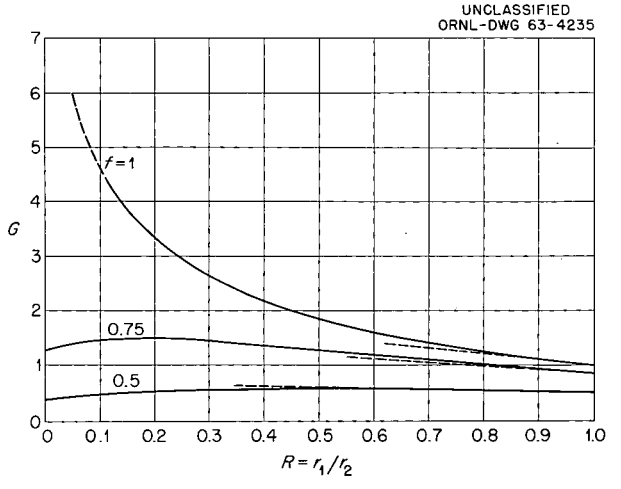

Fig. III-A-2. Annular Spacing for Continuous-Flow Centrifuge. Broken line, computed from simplified Eq. (6) for R close to unity.

Assume that we desire to remove all the virus, so that $f = 1$. Since R is close to unity, we can estimate G from Eq. (6) to obtain

$$G = 1 - \frac{1}{2}(-1)(1 - 0.9^2) = 1.095 . \quad (7)$$

The more accurate equation for G gives 1.109 for this case, so that the error of the approximation formula is only about 1.3%. The feed rate can now be computed from the known value of G:

$$Q = \frac{\pi r_2^2 \omega^2 Le}{G} \frac{D^2(\rho - \rho_1)}{9\eta}$$

$$= \frac{\pi(5^2)(2.094)^2(10^6)(25)(5.5)^2(10^{-12})(0.46)}{(9)(1.109)(0.015188)} , \quad (8)$$

$$Q = 0.790 \text{ cm}^3/\text{sec} = 2.84 \text{ liters/hr} .$$

Thus 50 liters of suspension can be processed in about 17.6 hr with this centrifuge. If the speed were 40,000 rpm the flow rate could be increased to about 11.4 liters/hr, and 50 liters could be processed in about 4.4 hr.

2. Effect of Transient Times and Coriolis Forces on Sedimentation Rates (Spherical Particles)

Under current operating conditions for virus concentration or separation, even a superficial examination of the equation of motion for the settling particle reveals that Coriolis effects will be small. Nevertheless, we wished to obtain an estimate of the dependence of the Coriolis effects and transient times on the properties of the centrifugal field, the virus, and the suspending medium. To obtain such estimates, the following equation of motion for a spherical particle settling slowly in a centrifugal field was examined:

$$\underbrace{-\frac{18\eta}{(\rho - \rho_1)D^2}\vec{v}}_{\text{Stokes resistance}} = \underbrace{\frac{\partial \vec{v}}{\partial t}}_{\text{Acceleration in rotating frame of reference}} + \underbrace{2\vec{\omega} \times \vec{v}}_{\text{Coriolis acceleration}} + \underbrace{\vec{\omega} \times (\vec{\omega} \times \vec{P})}_{\text{Centripetal acceleration}} . \quad (9)$$

In this equation $\vec{v}$ is the velocity vector of the particle, and $\vec{P}$ is its position vector; ρ and D are, respectively, the density and the diameter of the particle. The viscosity and the density (both assumed spatially constant) are η and ρ_1 respectively. The angular velocity vector of the rotor is $\vec{\omega}$. Since $\vec{v}$ is very small compared with $\vec{\omega}$ for current operating conditions, the Coriolis effect (proportional to ωv) will be small compared with the effect of the centrifugal field (proportional to $\omega^2 r$). The dependence on the properties of the system requires a solution of the above equation. For the present case it is convenient to use plane-polar coordinates. In this system the vector Eq. (9) yields

$$\beta v_r + \dot{v}_r - v_\theta(\dot{\theta} + 2\omega) - \omega^2 r = 0 , \qquad (10)$$

$$\beta v_\theta + \dot{v}_\theta + v_r(\dot{\theta} + 2\omega) = 0 , \qquad (11)$$

a pair of equations for the radial (v_r) and the tangential (v_θ) velocity components of the particle. In these equations, r is the radial position coordinate, θ is the angular position coordinate, ω is the angular velocity of the rotor, a dot over a quantity denotes the time derivative of that quantity, and β is given by

$$\beta = \frac{18\eta}{D^2(\rho - \rho_1)} . \qquad (12)$$

The terms $v_\theta(\dot{\theta} + 2\omega)$ and $v_r(\dot{\theta} + 2\omega)$ represent effects of the *total* Coriolis and centrifugal forces, that is, the forces on the particle produced by the rotation of the centrifuge with angular velocity ω, plus the secondary effects produced by the fact that the particle moves in a curved path (with angular velocity $\dot{\theta}$) relative to the rotating axes. Since in the problem of interest here, $\omega \gg \dot{\theta}$, the contribution made by $\dot{\theta}$ to these terms will be ignored.

With this simplification the pair of equations can be reduced to a single third-order differential equation for the radial position of the particle:

$$\frac{d^3r}{dt^3} + 2\beta \frac{d^2r}{dt^2} + (\beta^2 + 3\omega^2) \frac{dr}{dt} - \beta\omega^2 r = 0 . \qquad (13)$$

For ω/β small compared with unity, the solution for this equation is

$$r = a_1 \exp\left(\omega^2 \frac{t}{\beta}\right) + [a_2 \exp(2i\omega t) + a_3 \exp(-2i\omega t)] \exp\left[-\left(\beta + \frac{\omega^2}{2\beta}\right)t\right] , \qquad (14)$$

where a_1, a_2, and a_3 are constants of integration.

The transient time is seen to be very short and is approximately given by $(1/\beta)$ sec (about 10^{-10} sec for typical operating conditions and particles). Ignoring this transient effect, we find that the steady-state velocity components are given by

$$v_r = \frac{\omega^2 D^2(\rho - \rho_1)}{18\eta} r , \qquad (15)$$

$$v_\theta = \frac{\omega^3}{2}\left[\frac{D^2(\rho - \rho_1)}{18\eta}\right]^2 r . \qquad (16)$$

Thus the ratio of the tangential velocity (due to Coriolis effects) to the radial velocity is of the order $\omega/2\beta$ or 10^{-7} for typical current conditions and particles.

IV. Rotor Design

A. STABILITY STUDIES

D. A. Waters

1. General Considerations

The series A and C rotors developed during this program were designed from the outset to be stable, with suitable damping, at all speeds up to the designed maximum. The B-II rotor, however, has presented instability problems that were extremely difficult to analyze and that were not solved until very recently.

In the past, this rotor exhibited a marked instability between approximately 23,000 to 30,000 rpm. This instability is sufficiently severe to limit safe operating speed to about 20,000 rpm.

The instability has now been identified as an excitation of fast precession. The fast-precession curves for the B-II rotor, empty and full of water, are shown in Fig. IV-A-1. Although the exact mechanism which initiates this behavior is not known, past experience has shown that vibrations from a variety of sources can excite large-amplitude fast precession if the damping of the rotor is marginal. Consequently, when the amount of effective upper bearing damping was increased, the rotor could be driven successfully to the design speed of 40,000 rpm without sign of instability.

During the extensive analysis of the B-II system the rigid-body behavior of the rotor was analyzed. The runouts (variations in distance between a rotating mass and a proximity probe) of the various components of the rotor system, and of the rotor itself, are shown in Fig. IV-A-2. The upper suspension system encounters a rather severe resonance value at 34,000 rpm which may initiate the fast precession encountered experimentally at a somewhat lower speed. The analysis techniques used to investigate the behavior of the existing B-II rotor were used successfully to design and operate the C-series rotors.

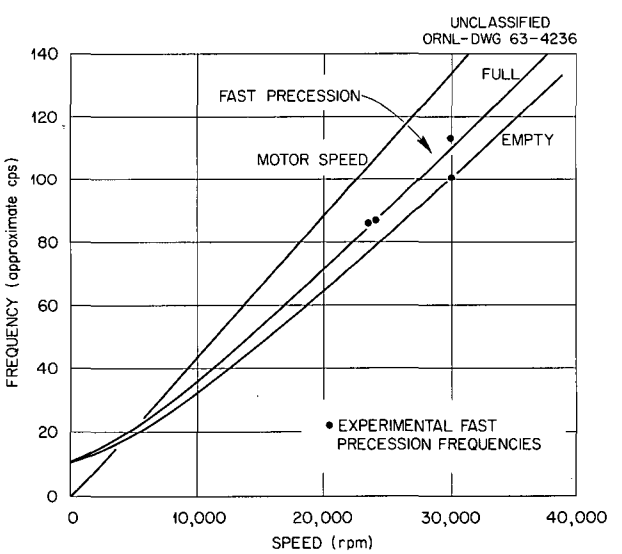

Fig. IV-A-1. Fast-Precession Curves for the B-II Rotor When Empty and When Loaded with Water.

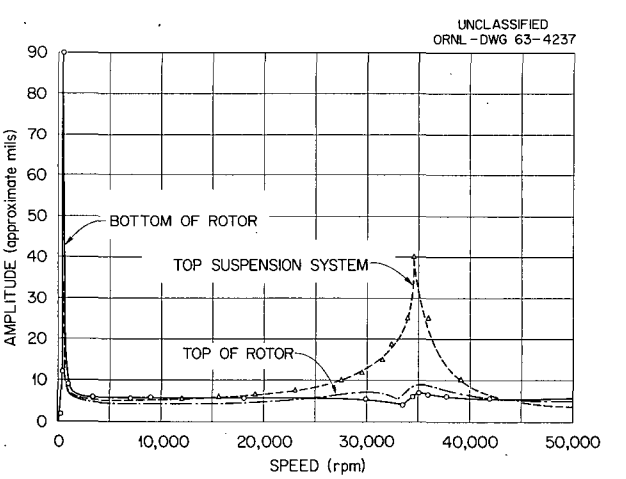

Fig. IV-A-2. Variations in Distance Between Rotor and Proximity Probe (Runout) of the Various Components of the B-II Rotor System as a Function of Speed.

2. Stability of the Liquid

Extensive experimental evidence has been obtained with regard to the high-speed mechanical behavior of a rotor when not filled with liquid.[1] The tests were conducted primarily on the B- and C-class rotors. No mechanical problems were encountered in either class of rotor when they were not filled. It has also been demonstrated that both classes of rotors can be run to design speed (40,000 rpm for the B-II, 141,000 rpm for the C-II) incompletely filled, with or without septa. As a result of this work, a new core with four centrally supported septa has been constructed and successfully tested (rotor B-V; see Chap. XVIIG).

B. THEORY OF ROTOR STABILITY AND ITS APPLICATION TO ROTOR DESIGN

D. A. Waters

1. General Considerations

The primary consideration in the design of a liquid centrifuge is the application, which dictates the capacity, loading and unloading procedure, rotational speed, and *g*-force. This section concerns the three critical design areas: (1) the ratio of the polar and transverse moments of inertia and the effect of this ratio upon shaft stiffness and the damping required to operate the machine, (2) the critical speed of the rotor, and (3) the stress in the rotor. Analysis has shown that two states of precession exist; one, a fast precession of the rotor symmetry axis in the same direction as the spin of the rotor, and the other, a slow precession of the rotor symmetry axis in the opposite direction of the spin of the rotor (Fig. IV-B-1). The dependence of the frequencies of fast precession upon the ratio of the polar and transverse moments of inertia should also be noted. As the ratio approaches unity, the expected frequency of fast precession increases until it approaches the value of the spin velocity of the rotor itself. When the ratio is equal to unity, the rotor behaves physically as a sphere, with its moments of inertia equal in all directions. Thus it has no principal axis to rotate about, and its spin axis will tend to wander continuously if the suspension systems are highly flexible.

UNCLASSIFIED
ORNL-DWG 63-4238

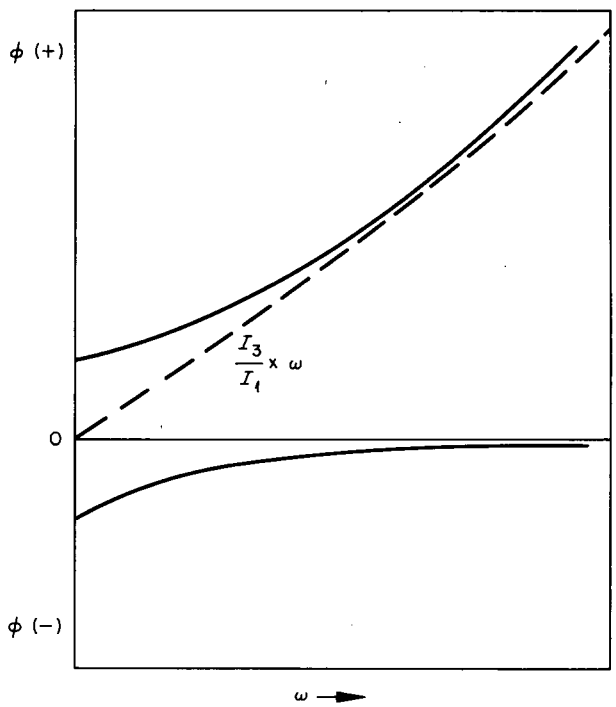

Fig. IV-B-1. Fast- and Slow-Precession Frequencies as a Function of Rotor Speed.

2. Critical Speed of the Rotor

The critical speed of the rotor itself must be determined when the required length-to-diameter ratio of the rotor is large. If flexible shafting is used to support the rotor, it can be demonstrated that the shafting exerts a negligible influence upon rotor critical speed. In such cases, the rotor can be treated quite accurately as a free beam. The Raleigh-Ritz method of analysis can be used to determine this frequency:

$$\frac{\partial}{\partial a_i} \int_0^L \left\{ \left[\frac{d^2\phi(x)}{dx^2} \right] - \psi[\phi(x)]^2 \right\} dx = 0 \ , \quad (1)$$

where

$$\phi(x) = \sum_{i=0}^{\infty} a_i (x/l)^{2i} \ ,$$

$$\psi = 4\pi^2 \nu^2 (A\gamma / EIg) \ ,$$

[1] *Joint NIH-AEC Zonal Centrifuge Development Program Semiann. Rept. Dec. 31, 1962,* ORNL-3415 (Special) p 25.

ν is the critical frequency (cps); A, cross-sectional area (in.^{2}); γ, density (lb/in.^{3}); E, Young's modulus (lb/in.^{2}); I, area moment of inertia (in.^{4}); g, 32.2 ft/sec^2; L, length of rotor; and l, $L/2$. The $\phi(x)$ function defines the shape of the rotor when it is operated at its critical speed. Assuming free-free end conditions, the shape function can be determined by invoking the boundary conditions

$$EI \frac{\partial^2 \phi(x)}{\partial x^2} = 0$$

and (2)

$$\frac{\partial}{\partial x}\left[EI \frac{\partial^2 \phi(x)}{\partial x^2}\right] = 0$$

at the ends of the rotor. Taking the midpoint of the rotor as the origin and applying the boundary conditions to the first four terms of the series, $\phi(x)$ yields the shape function

$$\phi(x) = a_0 + a_3\left(\frac{x^6}{l^6} - \frac{5x^4}{l^4} + \frac{15x^2}{l^2}\right). \quad (3)$$

The total mass of the end plugs will be assumed concentrated in a solid plug of uniform density and effective thickness, t_{eff}. From this assumption, t_{eff} can be derived from the ratio of the mass of the bowl, M_b, to the mass of the end plug, M_{ep};

$$\alpha = \frac{M_{ep}}{M_b} \simeq \frac{\rho_{ep}\pi r^2}{\rho_b \pi A r^2}\frac{t_{eff}}{l}$$

or

$$t_{eff} = \frac{\alpha}{K} l , \quad (4)$$

where K is the ratio of the cross-sectional area of the end plug, πr^2, to the cross-sectional area of the bowl, $\pi \Delta r^2$.

The range of integration of Eq. (1) is $0 \leqq x \leqq l$ for the bowl and $l \leqq x \leqq l(1 + \alpha/K)$ for the end plug. Furthermore, it will be assumed that the shape of the deflection curve, $\phi(x)$, will be constant throughout the end plug, the value of which is equal to the deflection at $x = l$ or

$$\phi(l) = a_0 + 11a_3 . \quad (5)$$

Substituting Eqs. (2–5) into Eq. (1) and integrating over the appropriate ranges yields the following simultaneous equations that can be solved for the critical frequency ν:

$$a_0(1 + \alpha) + a_3(4.1429 + 11\alpha) = 0 , \quad (6)$$

$$0.4063a_3 - \frac{\psi l^4}{300}[a_0(4.1429 + 11\alpha) + a_3(28.8504 + 121\alpha)] = 0 . \quad (7)$$

These equations can be solved quite easily by hand. However, they have also been included in a computer program to simplify multiple computations for optimum design.

A vibration test stand in which the rotor is excited by a loudspeaker is used to make a final check on the frequency computations. The rotor can be mounted either as a free-free beam in the test stand, or it can be mounted in its suspension system.

C. PHYSICAL PROPERTIES OF MATERIALS

H. P. Barringer

1. Design Calculations

The equations[1] for rotor wall thickness and optimum stress conditions for a completely filled centrifuge rotor can be written as

$$t = a\left\{\left[1 + \left(\frac{4\rho}{(3+\mu)\delta}\right)^{1/2}\right]^{1/2} - 1\right\} = ak_1 , \quad (1)$$

and the working stress,

$$\sigma = \frac{V_p^2}{g}\{\delta + \rho + [(3+\mu)\delta\rho]^{1/2}\} = V_p^2 k_2 , \quad (2)$$

where t is the optimum wall thickness (in.); a, inside rotor radius (in.); ρ, fluid density (lb/in.^{3}); δ, rotor material density (lb/in.^{3}); μ, Poisson's ratio (dimensionless); k_1, constant (dimensionless); σ, optimum tangential working stress (lb/in.^{2}); V_p, inside peripheral speed (in./sec); g, gravitational constant (in./sec^2); and k_2, constant (lb-sec^2/in.^{4}). Furthermore, the maximum centrifugal field that can be produced is

$$g_{max} = \frac{a\omega^2}{g} = \frac{V_p \omega}{g} , \quad (3)$$

where g_{max} is the centrifugal field (times gravity) and ω is the angular velocity (radians/sec). The

maximum inside length of a centrifuge is given by

$$L = \left\{ \frac{a_n}{\omega} \left[\frac{EI}{\mu_1} \right]^{1/2} \right\}^{1/2} = k_3 a , \qquad (4)$$

where L is the inside length of centrifuge (in.); a_n, constant to correct for constrains and end conditions (dimensionless); E, modulus of elasticity (lb/in.^{2}); I, moment of inertia (in.^{4}); μ_1, mass per unit length of beam (lb-sec^2/in.^{2}); and k_3, constant (dimensionless).

The volume of the centrifuge is usually of concern and can be expressed as

$$V = \pi a^2 L k_4 , \qquad (5)$$

where V is the volume (in.^{3}) and k_4 is a constant to compensate for the addition of septa, etc., to the rotor interior (dimensionless). Finally, the ratio of mass moments of inertia are to be considered to avoid an unstable configuration

$$\frac{I_{\text{spin}}}{I_{\text{trans}}} \ngtr 1 , \qquad (6)$$

where I_{spin} is the polar moment of inertia (in.-lb-sec^2) and I_{trans} is the transverse moment of inertia.

From these equations several obvious conclusions can be drawn for a given fluid density:

1. The maximum inside peripheral speed is a function of the strength-to-density ratio (σ/δ).
2. The maximum centrifugal field is proportional to the maximum peripheral speed of the material. Therefore, for a given material, high angular speeds are required to produce high g's.
3. For a given material and working stress level, a fixed ratio of L/a can be obtained. Long-length rotors that operate below their first flexural critical speeds can be lengthened primarily by reducing the rotor operating speed or changing the constant a_n.
4. The maximum volume of a rotor is proportional to the a^3 when Eq. (4) is used with Eq. (5).

2. Design Data

The selection of a centrifuge rotor material is usually based on the following conditions: (1) strength-to-density ratio, (2) ease of fabrication, (3) cost and availability, (4) corrosion resistance, and (5) operating temperature. Typical materials for use in rotor construction are shown in Table IV-C-1.

From the information in Table IV-C-1 a number of materials have been considered (see Table IV-C-2), and the data have been used to construct rotor design curves for various stress levels, assuming dense CsCl solutions are used, as shown in subsequent figures.

The data in Table IV-C-3 are given where N is the angular speed of the centrifuge rotor in rpm, and where a circumferential wrap is used for the Fiberglas-epoxy and steel wire–epoxy rotors. With such wraps, a metal liner is used to carry the axial hydraulic load.

Using the working stresses shown in Table IV-C-2 and the stress relations given in Table IV-C-3, another comparison (Table IV-C-4) can be made to show the maximum inside peripheral speed of the rotor. The table also points out the penalty for centrifuging heavy liquids.

The data in Table IV-C-2 have been plotted as design graphs in Fig. IV-C-1, using CsCl to determine the proper design of a liquid centrifuge.

3. Filament-Wound Vessels

From the data in the preceding section it is evident that higher peripheral speeds and resulting higher g-fields can be produced by using circumferential wraps of Fiberglas or steel wire over a liner. This technique has been used by aerospace firms for rocket motor cases,[2] and represents the simplest fabrication method. Two slightly different methods have been used to form rocket motor cases without the use of metal liners. These are (1) the balanced method which uses sets of longitudinal and circumferential wraps, such as those on the Polaris missile case[3] and (2) the method of winding the cases on a helix angle where the path of the glass or wire filament is that of a geodesic. Techniques for winding vessels with openings on either end of the cylinder, such as would be required with centrifuges, have also been developed for aerospace applications.

---

[2] C. N. Odell and W. E. Albert, *Aerospace Eng.* **21**, 33 (1962).

[3] F. J. Darms, *Optimum Filament-Wound Construction for Cylindrical Pressure Vessels*, ASTIA Rept. AD 292010, p 12 (April 1962).

Table IV-C-1. Typical Mechanical Properties of Various Materials

Material	Yield or Ultimate Strength, σ (psi)	Material Density, δ (lb/in.^{3})	Strength-to-Density Ratio, σ/δ (in.)	Trade Name
	$\times 10^3$		$\times 10^6$	
Acetate	138	0.0543	2.54	Fortisan 36
Aluminum	78	0.101	0.773	7178-T6
Beryllium	144	0.036	4.0	Beryllium wire
Glass	250	0.075	3.34	S-994 HTS
Magnesium	32	0.060	0.534	AZ31B-H24
Plastic	40	0.051	0.784	Mylar T film
Steel	300	0.289	1.04	Maraging steel
Steel	650	0.283	2.30	Rocket motor case wire
Titanium	220	0.175	1.26	13V-11Cr-2Al

Table IV-C-2. Typical Mechanical Properties of Materials for Liquid Centrifuges

Material	Ultimate Strength (psi)	(0.2%) Yield Strength (psi)	Elongation (%)	Working Stress (psi)	Rotor Material Density (lb/in.^{3})	Strength-to-Density Ratio[a]
	$\times 10^3$	$\times 10^3$		$\times 10^3$		$\times 10^6$
7075-T6 Aluminum	76	67	11	50	0.101	0.495
Beta-titanium	190	170	4	150	0.175	0.857
Maraging steel	286	280	11	250	210,000	0.865

[a]Based on working stress.

Table IV-C-3. Optimum Working Stresses and Wall Thicknesses for Liquid Centrifuge Rotors

Rotor Fluid	7075-T6 Aluminum		Beta-Titanium		Fiberglas Epoxy		Maraging Steel		Steel Wire Epoxy	
	σ	t	σ	t	σ	t	σ	t	σ	t
	$\times 10^{-6} N^2 a^2$		$\times 10^{-6} N^2 a^2$		$\times 10^{-6} N^2 a^2$		$\times 10^{-6} N^2 a^2$		$\times 10^{-6} N^2 a^2$	
CsCl[a]	0.865	$0.36a$	12	$0.285a$	7.32	$0.41a$	16.8	$0.23a$	14.7	$0.25a$
66% Sucrose[b]	7.83	$0.33a$	11.1	$0.255a$	6.6	$0.372a$	15.7	$0.21a$	13.6	$0.22a$
Water[c]	7.05	$0.29a$	10.1	$0.225a$	5.88	$0.33a$	14.6	$0.18a$	12.5	$0.20a$
Empty[d]	2.88	0	4.98	0	2.13	0	8.24	0	6.74	0

[a] $\rho = 0.06$ lb/in.^{3}.
[b] $\rho = 0.0476$ lb/in.^{3}.
[c] $\rho = 0.036$ lb/in.^{3}.
[d] $\rho = 0$.

Table IV-C-4. Maximum Inside Peripheral Velocity for Liquid Centrifuges[a]

Material	Rotor Fluid				Working Stress (psi)
	CsCl	Sucrose	Water	Empty	
					$\times 10^3$
7075-T6 Aluminum	(202)	(211)	(222)	(348)	
	7,950	8,360	8,820	13,800	50
Beta-titanium	(295)	(308)	(322)	(458)	
	11,700	12,200	12,800	18,200	150
Maraging steel	(322)	(333)	(356)	(458)	
	12,800	13,200	13,700	18,200	250

[a] Values in parentheses in m/sec, others in in./sec.

UNCLASSIFIED
ORNL-DWG 63-4239

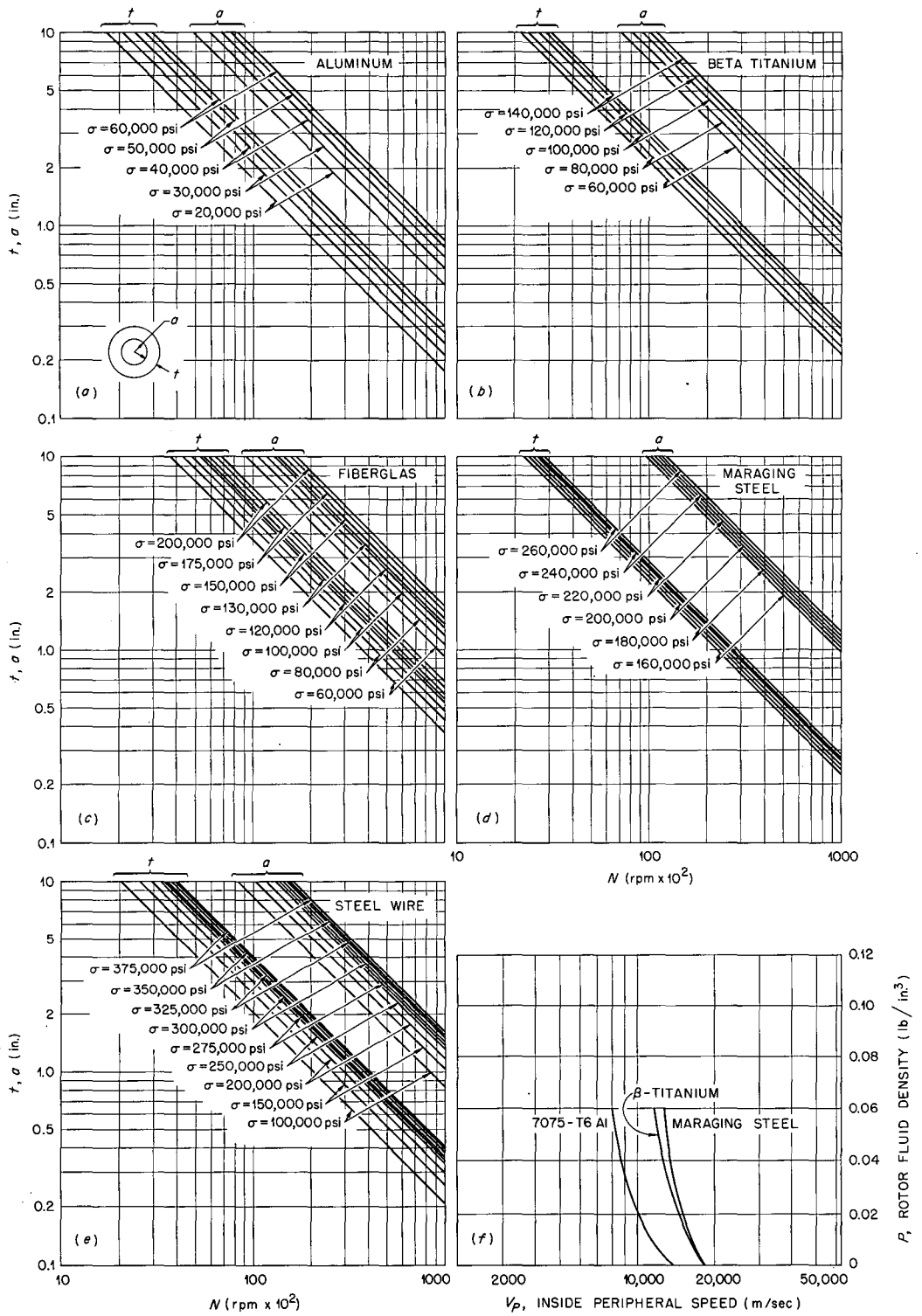

Fig. IV-C-1. Design Graphs for Liquid-Filled Centrifuges. (*a*–*e*) Optimum wall thickness of rotor and inside radius as a function of rotor speed using various materials. Cesium chloride was used in all cases at 0.060 lb/in.^{3} in liquid-filled centrifuge. (*f*) Inside peripheral speed compared with fluid density for materials of rotor construction.

Material	Working Stress, σ	Wall Thickness, t
	$\times 10^{-6} N^2 a^2$	
Aluminum (0.101 lb/in.^{3})	8.65	$0.36a$
β-Titanium (13V-11Cr-3Al) (0.175 lb/in.^{3})	12	$0.285a$
Fiberglas (0.075 lb/in.^{3})	7.32	$0.41a$
Maraging steel (0.289 lb/in.^{3})	16.8	$0.23a$
Steel wire (0.237 lb/in.^{3})	14.7	$0.25a$

Figure IV-C-2*a* shows a portion of a rotating centrifuge filled with liquid and helically wrapped with high-strength filaments. Figure IV-C-2*b* shows an enlarged view of a filament, with unit width and depth in the direction of the wrap, along with the area of the other surfaces. The stress and force diagrams are shown in Fig. IV-C-2*c* and -2*d* from which the helix angle can be found.

The value $\sigma \sin^2 \phi$ represents the circumferential stress and $\sigma \cos^2 \phi$, the axial stress, thus

$$\sigma \sin^2 \phi = \sigma_\theta , \tag{7}$$

$$\sigma \cos^2 \phi = \sigma_A , \tag{8}$$

or

$$\frac{\sigma \sin^2 \phi}{\sigma \cos^2 \phi} = \frac{\sigma_\theta}{\sigma_A} . \tag{9}$$

Then

$$\phi = \tan^{-1} \sqrt{\frac{\sigma_\theta}{\sigma_A}} , \tag{10}$$

where σ_θ is Eq. (2); the axial stress is the hydraulic load acting on the end caps of the centrifuge,

$$\sigma_A = \frac{\pi \rho \omega^2 a^4 / 4g}{2\pi a t} = \frac{\rho \omega^2 a^3}{8gt} , \tag{11}$$

where the wall thickness t is given by Eq. (1).

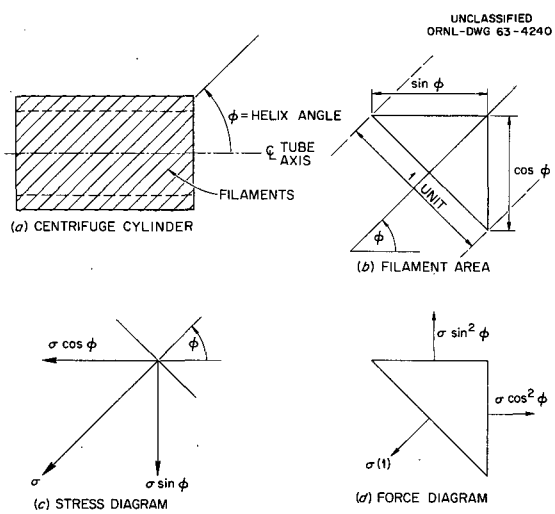

Fig. IV-C-2. Force and Stress Analysis for Helically Wrapped Rotors. (*a*) Portion of a rotating centrifuge filled with liquid and helically wrapped with high-strength filaments. (*b*) Enlarged view of filament, with unit width and depth in the direction of the wrap, together with the area of the other surfaces. (*c*) Stress diagram from which the helix angle can be found. (*d*) Force diagram.

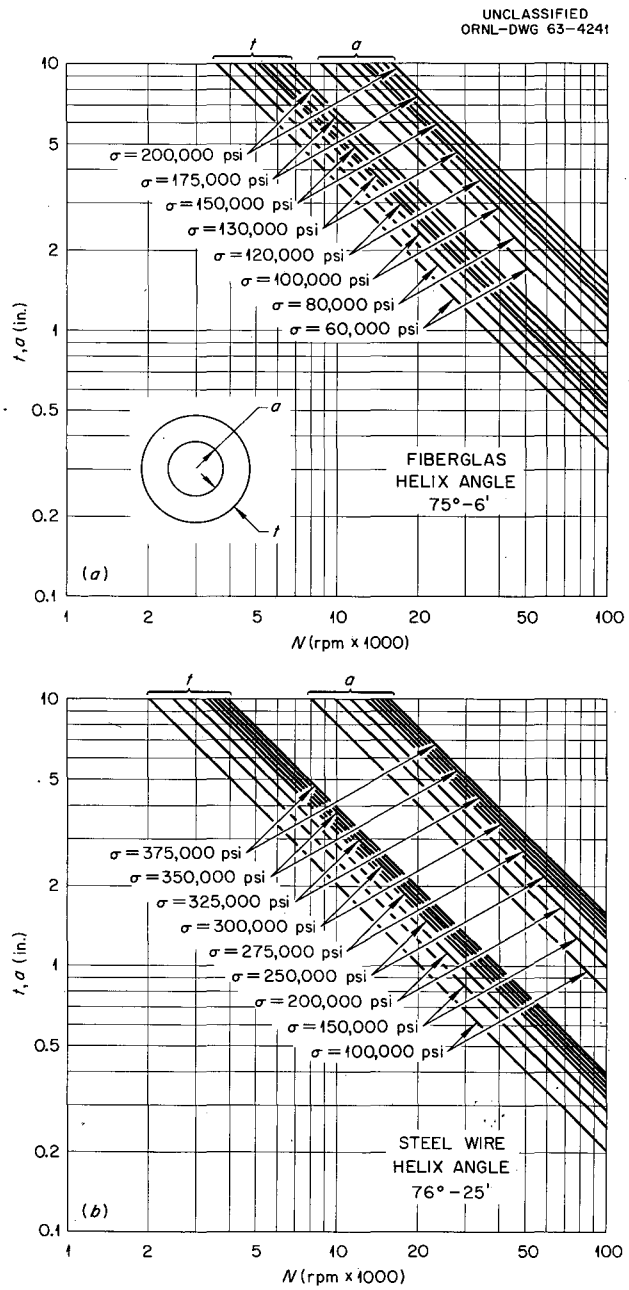

Fig. IV-C-3. Design Data for Fiberglas and Steel Wire Helically Wound Centrifuge Rotors. Cesium chloride (0.060 lb/in.^{3}) was used in liquid-filled centrifuges in both cases.

Material	Working Stress, σ	Wall Thickness, t
	$\times 10^{-6} N^2 a^2$	
Fiberglas (0.75 lb/in.^{3})	7.85	0.41*a*
Steel wire (0.273 lb/in.^{3})	15.6	0.25*a*

Table IV-C-5. Optimum Working Stresses, Wall Thicknesses, and Helix Angles for Helically Wound Liquid Centrifuge Rotors

Rotor Fluid	Helical Wrap Fiberglas				Helical Wrap Steel Wire			
	σ	t	σ/σ_A	ϕ	σ	t	σ/σ_A	ϕ
	$\times 10^{-6} N^2 a^2$				$\times 10^{-6} N^2 a^2$			
CsCl	7.85	0.41a	14.1	75°-6'	15.6	0.25a	17.1	76°-25'
Sucrose	7.06	0.372a	14.5	75°-17'	14.4	0.22a	17.7	76°-38'
Water	6.27	0.33a	15.1	75°-35'	13.2	0.20a	19.6	77°-19'
Empty	2.13	0	∞	90°	6.74	0	∞	90°

When Eqs. (1), (2), and (11) are substituted into Eq. (10), the helix angle becomes

$$\phi = \tan^{-1} \sqrt{\frac{8}{\rho}\left[\sqrt{1 + \sqrt{\frac{4\rho}{(3+\mu)\gamma}}} - 1\right]\left[\gamma + \rho + \sqrt{(3+\mu)\gamma\rho}\right]} \,. \qquad (12)$$

The filament working stress for helically wound rotors can be no higher than for cylindrical wrap; therefore, the circumferential working stress must be reduced by the relation of Eq. (7).

The data from Table IV-C-5 have been assembled in the form of design graphs, using CsCl, for finding the proper design of a liquid centrifuge, as shown in Fig. IV-C-3.

D. METALLURGICAL STUDIES

K. T. Ziehlke W. S. Dritt H. P. Barringer

Several problems prompted extensive metallurgical investigations on the C-II and C-III rotors.

The C-III biological centrifuge failed at 5:10 AM on May 7, 1963, at 81,000 rpm, after 40 hr of operation with DNA and CsCl. At the time the failure occurred, the 7075 aluminum-alloy rotor was at a calculated stress of 52,300 psi. Severe fragmentation occurred.

To simplify the diagnosis and to determine where the failure initiated, the major fragments were first reassembled for study. The reconstruction is shown in Fig. IV-D-1 and includes the bowl, end plugs, and motor plate. Areas of interest were sectioned for microstructural study. To aid in diagnosis, hardness and impact tests and heat treatment studies were made on pieces of the bar stock from which the rotor had been machined.

The outstanding characteristic of the fracture surfaces is their fibrous character, seen in greater detail in Fig. IV-D-2. The failure appears to have originated at a design notch, the corner just outside of the O-ring groove (Fig. IV-D-3) at the end of the rotor.

A high density of massive, second-phase stringers that were oriented with the bowl axis was noted in examination of the microstructure of the bowl fragments (Fig. IV-D-4*a*), and of the forged 7075-T6 bar stock from which the bowl was machined. These stringers are weak and will serve as paths along which cracks, once initiated, will readily propagate (Fig. IV-D-4*b*).

The nominal operating stress on the material was about 52,000 psi. Hardness test results of 139 Brinell hardness number (BHN) indicated a marginally low-heat treatment accomplishment, but one which should have resulted in a yield strength of about 65,000 psi. Since the fracture surfaces showed a strong orientation in the direction of the microstructural stringers, impact tests were run to evaluate directional weakness. The results of these tests showed the stock to be very weak

transversely. The impact test specimens failed by cleavage, a brittle fracture mechanism, and revealed a pattern (Fig. IV-D-5) similar to that seen in the rotor that failed.

The microstructural stringers are a residue of the cast ingot structure. They are broken up and given their directional orientation during the forging operation and would be largely taken into solution in an adequate heat-treatment cycle. Samples of the forged bar stock were reheat-treated in a cycle determined to give maximum mechanical properties which included solution heat treatment

UNCLASSIFIED
PHOTO 62563

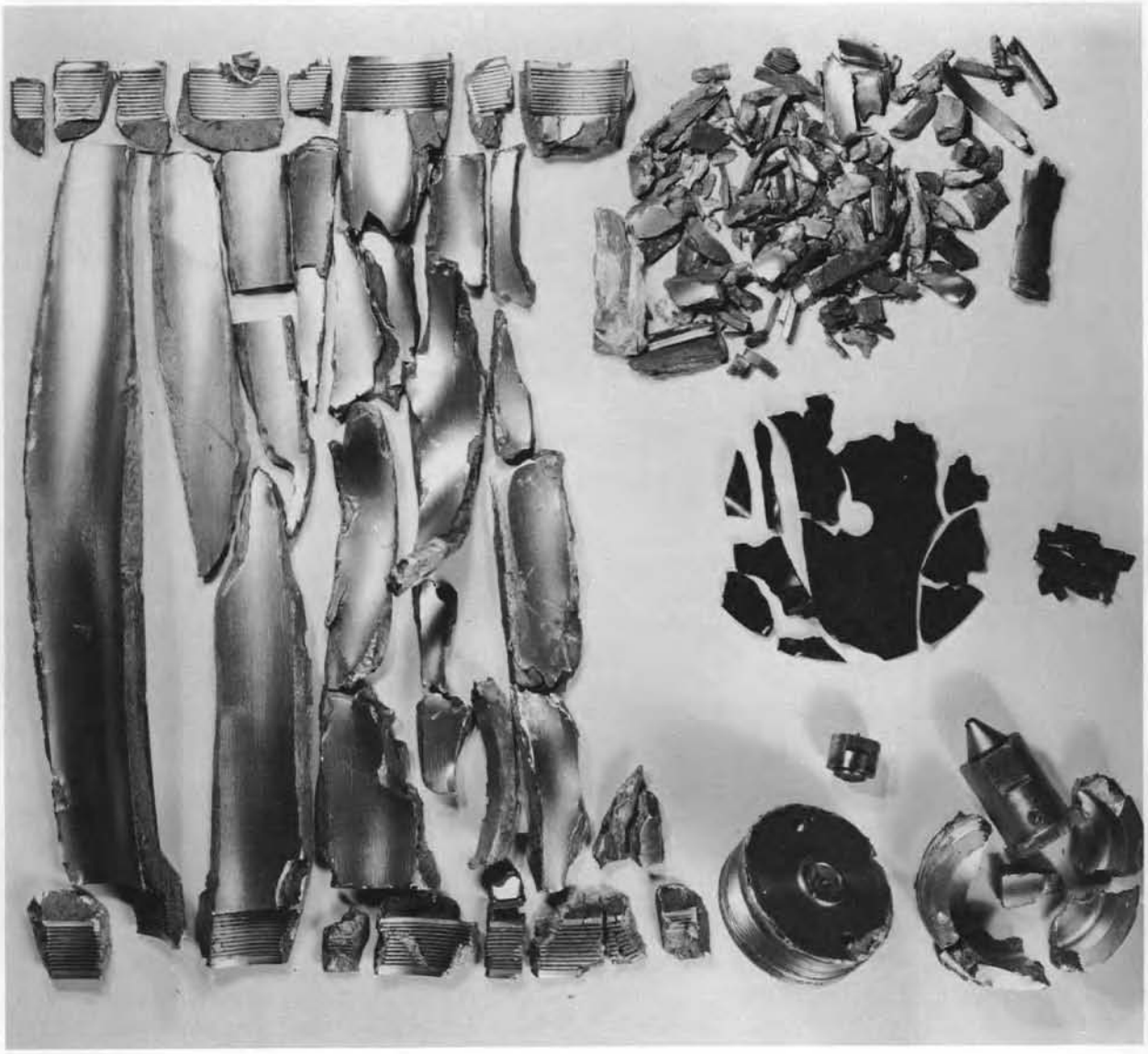

Fig. IV-D-1. Reconstruction of C-III Rotor. The rotor was approximately 11 in. long.

UNCLASSIFIED
PHOTO 62583

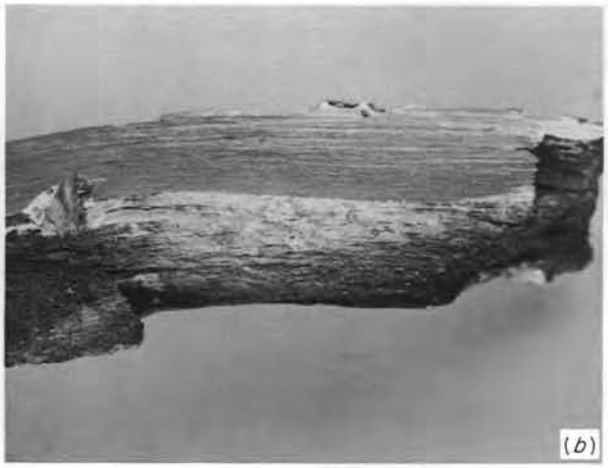

Fig. IV-D-2. Outstanding Characteristic of the Fracture Surface. (*a*) Cleavage and tensile fractures at opposite ends of rotor. 2X. (*b*) Radial cleavage fracture at rotor midsection. $3\frac{1}{2}$X. Reduced 29%.

UNCLASSIFIED
PHOTO 62584

Fig. IV-D-3. Crack in Area of Stress Concentration. 5X.

for 30 min at 870°F, 1 hr at 890°F, water quenched, and aged for 26 hr at 250°F. The resulting microstructure is shown in Fig. IV-D-6. In addition to the reduction in the number and size of the β-phase stringers, the material hardness was increased from 139 to 155 BHN, and the transverse impact strength was more than doubled, to a level only 18% below the impact strength longitudinally.

It is concluded that the failure initiated at one end of the rotor in the relatively sharp corner formed at the end of the threaded section against the plane surface that forms the seat for the end plug. The fractures at this end, and the longitudinal fragmentation in the body of the bowl, were cleavage fractures, following a fairly dense pattern of longitudinal stringers of the β(Zn) phase in the microstructure. At the other end, the fractures were predominantly tensile. The failure resulted, therefore, from the combination of stress concentrations at a sharp corner and the low transverse strength of the material due to the presence of the second-phase stringers. These stringers would have been largely eliminated by an adequate solution heat treatment. Reheat-treated samples showed a decrease in the stringers in the microstructure, accompanied by an increase in hardness and a doubling of the transverse impact strength. In the future, samples of rotor material stocks will be subjected to metallurgical examination before the rotors are fabricated.

UNCLASSIFIED
PHOTO 62585

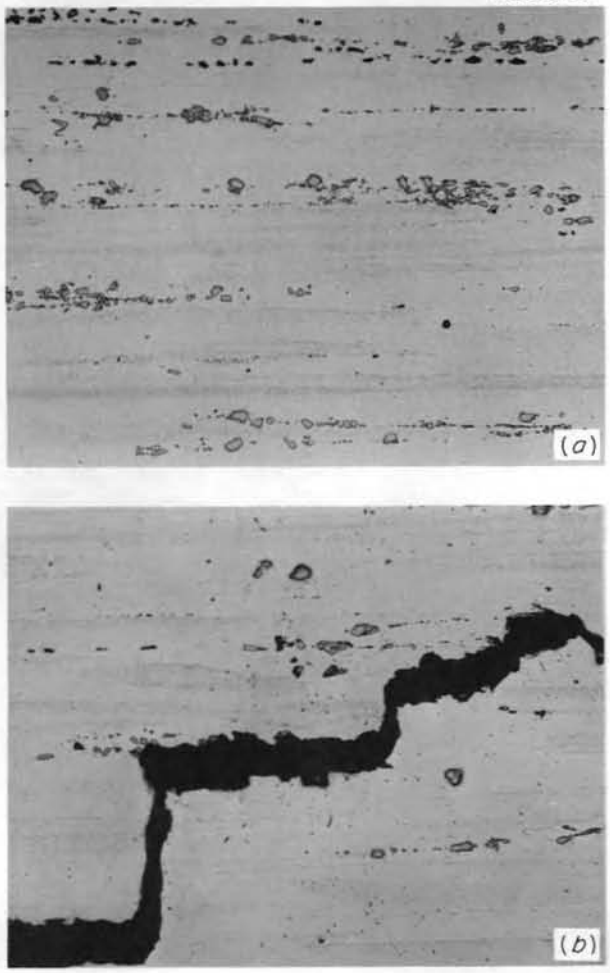

Fig. IV-D-4. Microstructure of the Bowl Fragments. (*a*) Microstructure of 7075 alloy rotor. The black stringers contain most of the iron and silicon impurities in the alloy. The gray massive particles in parallel-line arrays are the proeutectic β(Zn) phase, resulting from nonequilibrium solidification of the primary ingot and not taken into solution during subsequent solution heat treatment. Etchant, 0.5% HF. 250X. (*b*) Crack propagating along β-phase stringers. Most of the threaded section at this end of the rotor separated in this way. The rotor axis was parallel to the stringers. Etchant, 0.5% HF. 250X. Reduced 29%.

UNCLASSIFIED
PHOTO 62586

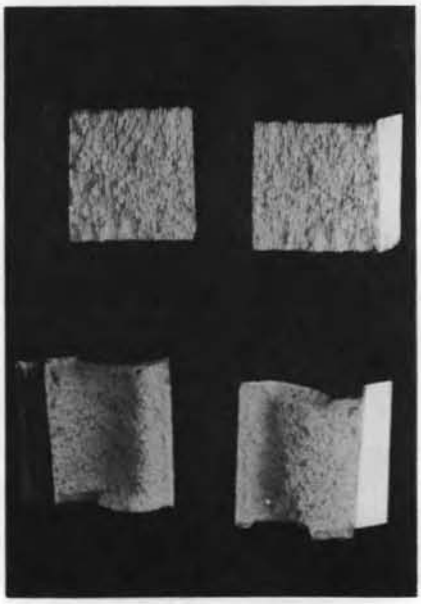

Fig. IV-D-5. Impact Fractures in 7075 Alloy Forged Bar Stock. Note the similarity in texture of the transverse fracture surface (top) and the cleavage fractures in the rotor shown in Fig. IV-D-2. Charpy V-notch samples had an average transverse impact strength of 3.0 ft-lb and an average longitudinal strength of 7.7 ft-lb. 2X. Reduced 9%.

UNCLASSIFIED
PHOTO 62587

Fig. IV-D-6. Microstructure of Reheat-Treated Bar Stock. Compare the number and volume of the β-phase stringers with those in the original structure shown in Fig. IV-D-4a. The transverse impact strength of this material has been raised from 3.0 to 6.3 ft-lb. Hardness is 155 BHN compared to the as-received hardness of 139 BHN. Etchant 0.5% HF. 250X.

E. CORROSION STUDIES

W. S. Dritt K. T. Ziehlke

The failure of one C-III rotor and the discovery of apparent cracks in another rotor and in two end plugs raised the possibility of corrosion in the 7075 aluminum alloy used in their machining. Both anodized and nonanodized rotors have been tested when filled with CsCl solution. These surface conditions were duplicated in tests run on 7075 alloy sheet stock. Samples were loaded to the nominal operating stress level of 52,000 psi. The strain gages were then removed and the samples submerged in an agitated, saturated solution of CsCl at room temperature. The loaded, bend-test fixtures used in the CsCl exposures are shown in Figs. IV-E-1 and IV-E-2. Since samples loaded in this type of fixture expose a relatively large area of constant stress to the corroding medium, the interpretation of the test results is simplified. Samples were exposed in the as-received condition and after an anodizing treatment similar to

UNCLASSIFIED
PHOTO 62588

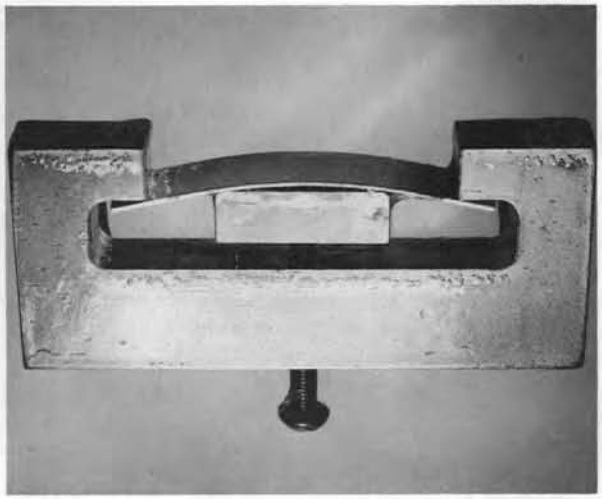

Fig. IV-E-1. Nonanodized 7075-T6 Aluminum After 20 hr in Saturated CsCl. The polyvinyl chloride point used to electrically insulate the test strip from the dissimilar metal holder can be seen at the ends of the sample. 1X. Reduced 22½%.

UNCLASSIFIED
PHOTO 62589

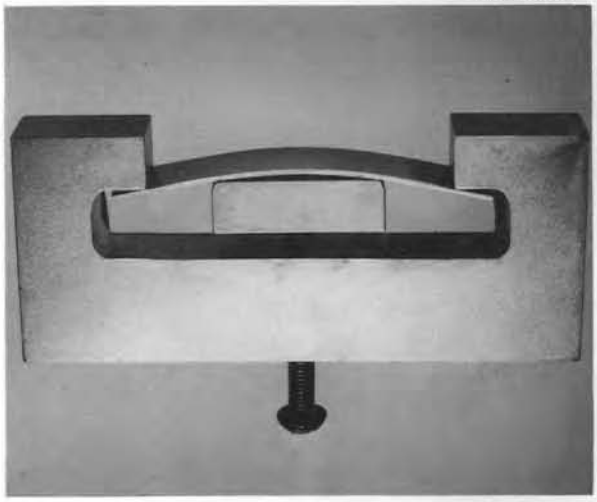

Fig. IV-E-2. Anodized 7075-T6 Aluminum After 110 hr in Saturated CsCl.

that given to the rotors and end plugs. Specimens were taken from the starting sheet both longitudinally and transversely. They were examined after 20 hr and after the test was terminated at 110 hr. A nonanodized bend sample removed from test after 20 hr is shown in Fig. IV-E-1. There is no evidence of reaction except for a slight darkening of the initially bright surface. Figure IV-E-2 shows an anodized sample after 110 hr of exposure. This sample shows no evidence of corrosive attack by CsCl. The darkening of the unprotected aluminum that occurred in the sample of Fig. IV-E-1 is not related to the condition of stress. The same degree of darkening was also observed in an unstressed sample shown in Fig. IV-E-3 when compared with the unprotected sheet stock before immersion.

The 7075 aluminum alloy is sensitive to galvanic attack if coupled to an electrically dissimilar material in the CsCl electrolyte. The samples shown in Fig. IV-E-4 were not insulated from the nickel-plated steel bend fixtures. These samples were exposed for 20 hr. The directional pattern of rolling is apparent in the corrosion product on the nonanodized samples, the first and third bars being longitudinal samples, and the second and fourth being transverse. This pattern results from differences in corrosion rate from point to point because of differences in electrode potential between the two principal phases in the alloy. The anodized samples, in contrast, show no attack except where the film cracked as a result of the applied load. We noted that the film is apparently most susceptible to cracking when the bend axis parallels the sheet rolling direction (transverse samples). The β-phase stringers are oriented toward the bend axis in the transverse specimens, and therefore tend to induce discontinuities in the anodized film.

UNCLASSIFIED
PHOTO 62591

Fig. IV-E-4. Galvanic Attack on Samples Coupled to Electroless Nickel-Plated Steel. The two samples on the left were in the "as-received" condition. The two on the right were anodized before exposure to the saturated CsCl. 1X. Reduced 28½%.

UNCLASSIFIED
PHOTO 62590

Fig. IV-E-3. Discoloration of Unstressed Sample After 20 hr in Saturated CsCl. Left, "as-received"; right, after exposure. 1X. Reduced 28½%.

No failures were experienced in any of the bend samples and no evidence of susceptibility to stress corrosion could be found in metallographic examination of exposed samples. It is concluded that the 7075-T6 aluminum is not sensitive at the design stress to stress corrosion in saturated CsCl. A general attack of a shallow-pitting nature was observed on some of the nonanodized samples, which was probably galvanic in origin, since the samples were not electrically isolated from the nickel-plated steel bend fixtures. Electrically insulated samples did not pit and showed only a slight discoloration.

F. DYE-PENETRATION STUDIES

W. S. Dritt K. T. Ziehlke H. P. Barringer

Two liquid centrifuge (C-II) rotors and two sets of end plugs were examined to determine the cause of leaks in service. The first rotor examined had been in service for approximately 50 hr at speeds up to 90,000 rpm. It was then anodized and returned to service for a period of 400 hr at speeds as high as 141,000 rpm, at a nominal stress of 52,000 psi. A dye penetrant was used to detect cracks, which might serve as leak paths, in this rotor. The rotor and two of the end plugs were then examined destructively. A second C-II rotor and the other two end plugs were also examined by the dye-penetrant method. They did not contain cracks and were returned to service.

Figure IV-F-1*a* shows an end of the first rotor and a crack on the inside surface parallel to the rotational axis and extending to the sealing lip. Figure IV-F-1*b* shows a crack on the opposite end of the rotor approximately 120° from the first crack. A section through this crack is shown in Fig. IV-F-1c. The crack contains anodized film on the

UNCLASSIFIED
PHOTO 62592

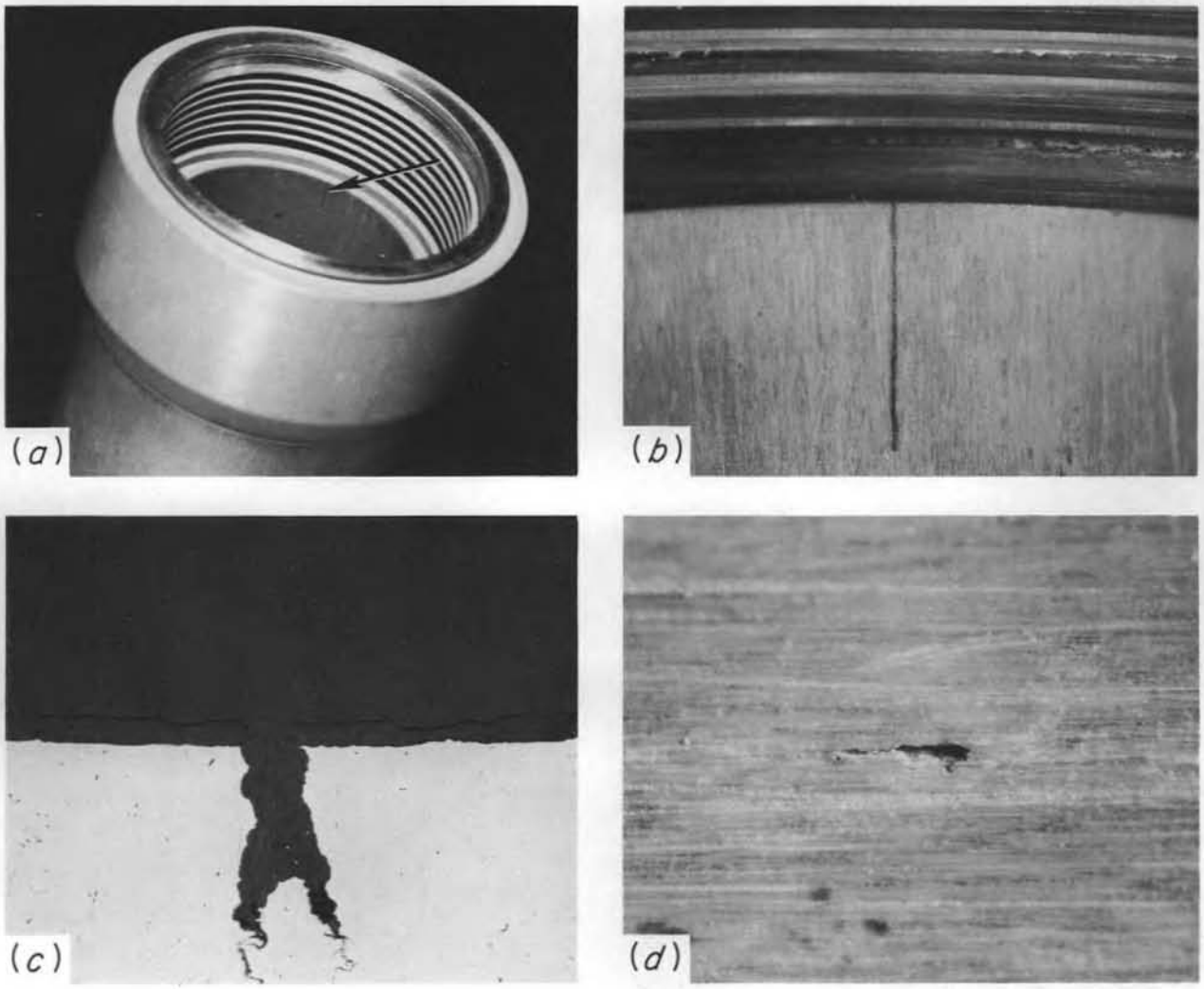

Fig. IV-F-1. Cracks in Rotor. (*a*) Crack on one end of rotor. 1½X. (*b*) Crack on opposite end of rotor. 5X. (*c*) Section through crack in rotor showing anodized film in crack. 100X. (*d*) Crack in rotor away from ends. 25X. Reduced 22%.

interior surfaces of the crack, indicating that the crack was present before the rotor was anodized. A crack in the inside surface of the rotor is shown in Fig. IV-F-1*d*. A section through a top end plug (Fig. IV-F-2) shows a second-phase stringer which resulted in a discontinuity on the oxide film on the anodized surface.

The cracks in the rotor were formed before the rotor was anodized. The aluminum-alloy material (7075-T6) from which the rotor and the end plugs were made contained striations similar to those found in the structure of the material used for the C-III rotor which failed (see preceding sections). These second-phase stringers, which were present in quantities indicative of incomplete solution heat treatment, served as foci for the initiation of cracks.

UNCLASSIFIED
PHOTO 62593

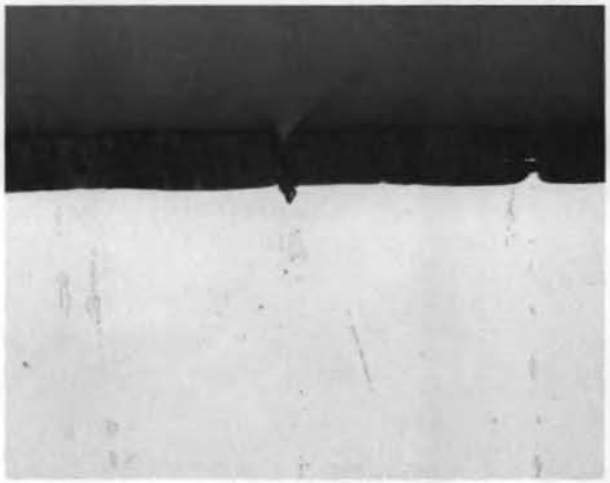

Fig. IV-F-2. Section Through Top End Cap Showing Discontinuity in Oxide Film at Location of Surface.

V. Low-Speed Zonal Rotors

H. P. Barringer

A. ROTOR A-VIII

Rotor A-VIII is a conversion of the B-III rotor for use on the International Equipment Company model PR-2 centrifuge drive system. The A-VIII does not represent an extremely stable rotor due to its configuration, but satisfactory mechanical operation has been obtained by attaching a conversion section to the drive shaft of the International PR-2. A locating system is used to attach the rotor to the conversion section. The centrifuge has been operated at its top design speed of 6000 rpm. The rotor runout is shown in Fig. V-A-1 with the four large peaks representing natural critical frequencies of the drive system. The rotor is shown in Fig. V-A-2. Data on the performance of this rotor will be presented in a subsequent report.

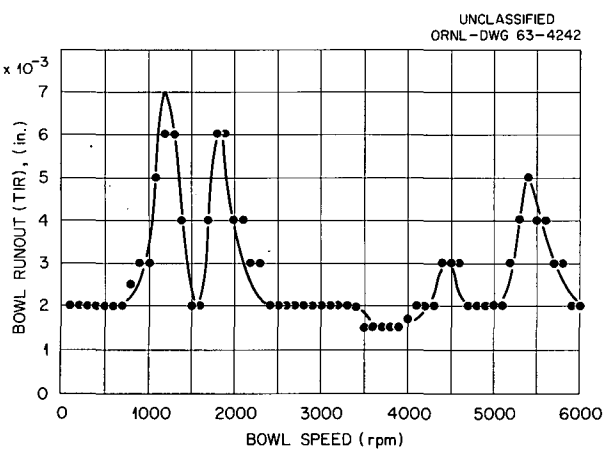

Fig. V-A-1. Runout of Rotor A-VIII When Driven by International PR-2 Centrifuge.

B. ROTOR A-IX

Rotor A-IX, shown in Fig. V-B-1, has been designed to replace rotor A-V. The new design permits higher speed and more stable operating characteristics. The centrifuge has thick transparent end caps to permit visual studies when used on the International Equipment Company model PR-2 centrifuge drive. The rotor volume of 1300 ml is divided into eight sector-shaped compartments. Each compartment is $^{9}/_{16}$ in. deep and has a maximum radius of 7 in. The central core is a single 45° cone with a maximum radius of 1.86 in. Flow lines to the rotor edge pass over the septa, thus leaving the entire sector-shaped compartment unobscured. The rotating seal is described in Chap. X.

It was necessary to disassemble the drive systems and regrind each taper to the manufacturer's specified values. When proper mating fits have been established between the male drive shaft and the female taper on the centrifuge, the A-IX is held in position by its weight – approximately 50 lb.

Numerous tests have been made spinning the rotor at approximately 4000 rpm both empty and when filled with water. The design speed of 6000 rpm has not been reached due to the limited power of the drive system. Rotor runout when empty and filled with water is shown in Fig. V-B-2. It should be noted that these rotors have not required balancing to run satisfactorily. The high runouts encountered at 400 and 900 rpm when the rotor is filled are natural critical frequencies of the centrifuge system. Tests with water have

Fig. V-A-2. Rotor A-VIII.

Fig. V-B-1. Rotor A-IX. 6000 rpm, 7150 × *g*, 1.3 liters.

shown that the centrifuge will make a satisfactory continuous-flow device for large particles as well as a rate-zonal centrifuge. Estimated flow rates of 1 liter/min appear feasible with low-viscosity materials.

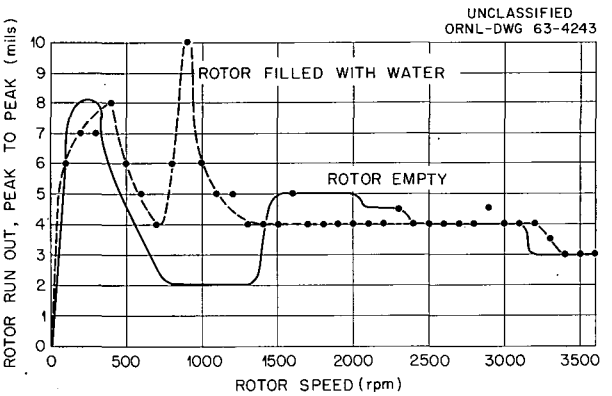

Fig. V-B-2. Runout of Rotor A-IX-b on International Model PR-2 Centrifuge Drive.

VI. Intermediate-Speed Zonal Rotors

A. ROTOR B-II SYSTEM

H. P. Barringer C. Nunley D. A. Waters

The B-II rotor was originally designed for operation at 40,000 rpm. In the original tests, low-speed instabilities were observed in the region around 5000 rpm which diminished when the number of septa was increased. With 36 septa, acceptable operation at speeds up to 25,000 rpm has been obtained. However, at higher speeds instabilities are encountered. Since the B-II system will probably be the first instrument developed under this program to come into general use, it has been considered of paramount importance to determine the nature of the instabilities previously encountered and to modify the system so that high-speed operation may be routinely obtained.

For definitive studies, proximity probes have been deployed in four positions to monitor vibrations occurring in the upper bearing, in the top and bottom plugs of the rotor, and in the transmission of the centrifuge drive. The outputs are simultaneously displayed on a four-channel oscilloscope or recorded on tape up to 180,000 cycles/min and photographs were taken of oscilloscope traces. The phase relation of the motions at various points may be observed along with the frequencies of vibrations (the oscilloscope has a time-calibrated sweep rate) and the amplitudes. As shown by the oscillograms in Fig. VI-A-1, the instabilities of the B-II rotor exhibit characteristic precessional instability. Efforts to eliminate this vibration involved three areas of the system: (1) drive quill and lower damper bearings, (2) transmission box mounting system, and (3) top centrifuge damper bearing. The first two were investigated in detail and found not to be the primary cause of the instabilities observed at the higher speeds.

The original design of the B-II top bearing was revised to incorporate more damping and lower spring rate between the bearing and the vacuum chamber. Immediate improvements in the instability were noted. The maximum amplitude of the instability was reduced from greater than 0.120-in. total indicator reading (TIR) to the maximum amplitude of 0.003 in. TIR, as shown by the oscillogram in Fig. VI-A-2. This amplitude produced no detectable noise, and at about 33,000 rpm the amplitude markedly diminished, permitting the rotor to be driven successfully to 40,000 rpm. The low-amplitude frequency (rotor runout) is smaller (see Figs. VI-A-1*b*, *c* and VI-A-2) due to the use of rotor B-II-b fabricated by Union Carbide Corporation, Nuclear Division. The actual value of the runout of the original B-II system during unstable operation at 30,000 rpm is not known since the probes positioned 0.060 in. from the rotor were completely destroyed.

An experimental damper bearing with built-in seal holder is shown in Fig. VI-A-3. This bearing eliminates the instability completely, with satisfactory operation to the design speed of 40,000 rpm. Approximately 50 test runs have been made using this bearing with no instability encountered.

Tests with and without the improved damper bearing show that the rotor can be operated without the 36 septa shown in Fig. VI-A-4 when the rotor is partially or completely filled with water, and that fluid perturbations are not responsible for the instability.

A new core with only four septa, which are centrally supported, has therefore been constructed. Preliminary tests with T2 phage show that this core gives the same resolution obtained with the original B-II core. The four-vaned core assembly is designated B-V.

UNCLASSIFIED
PHOTO 62565

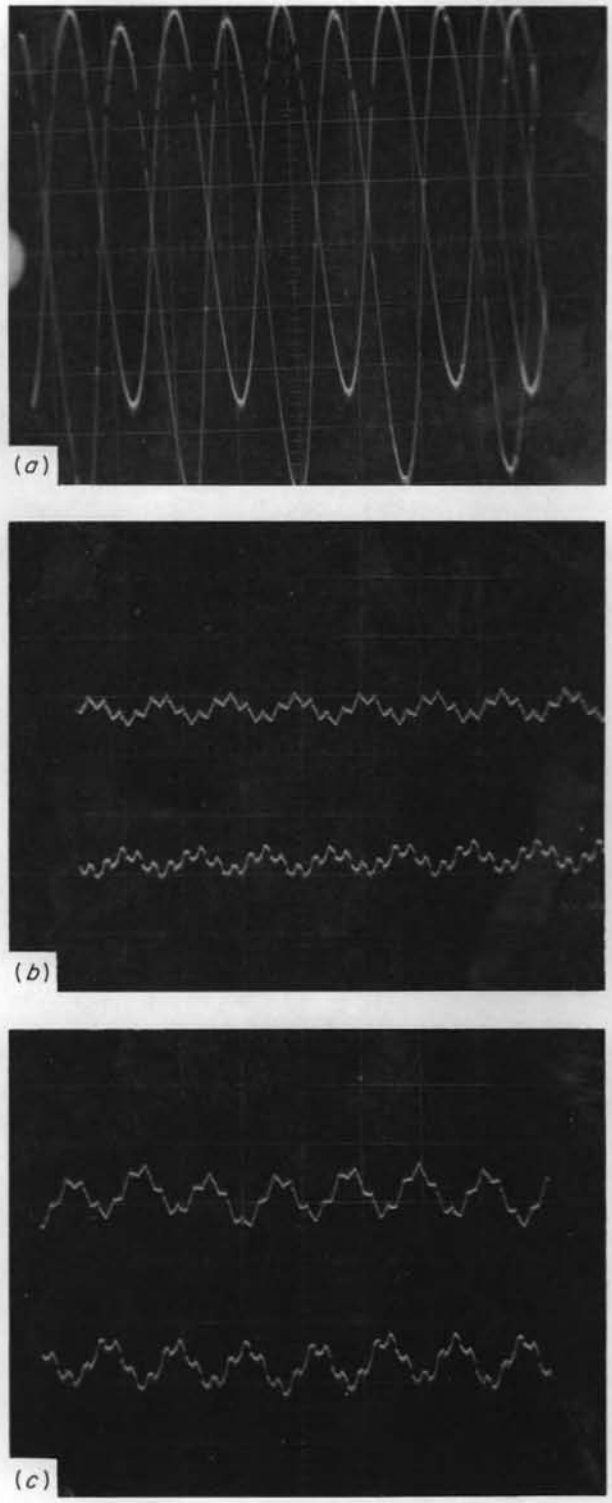

Fig. VI-A-1. Oscillograms of B-II Rotor Taken at Three Speeds. The upper traces are monitoring the top end cap, the lower trace the bottom end cap. (*a*) Taken at 28,000 rpm; vertical sensitivity 0.005 in./cm; horizontal sweep rate 0.005 sec/cm; high-amplitude frequency, 114 cps; low-amplitude frequency, not detectable but approximately 28,000 rpm. (*b*) Taken at 23,500 rpm; vertical sensitivity, 0.005 in./cm; horizontal sweep rate, 0.010 sec/cm; horizontal sweep rate, 0.010 sec/cm; high-amplitude frequency, 86.5 cps; low-amplitude frequency, approximately 23,500 rpm. (*c*) Taken at 23,000 rpm; vertical sensitivity 0.005 in./cm; horizontal sweep rate, 0.010 sec/cm; horizontal sweep rate, 0.010 sec/cm; high-amplitude frequency, 87 cps; low-amplitude frequency, approximately 23,000 rpm.

UNCLASSIFIED
PHOTO 62566

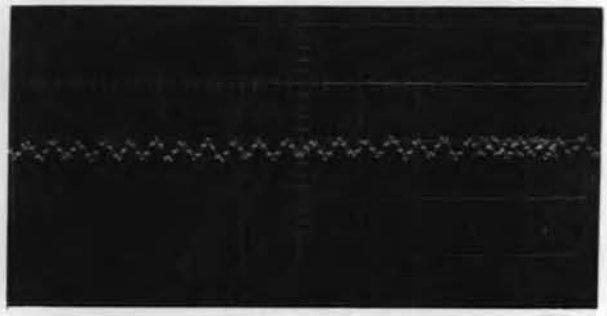

Fig. VI-A-2. Oscillogram of B-II Rotor Taken at About 30,000 rpm. Vertical sensitivity, 0.005 in./cm; horizontal sweep rate, 0.02 sec/cm. The trace is monitoring the bottom end cap. High-amplitude frequency is 111 cps; low-amplitude frequency, about 30,000 rpm.

UNCLASSIFIED
ORNL-DWG 63-4244

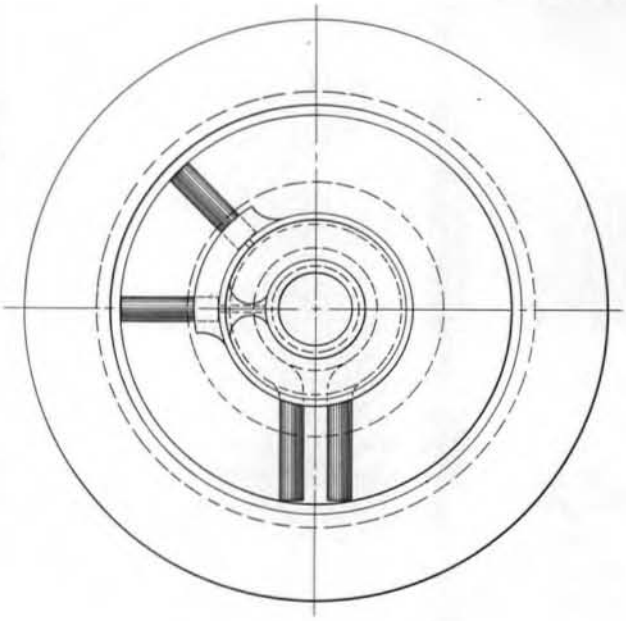

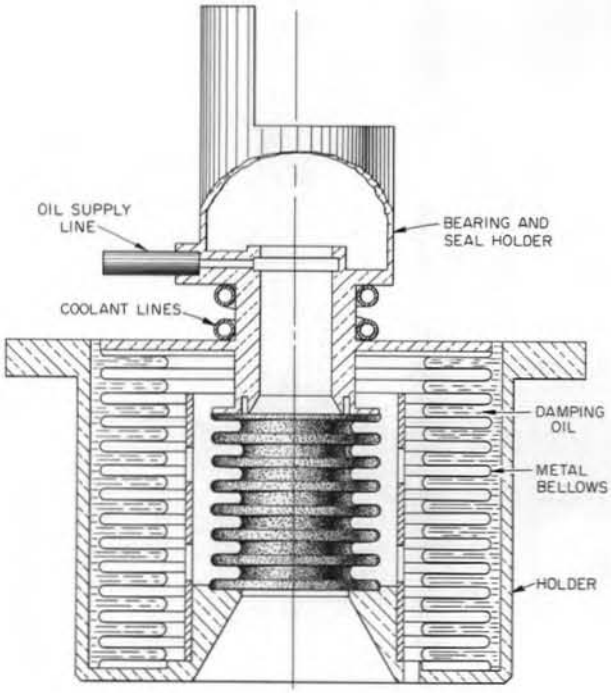

Fig. VI-A-3. Damper Bearing for Rotor B-II.

UNCLASSIFIED
PHOTO 62567

Fig. VI-A-4. Rotor B-II-b, End Caps Removed, Septa in Foreground.

VII. High-Speed Zonal Rotors

H. P. Barringer

A. GENERAL CONSIDERATIONS

To achieve high centrifugal fields in the speed range from 40,000 to 141,000 rpm a number of very difficult problems must be solved. If the B-II configuration is used as the prototype, then high-speed seals and drives in addition to new rotors would be required. For initial explorations, simple tubular centrifuges using the reorienting gradient principle previously described have been employed. These may be used for isopycnic separations with either preformed or centrifuge-produced gradients; or rate-zonal separations may be made using gradients and sample layers introduced into the rotor at rest. One-piece, quadri-sector cores are used to minimize laminar mixing during acceleration and deceleration. The simplicity of the basic design is a great advantage when hazardous materials are to be handled in either a glove box or a remotely controlled installation.

B. ROTOR C-II

Rotor C-II shown in Fig. VII-B-1 has run a total of 300 hr. Six centrifuges of this configuration have been constructed, and metallurgical studies have been done on components of two rotors.

The centrifuge system with the supporting equipment is shown in Fig. VII-B-2. The operation of this centrifuge was discussed in a previous report.[1]

[1]H. P. Barringer, *Joint NIH-AEC Zonal Centrifuge Program Semiann. Rept. Dec. 31, 1962*, ORNL-3415 (Special), p 51.

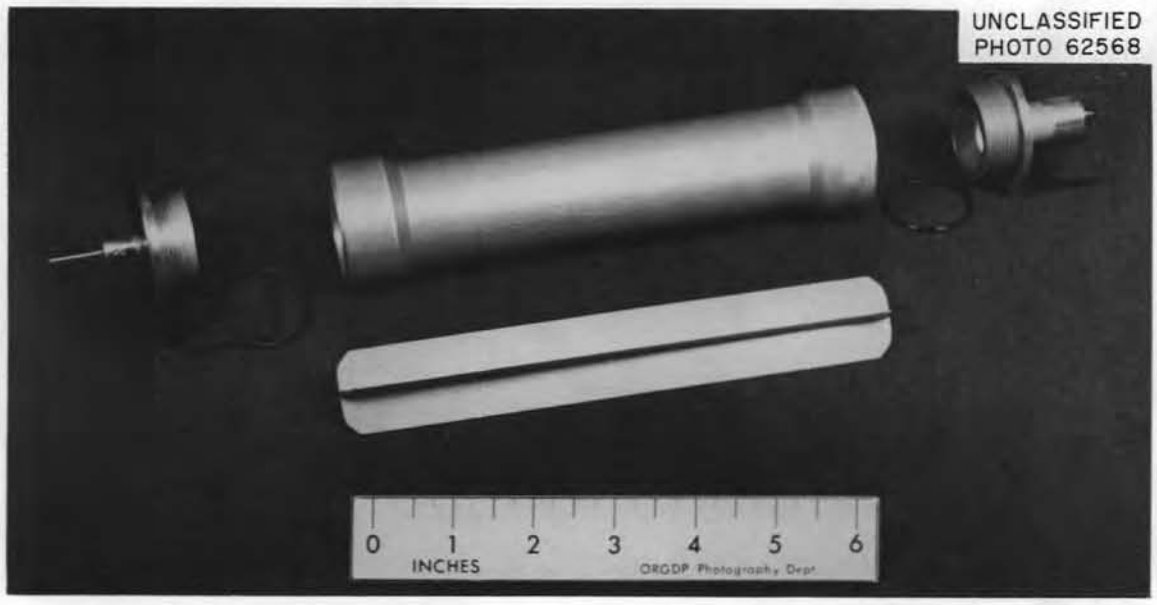

Fig. VII-B-1. C-II Zonal Ultracentrifuge. 141,000 rpm, 310,000 × *g*, 100 ml.

Fig. VII-B-2. Centrifuge System with Supporting Equipment.

C. ROTOR C-III

Rotor C-III has a design speed of 81,000 rpm (172,000 × g at R_{max}) when loaded with 500 ml of fluid with a density of 1.7. The rotor is a hollow, tubular, reorienting gradient-type zonal centrifuge, which is loaded and unloaded at rest. The density gradient may be formed with a suitable gradient engine and introduced together with the sample zone at rest for rate-zonal sedimentation studies, or the gradient may be formed by the centrifugal field as for isopycnic zonal centrifugation.

The rotor is shown with all rotating components in Fig. VII-C-1. The motor armature attached to the lower end cap can be seen at left. The core is shown in the foreground, and the bore of the centrifuge rotor is shown in the background. One part of the upper magnetic bearing can be seen at the extreme right. This magnet is press-fitted into the adjacent end cap. The centrifuge spins with its axis in the vertical plane, resting on the pivot bearing at the bottom, and using a magnetic bearing at the top end of the centrifuge; that is, at the top end there is no contact between rotating

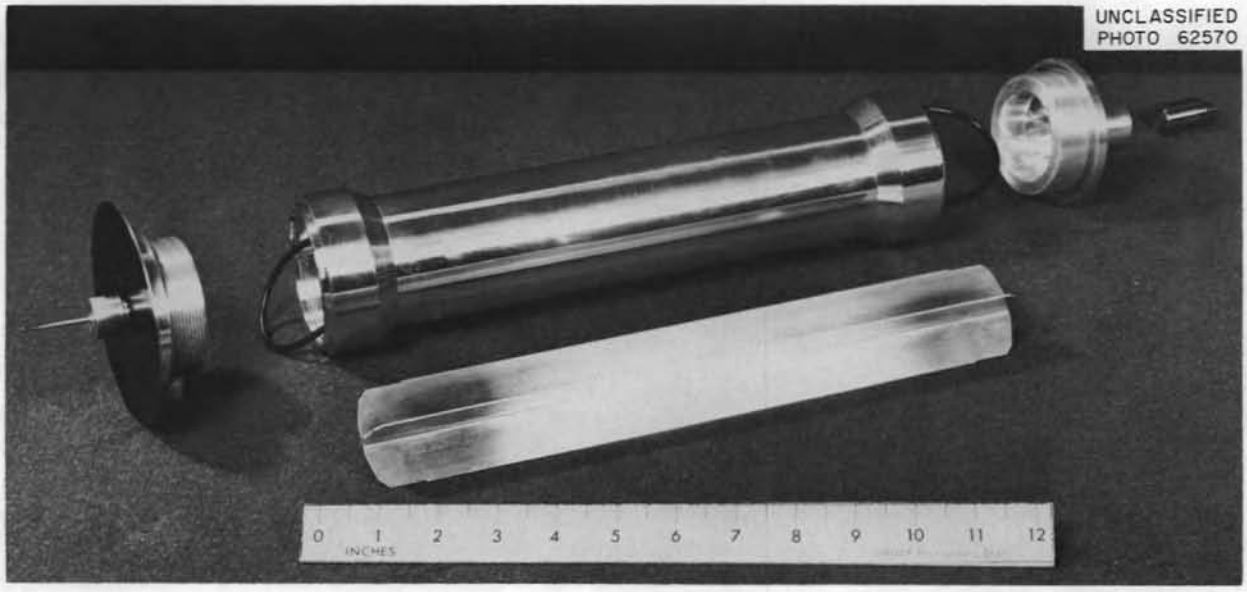

Fig. VII-C-1. C-III Zonal Ultracentrifuge. 81,000 rpm, 172,000 × g, 500 ml.

and nonrotating surfaces. The entire centrifuge is operated in a vacuum, and all parts of the centrifuge system, motor, bearings, etc. are inside the vacuum chamber.

The fragments of one C-III rotor which failed at 81,000 rpm are shown in Chap. IV. Minor damage was done to the vacuum chamber.

D. ROTOR C-IV

Figure VII-D-1 shows rotor C-IV, which operates at 66,000 rpm (143,000 × g at R_{max}) and has an internal volume of 1000 ml. This rotor is similar to those described above and has been operated successfully at full speed with CsCl.

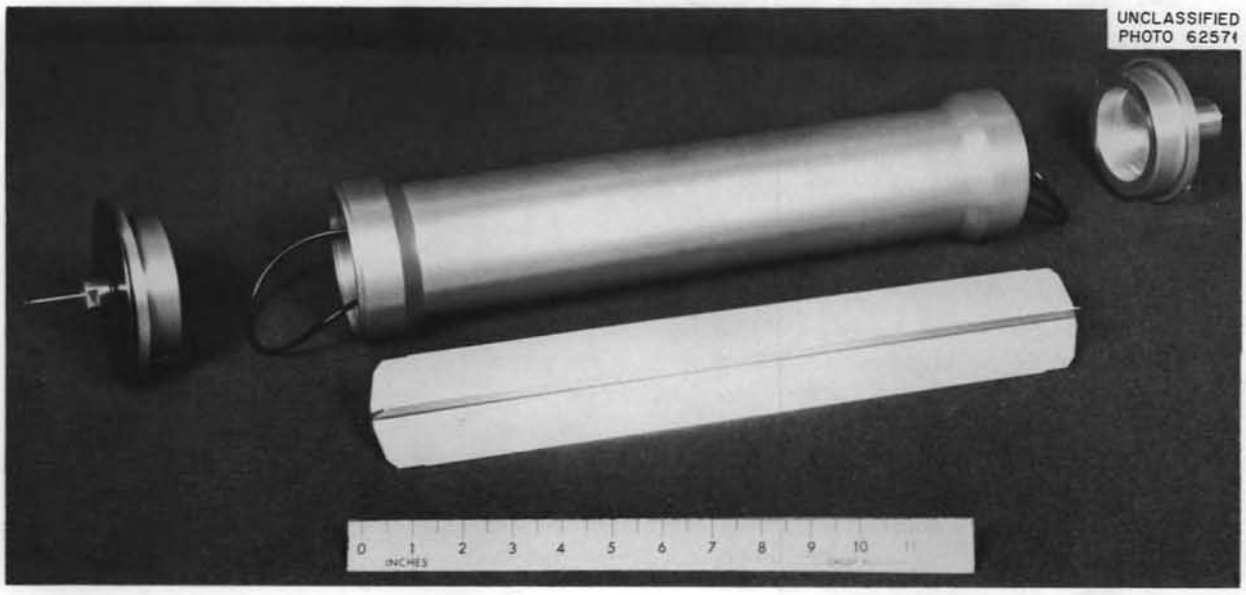

Fig. VII-D-1. C-IV Zonal Ultracentrifuge. 66,000 rpm, 143,000 × g, 1000 ml.

E. ROTOR C-V

Rotor C-V is similar to the B-II and C-series rotors. It has an internal volume of 5000 ml and operates at 40,000 rpm (91,000 × g at R_{max}). Figure VII-E-1 shows the rotor as it would be for use with the pivot bearing support system. Figure VII-E-2 shows the rotor with modified end caps for testing on the Spinco model L centrifuge drive system. The rotor can be operated as a batch-type centrifuge on either system, or it can be converted into a continuous-flow centrifuge machine by using a different core. All the rotating-components C-series rotors are machined to an accuracy of 5×10^{-4} in., or less, total indicator reading (TIR).

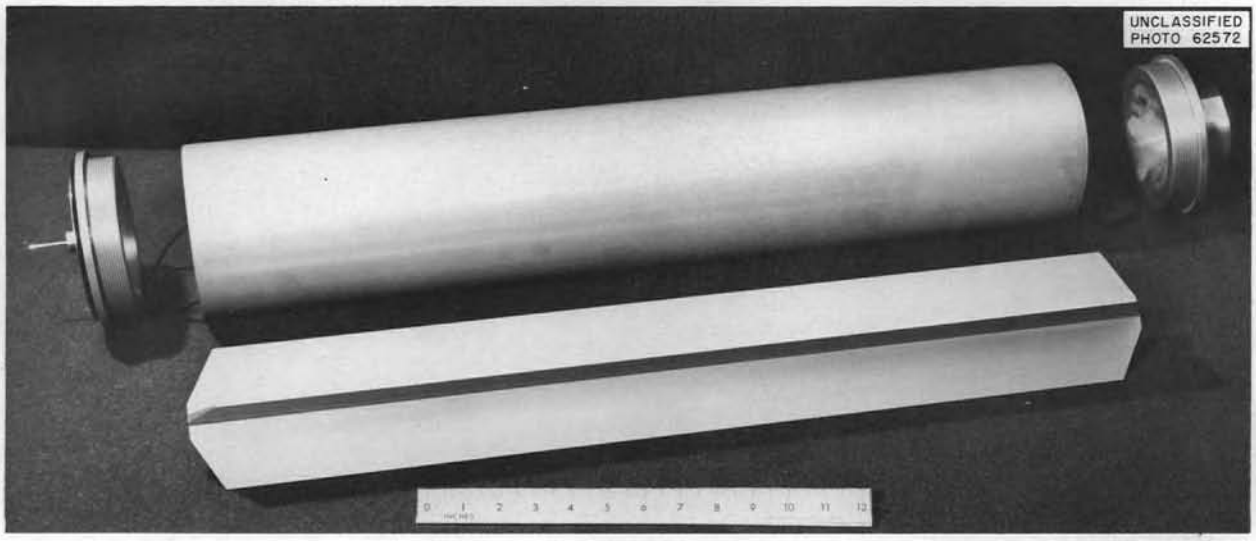

Fig. VII-E-1. C-V Zonal Ultracentrifuge. 40,000 rpm, 91,000 × g, 5000 ml.

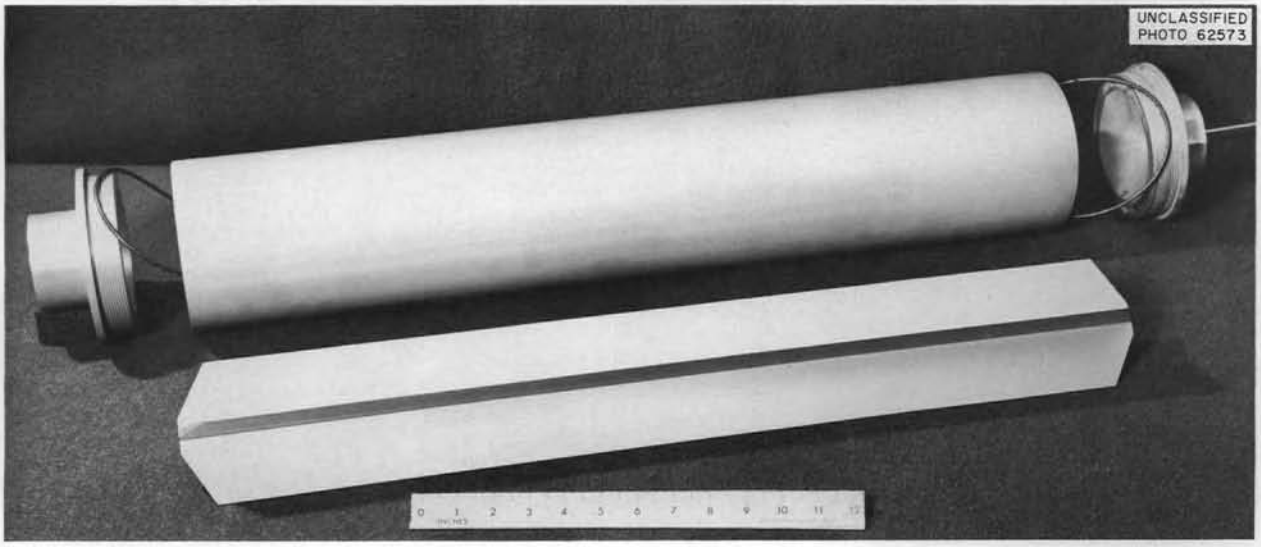

Fig. VII-E-2. C-V Zonal Ultracentrifuge with Modified End Caps for Testing on Spinco Model L Centrifuge Drive System. 40,000 rpm, 91,000 × g, 5000 ml.

F. FUTURE C ROTORS

For the processing of some biological materials a large number of conventional angle-head centrifuges are required for prolonged equilibrium runs. Since the centrifuge drives are not ordinarily used more than the recommended 400 hr before being replaced, a large number of drive systems would be required to sustain continuous operation of, for example, 12 angle heads operating 24 hr per day five days per week. However, the bearing system used with the C-series rotors can be used for much longer periods than conventional drive systems.

In a multiple angle-head operation, several angle heads and their associated motors and bearings could be stacked like shelves into a common vacuum chamber to minimize expense.

A 40,000-rpm angle-head rotor has been adapted for use on a magnet-pivot system for preliminary testing. The results show the system is feasible and practical.

VIII. Ultrahigh-Speed Rotor Systems

W. W. Smith W. G. S. Fort H. F. Dunlap H. P. Barringer

A. ROTOR D-I

The D-I rotor shown in Fig. VIII-A-1 is designed to operate at 400,000 rpm (1,200,000 × g at R_{max}) and contains 10 ml of fluid with a density of 1.7. The rotor is fabricated from 18% nickel maraging steel with a yield strength of 260,000 psi and an elongation of 11% at the tensile strength of 268,000 psi. All internal surfaces that will be exposed to CsCl have been Kanigen nickel-plated to prevent corrosion, while the external surfaces have been given a black oxide coating to increase heat transfer.

To date, the rotor has been driven to 300,000 rpm on the magnet-pivot suspension by means of the stator from an ultrahigh-speed electric motor. The system shows promise for reaching the design speed of 400,000 rpm.

The rotor has been designed to operate with steel end plugs as a preparative centrifuge or with transparent materials for visual analytical studies. When transparent windows are used, optical studies of the rotor contents similar to those performed in the conventional analytical ultracentrifuge can be made. However, for optical studies the magnet-pivot support system restricts the field of view so that a magnetic support system is desirable.

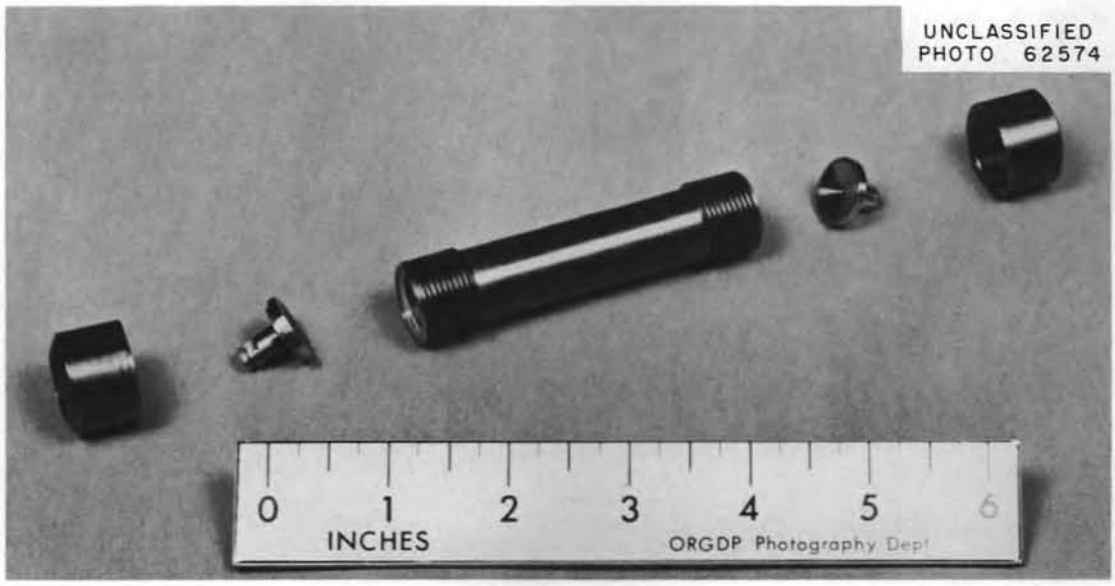

Fig. VIII-A-1. D-I Zonal Ultracentrifuge. 400,000 rpm, 1,250,000 × g, 10 cc.

B. MAGNETIC SUPPORT SYSTEM

The support of rotating bodies in a magnetic field with no contact between the rotating member and any stationary object has been demonstrated and summarized by J. W. Beams[1] at the University of Virginia. Stable operation and ultrahigh speeds for producing high-*g* fields are two of the advantages of full magnetic supports.

The approach taken at ORGDP has been that of utilizing a design incorporating transistorized circuits in place of vacuum tubes. A magnetic support system has been built for the D-I rotor and has been tested at low speeds. Fabrication of the mechanical vibration damping components for high-speed testing of the centrifuge is now under way. The operation of the system will be described in subsequent reports.

The electronic components are shown diagrammatically in Fig. VIII-B-1. The distance between the stationary, nonrotating proximity coil (*A*) and the rotor is sensed and amplified by (*B*), and a signal is sent to an amplifier (*C*) for phase correction and control of the set point or elevation of the D-I rotor. The computer amplifier (*D*) determines the first derivative of the distance signal and sends the signal to amplifiers (*E* and *F*) for determination of the second derivative and control of the vertical damping of the centrifuge rotor. The control signals are amplified (*G* and *H*) by units that operate a transistor gate to control the programmable transistorized high-current power supply (*I*), which, in turn, regulates the flux in the magnet (*J*). All items are commercially available, and preliminary tests show the system is stable.

[1] J. W. Beams, *Phys. Today* 12(7), 20–27 (1959).

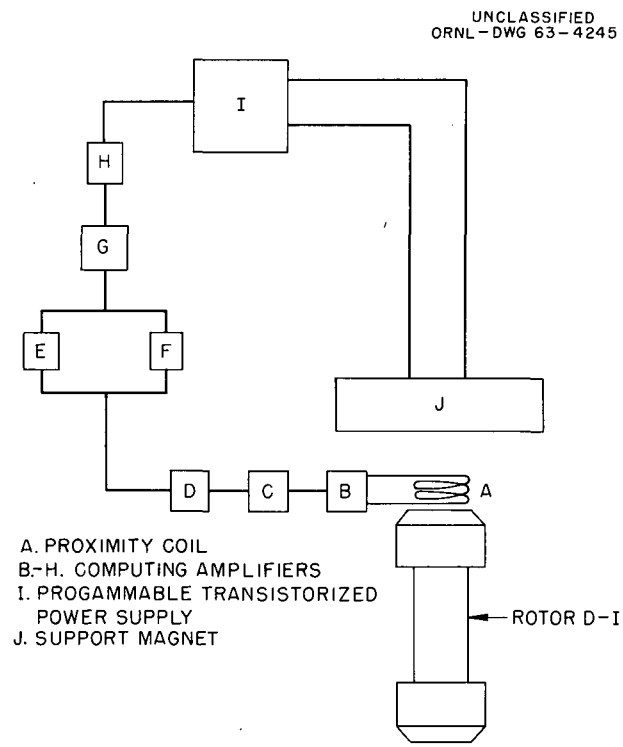

Fig. VIII-B-1. Diagrammatic Representation of Electronic Components of ORGDP Magnetic Support System.

IX. Density-Gradient Centrifugation in Angle-Head Rotors

W. D. Fisher G. B. Cline N. G. Anderson

Preparative isopycnic density-gradient centrifugation is ordinarily done in high-speed swinging-bucket rotors, such as the Spinco SW39 and SW25. In addition to requiring this special equipment, the technique is severely limited by the small number of samples and the low total sample volume that may be used. In recent studies on methods for isolating small numbers of virus particles from tissues and for separating nucleic acids which differed in density, we required means for centrifuging many samples simultaneously. We investigated the possibility of making such separations in ordinary angle-head rotors, which are widely available and have a large number of tubes and high capacities. This application of angle-head rotors depends on reorientation of the density gradient from horizontal to vertical during deceleration, which, in effect, replaces the mechanical transition of the tubes in the swinging-bucket rotor. This approach appeared feasible since the same basic principle has been applied to the construction of hollow, cylindrical, reorienting gradient rotors (C-series rotors) in which a density gradient formed at rest is reoriented radially during centrifugation and is subsequently recovered at rest after deceleration.

Figure IX-1 illustrates the principal results obtained in a test system of T3 bacteriophage in CsCl (ρ = 1.519). After the rotor coasted to rest without braking, the tubes were removed and unloaded through a length of stainless steel tubing inserted to the bottom of the tube. The sample was passed through a flow cell in a Beckman DB spectrophotometer and a Waters model 34H refractometer, which displayed optical density at 260 mμ and refractive index on a Brown 12-point recorder. The results show that (1) the gradient produced approached the predicted equilibrium condition, (2) good banding was obtained, and (3) the reorientation of the gradient column did not cause appreciable disturbances of the gradient or sample zone.

Results similar to those for the No. 40 rotor were obtained with the Nos. 30 and 50 Spinco rotors. DNA, adenovirus, and R17 bacteriophage have been separated isopycnically in angle-head rotors.

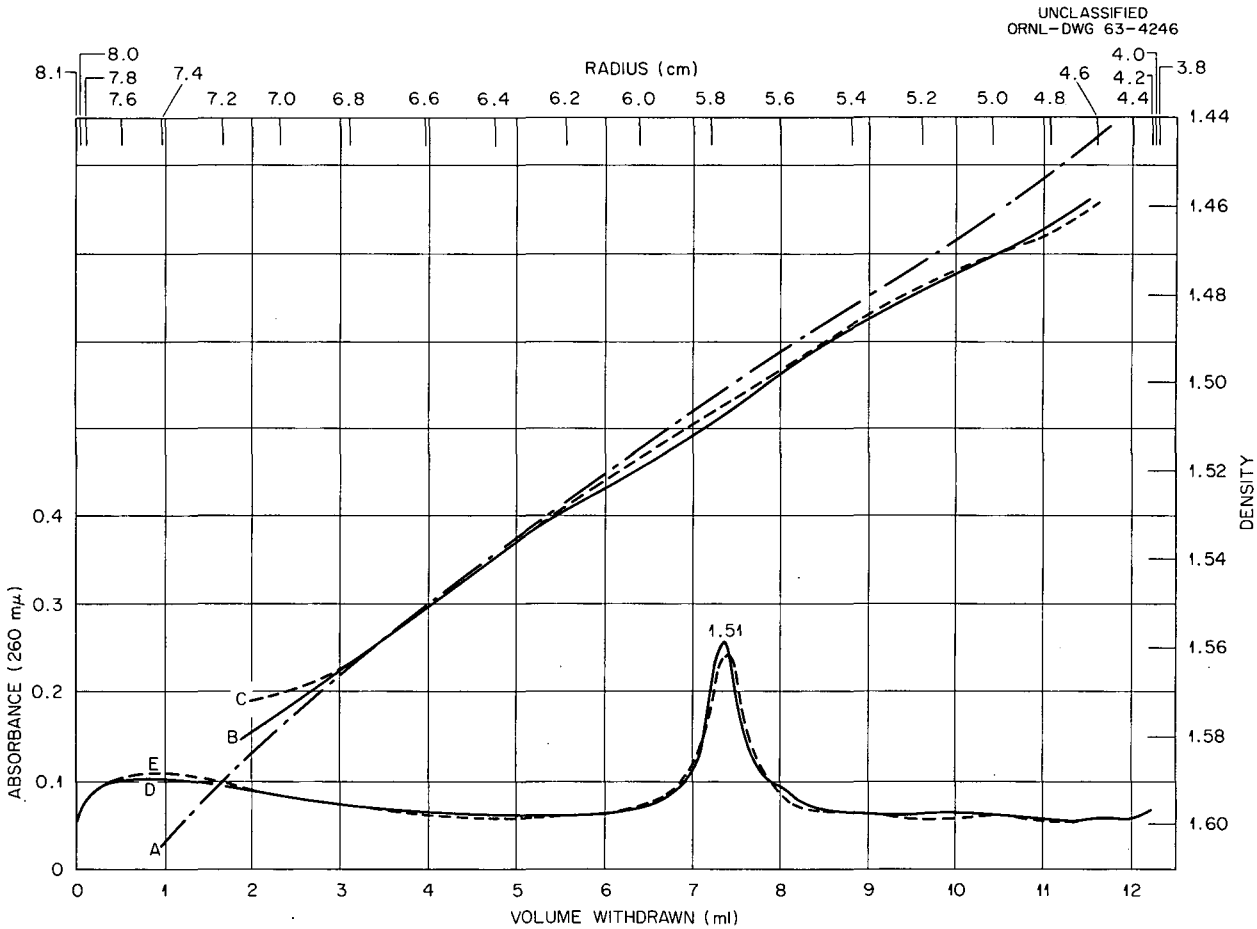

Fig. IX-1. T3 Bacteriophage Banded in CsCl. Curve *A* is the calculated gradient at equilibrium. Curve *B* was obtained after centrifuging for 30 hr at 33,000 rpm in a No. 40 rotor in a Spinco model L centrifuge. Curve *D* is the corresponding optical density tracing. Curves *C* and *E* were obtained after a 1-min recentrifugation at 33,000 rpm of previously banded phage.

X. Seal Development

C. E. Nunley

A. SEAL DESIGN

The face seal is used for applications requiring a high order of sealing effectiveness when relative motion between static and dynamic surfaces is limited. The face seal can be made to accommodate fluids over a wide range of viscosities. The major advantage afforded by this seal, however, arises from the fact that primary sealing takes place in a radial plane; this permits the face seal to be more easily pressure-balanced.

Most seal applications involve an accumulation of relative axial motions, arising from such factors as thrust bearing endplay and differential thermal expansion between shaft and housing. Moreover, manufacturing tolerances account for a degree of uncertainty as to the relative axial position of the primary sealing elements after assembly. To ensure continuing contact between static and dynamic sealing surfaces, it is necessary to provide a degree of axial freedom for one of the primary sealing members, usually the seal ring. This necessity then implies a requirement for an additional, relatively static seal between the translating seal ring and the housing. This "secondary seal" may take a variety of forms; however, the O-ring is commonly used in seals for low-temperature applications.

To complete the function of maintaining contact between the primary sealing members, there must be some axial driving force to move the seal ring. One or more axial springs are used to provide the required driving force which prevents the seal faces from becoming separated during operation.

B. SEAL TYPES

1. A-Type Rotor Seal

The A-type seal, designed for relatively low-speed rotors, is shown in Fig. X-B-1. The operation of a flexibly mounted rotating seal without an upper bearing to assist alignment of the two surfaces requires some means to ensure reproducible alignment. The cone-shaped alignment plug (9) shown in Fig. X-B-1 mates with a similar-shaped hole in the dynamic face seal (8) as shown in Fig. X-B-2.

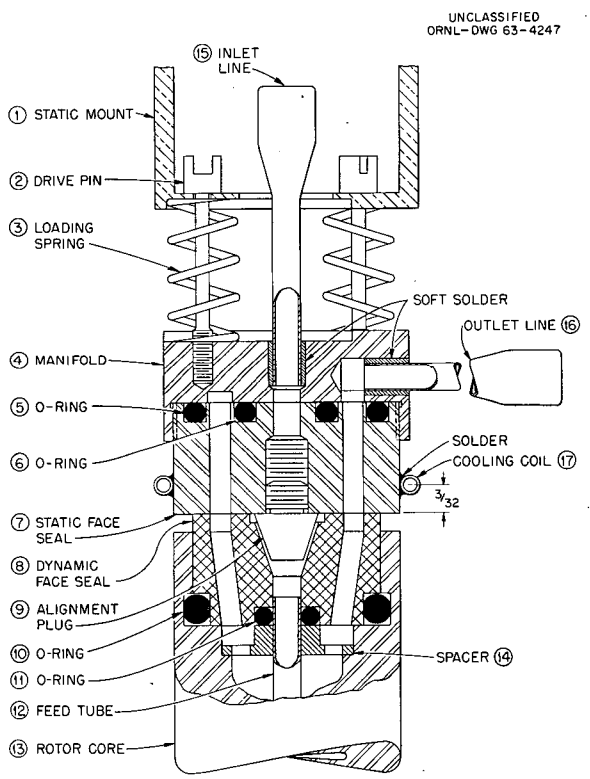

Fig. X-B-1. A-Type Seal Assembly.

Fig. X-B-2. Portion of A-Type Seal.

This seal can be designed so that it may be removed after the gradient and sample have been introduced or while the rotor is operating at full speed, then reengaged after the rotor has returned to unloading speed; or the seal can be left engaged during high-speed operation and cooled by coil (17) (Fig. X-B-1). This seal has operated satisfactorily on the A-VI rotor, and tests indicate it will operate equally well on other A-type rotors such as the A-IX.

2. B-Type Rotor Seal

For work with pathogenic viruses, seals are required which (1) show minimum cross leakage between inlet and outlet streams during operation, (2) do not allow virus leakage out of the seal enclosure, and (3) have provision for the inactivation of any live virus particles which may escape from the sealing faces. The seal illustrated in Fig. X-B-3 meets the above specifications. It assembles into a single unit which attaches to the upper rotor shaft as shown in Fig. X-B-4. The seal is totally enclosed and is cooled by circulating fluid which may contain a disinfectant. This seal is currently being used on the B-II rotors.

3. C-Type Rotor Seals

Seals for C-III and C-IV rotors are now in a developmental stage.

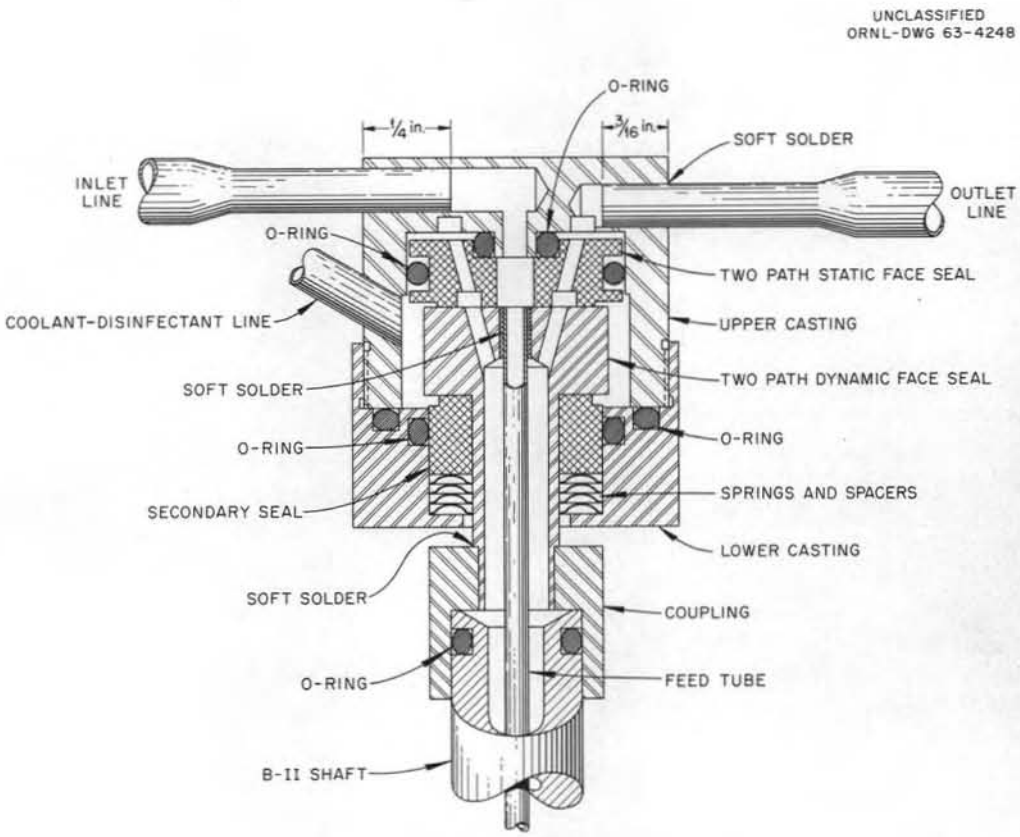

Fig. X-B-3. B-Type Seal Assembly.

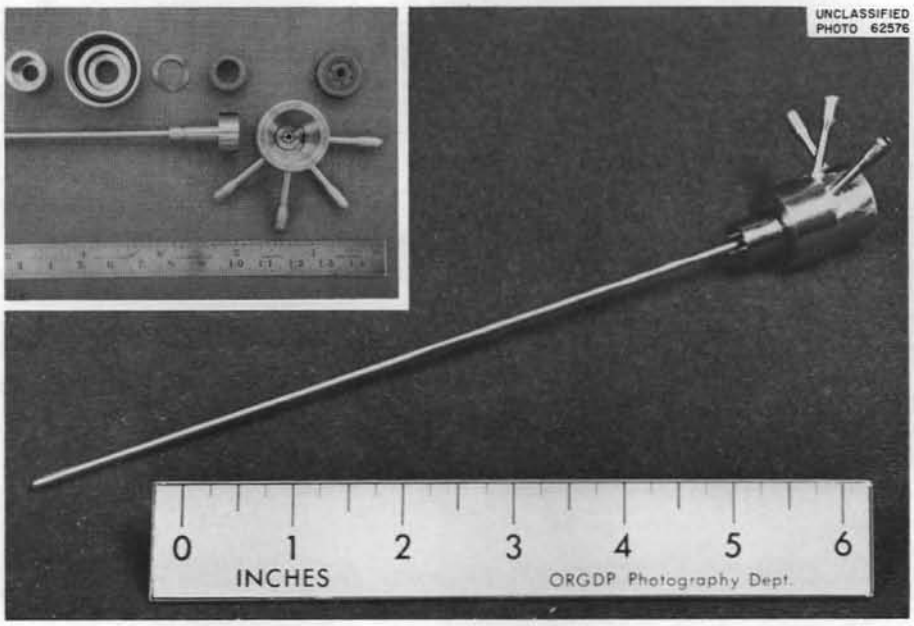

Fig. X-B-4. Components of B-Type Seal.

XI. Reprocessing of Cesium Chloride

A. INTRODUCTION

C. W. Weber

In several rotor systems now under development, large amounts of CsCl are used. The B-II rotor, for example, requires about 2 liters of a solution of density 1.7 for one isopycnic separation, while the C-V rotor requires 5 liters. It is desirable to recover the CsCl for reuse.

Cesium chloride above 99% purity, with total divalent cation impurities below 0.01%, is required. The optical density of the saturated solution should be less than 0.1 higher than a standard saturated solution, at 260 mμ with a 1-cm light path.

Initial tests indicate that a laboratory-scale method of reprocessing has been achieved. The waste CsCl is autoclaved to inactivate virus contaminants, organics are carbonized and filtered out, and metallic impurities are removed. The chemical and spectrochemical analyses of the combined reprocessed CsCl batches are shown in Table XI-A-1. Also studied, but not reported, was a hybrid system.

B. REMOVAL OF METALLIC IMPURITIES

1. Method

An organic extraction method for the recovery and purification of cesium has been used at ORNL by Crouse and Arnold.[1–3] In this method, cesium is reacted with a phenolic compound and the cesium subsequently removed from the organic salt by treatment with a mineral acid.

The process of CsCl recovery with 4-*sec*-butyl-2-(alpha-methylbenzyl)phenol (BAMBP) is presented. A Varsol solution of the ion exchange liquid

[1]D. J. Crouse and W. D. Arnold, Jr., private communications, April–May, 1963.

[2]D. E. Horner *et al.*, *Chem. Technol. Div., Chem. Develop., Sec C, Progr. Rept. April–June 1962*, ORNL TM-265.

[3]D. E. Horner *et al.*, *Chem. Technol. Div., Chem. Develop., Sec C, Progr. Rept. July–December 1962*, ORNL TM-449.

Table XI-A-1. Analysis of Reprocessed Cesium Chloride[a]

Spectrochemical		Chemical	
Element	Concentration of Each Element (ppm)	Measurement	Concentration
Ag, Al, Be, Ca, Cr, Cu, Fe, Mg, Mn, Mo, and V	<1	CsCl	1242 g/liter
Pb and Ti	<5	P as PO_4^{3-} (colorimetric)	<5 ppm
Bi, Cd, Co, Ni, Si, and Sn	<10	Nitrogen (Kjeldahl)	<25 ppm
P and Zn	<50	Density	1.91 g/ml
Na (flame photometry)	500	Optical density at 260 mμ vs H_2O	0.047
K (flame photometry)	80		

[a]Ten pound batch.

BAMBP, in the hydrogen form (ROH), is reacted with the impure CsCl solution:

$$ROH + Cs^+ + OH^- \longrightarrow ROCs + H_2O .$$

Cesium is stripped from the organic phase by dilute hydrochloric acid:

$$ROCs + H^+ + Cl^- \longrightarrow ROH + Cs^+ + Cl^- .$$

Flame photometry and emission spectroscopy, as well as nitrogen determination, have been used to measure metallic ions and protein content of the CsCl rotations.

The prototype laboratory-scale system consists of five contactors as illustrated in Fig. XI-B-1. The impure CsCl solution is introduced into the extractor. Then the BAMBP solution (1 *M*) is circulated through the extractor, two water scrubbers, the hydrochloric acid stripper, and a third water scrubber. For each mole of CsCl being processed, one mole of sodium hydroxide is added to the extractor and one mole of hydrochloric acid is added to the stripper. A slight excess of the acid and base reagents is required for complete cesium transfer.

2. Tests and Results

A waste CsCl solution was processed in the laboratory system shown in Fig. XI-B-1. The scale of studies was limited to 500-ml-volume contactor stages. Table XI-B-1 presents results of the initial cesium extraction test. The organic phase was circulated at 100 ml/min for 45 min, probably exceeding the requirements for acceptable purification.

Cesium removal from the feed was 99.8%. The product recovered in the stripper exceeded 99.9% purity. The product solution was then evaporated to dryness, dissolved in water, and filtered. The optical density of the saturated filtrate was 0.31, which compared with 0.30 for a purified standard, at 260 mμ and 1-cm light path.

Although the test did not cover the full range of possible impurities, the purification is acceptable for divalent cation removal and total optical-density measurements.

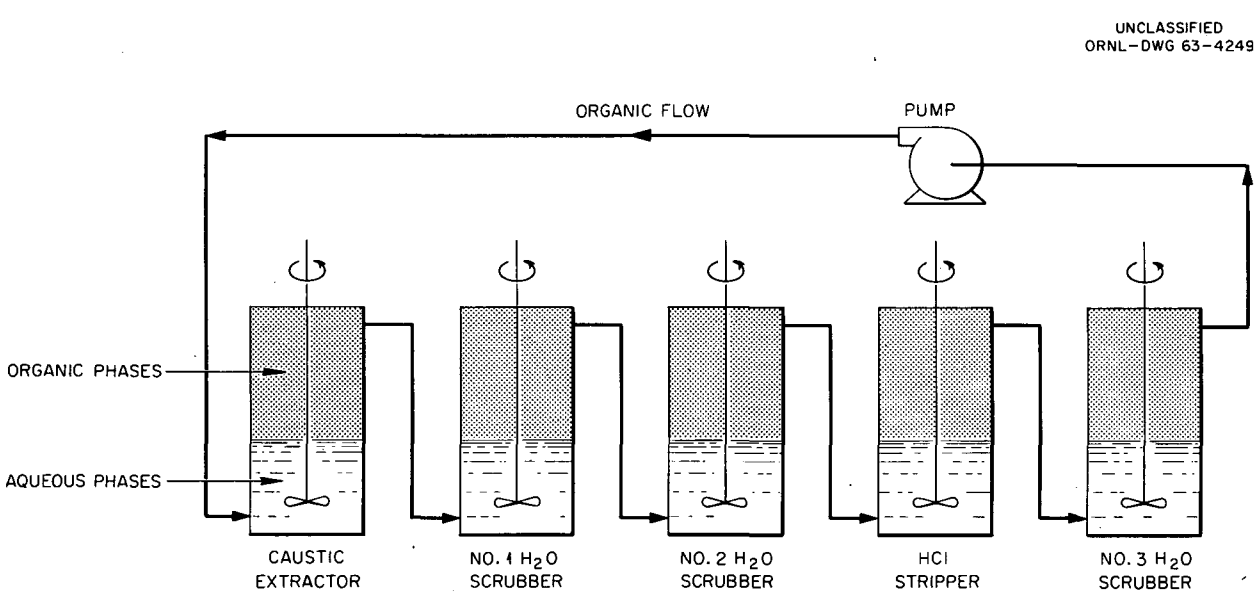

Fig. XI-B-1. Laboratory System for Reprocessing Cesium Chloride.

Table XI-B-1. Initial Test Data from Cesium Chloride Reprocessing System

	Organic Volume (ml)	Aqueous Volume (ml)	Concentration (g/liter)[a]					Normality		
			CsCl	Na	K	Ca	Mg	Cs^+	OH^-	HCl
Extractor										
Initial	330	250	112.1	21.0[b]	0.1	0.07[c]	0.003[c]	0.666	0.86	
Final	330	250	0.25	Strong	0.1	0.001[c]	0.00005	0.0015	0.06	
No. 1 Scrubber										
Final	455	125	1.1	0.25	0.01	0.02	0.0002		0.015	
No. 2 Scrubber										
Final	455	125	3.0	0.11	0.04	0.01	0.0003		0.012	
Stripper										
Initial	330	250	0	0	0	0	0	0	0	0.875
Final	330	250	101.3	0.03	0.005	0.002	0.0001	0.602		0.19
No. 3 Scrubber										
Final	330	250	1.5	0.006	0.001	0.00076	0.00015			

[a]Aqueous.

[b]As NaOH and NaCl.

[c]Prior to filtering where some Mg and Ca was removed.

XII. Containment and Sterilization

V. H. Kiplinger

A. BIOHAZARDS

To prevent contamination of virus cultures and to avoid any loss of the material during centrifugation it is necessary to consider methods of sterile operation for the complete containment of the rotor and all virus handling systems. The requirements for the safe handling of virus-containing materials are being set up by the ORNL Biohazards Committee and will be reviewed in a subsequent report. The extensive experience of personnel at ORNL in developing systems for work with high-level radioactivity and toxic gases will be utilized in the development of these systems.

B. CONTAINMENT

A stainless steel biological safety cabinet (Fig. XII-B-1) approximately 6 ft in length, 2 ft in

Fig. XII-B-1. Containment System Designed for B-II Ultracentrifuge.

height, and 2 ft in depth has been designed and fabricated for the routine operation of rotor B-II. This unit encloses the top of the centrifuge and houses the uv monitor system. The end of the unit has a double-door arrangement enclosing a compartment 18 × 14 in. so that materials put into the system may be gas-sterilized before entry into the main portion of the presterilized cabinet. In this way, filling and emptying of the rotor are accomplished under sterile conditions, and contamination either into or out of the system is eliminated.

Since modification of the existing cabinet will be necessary for specific application, plastic cabinets will be constructed in the future. The essential equipment for this work, including heat-sealing equipment for plastic bonding, has been procured.

XIII. Pressure Ultrafiltration

A. FLOW RATES THROUGH VISKING DIALYSIS TUBING

D. E. Fain

Flow rates of distilled water and of 1% bovine serum albumin (BSA) have been measured through Visking cellulose dialysis tubing, using pressure differentials up to 500 psi. This work was undertaken to aid in separating virus particles by reducing the total volume of solution before centrifugation. It is desirable to reinforce the membrane so that large pressure differentials can be used to obtain greater flow rates. The experiments reported utilized reinforced membranes for high-pressure tests in order to obtain data useful for estimating the size of equipment and amount of membrane material needed for specific purposes.

Three techniques for reinforcing dialysis tubing were evaluated. The best system involves the use of a wire spring (Fig. XIII-A-1) used as a support mechanism for the tubing. Another, that of using a porous tube as support (Fig. XIII-A-2), was tested. The third method, using glass beads within the cellulose tubing, causes difficulty due to the extra weight and subsequent leakage (Fig. XIII-A-3). The method of reinforcement, in general, did not affect the flow rates. We conclude, therefore, that any technique which proves convenient may be used.

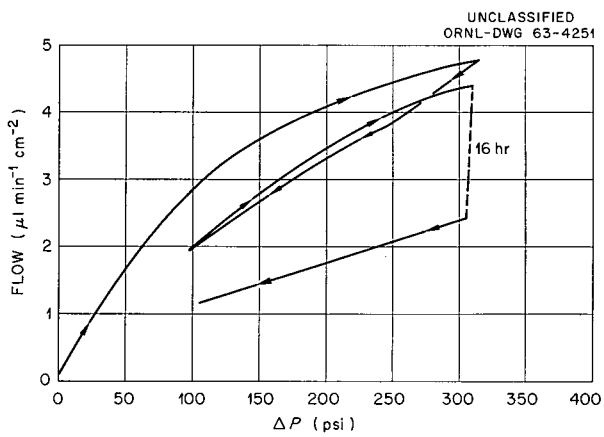

Fig. XIII-A-2. Flow of 1% BSA Through Two Samples of Dialysis Tubing. Porous-tube support.

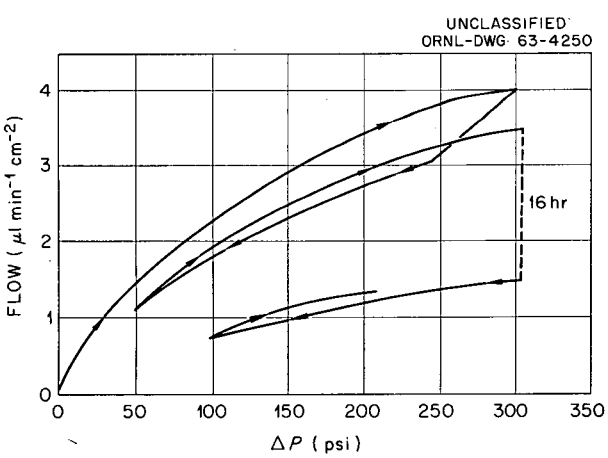

Fig. XIII-A-1. Flow of 1% BSA Through Dialysis Tubing. Helical-wire support.

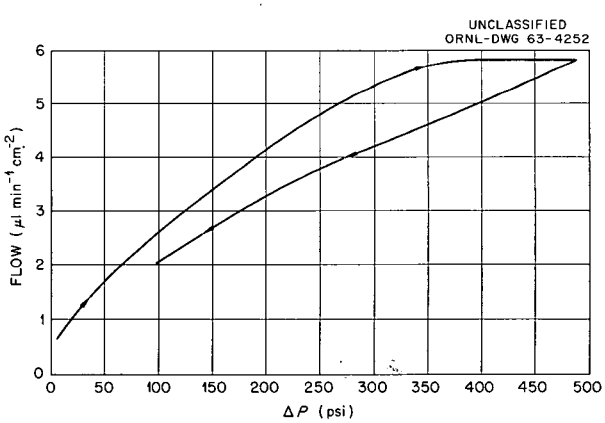

Fig. XIII-A-3. Flow of 1% BSA Through Dialysis Tubing. Glass-bead support.

Differences from sample to sample of dialysis tubing were observed, and general conclusions are difficult to draw with respect to flow properties. However, it appears that flow is not linear with pressure drop across the membrane, since proportionally smaller flow increase is observed with pressure increase.

Flow appears to be nearly inversely proportional to the thickness of the membrane (Figs. XIII-A-4 and -5). When the tubing is reinforced with interstitial hemp, the flow rate does not show an apparent decrease (Fig. XIII-A-6). The hemp may increase the structural strength, however, so that the flow vs pressure difference relation is more nearly linear (Fig. XIII-A-5).

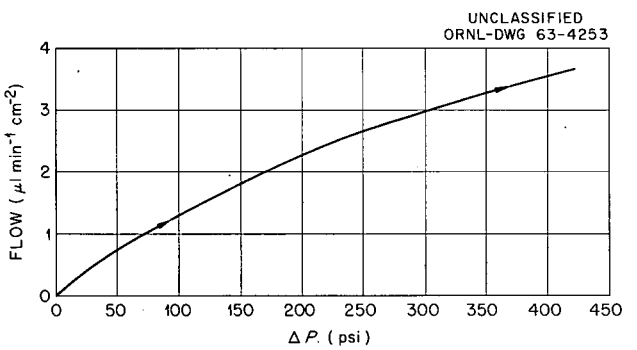

Fig. XIII-A-4. Flow of Water Through 3.5-mil-Thick Flat Sample of Dialysis Tubing.

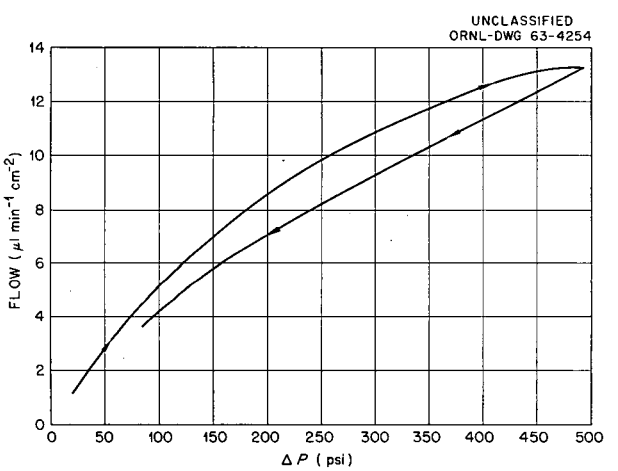

Fig. XIII-A-5. Flow of Water Through 0.8-mil-Thick Flat Sample of Dialysis Tubing.

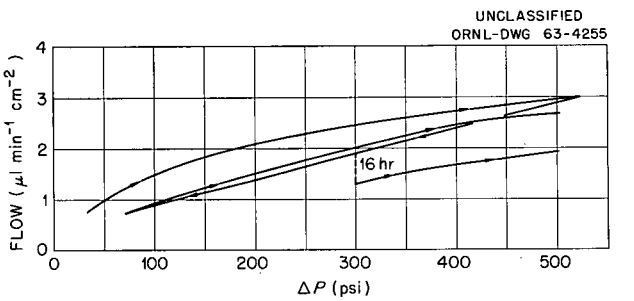

Fig. XIII-A-6. Flow of 1% BSA Solution Through 3.5-mil-Thick Flat Sample of Hemp-Reinforced Dialysis Tubing.

B. DESIGN OF CONCENTRATION SYSTEMS

H. P. Barringer

Conceptual designs are being considered which utilize Visking's No. 12 uncolored fibrous casing as the dialysis membrane. This material has a dry uninflated circumference of 18.2 in. and pore radii of 12.2 A.

The casing is 3.5 mils thick and is reinforced with fibrous hemp for additional strength required in a large separation facility.

The use of the membrane supported on a porous bed of glass beads, similar to normal filtration methods, has given good results. Other methods of reinforcing the membrane for large area exposures are being tested.

XIV. Data Reduction

A. COMPUTER PROGRAM FOR DETERMINING SEDIMENTATION COEFFICIENTS USING SUCROSE GRADIENTS IN THE B-II ZONAL CENTRIFUGE

E. F. Martin N. G. Anderson
R. Elizabeth Lybarger

1. General Considerations

During centrifugation in the zonal centrifuge, a particle migrates through the density gradient at a rate determined by the amount and duration of the applied acceleration, the size and density of the particle, and the density and viscosity of the suspending medium. It is of interest to calculate from data obtained with the zonal centrifuge the sedimentation coefficients of particles of a given size and density at 20°C in water. Since the computations are very laborious, a computer program has been developed to calculate the required information.

In the zonal centrifuge, sedimentation begins as soon as the particle is introduced into the rotor and continues until the gradient has been completely recovered at the end of the run. It is therefore necessary to determine $\int \omega^2 \, dt$ for the entire run, that is, immediately after introduction of the sample, through acceleration to operating speed, operation at speed, deceleration, and unloading. This is now done electronically as shown in Chap. XV.

At the conclusion of centrifugation the contents of the rotor are withdrawn into sample containers, in some instances with a concurrent flow of material into auxiliary analytical devices. Therefore, the material in a single sample tube may be the total quantity withdrawn from a toroidal section of the rotor; or it may be representative of a slightly larger volume, a small portion of which enters the auxiliary analytical systems. In either case the average properties of the material in the tube are equivalent to the average of the total quantity removed from a specific section of the rotor. In the calculations, therefore, the contents of a specific tube are correlated with a radial location in the rotor. Since the material is withdrawn through the rotor axis, the initial tubes (fractions or cuts) will contain the overlay. The calculation of sedimentation coefficients is started with the portion of the material which represents the volumetric center of the starting particle sample layer.

The time required to fill each sample container is recorded during removal of the solution from the rotor. This allows the calculation of the amount of gradient entering the auxiliary analytical device, if it is in operation. When the rotor has been emptied, the average sucrose concentration in each sample tube is determined refractometrically. Data from each experiment are supplied on the sucrose concentration for each collected fraction; if auxiliary analytical systems are used, the time required to fill each tube is supplied also. The other data items required are all single valued.

Since the centrifuge program is concerned initially with virus isolation, osmotic changes occurring in the gradient have not been considered in this study.

Often particles with different densities are present in the same gradient. It is desirable, therefore, to calculate sedimentation coefficients for particles with several different densities and to plot the data in such a way that the sedimentation coefficient of a particle of any given density may be determined.

2. The Program

We require a program to calculate sedimentation coefficients corresponding to the center of each of from 40 to 100 fractions and to report this value correlated with each fraction. The basic equation for the calculations is:

$$S_i = \frac{\dfrac{\eta_i}{\left(\rho_{s_i} - \rho_{m_i}\right)\cdot(R_i)}(R_i - R_{i-1})}{\omega^2 t} \times \frac{(\rho_s - \rho_{20,w})}{\eta_{20,w}}, \quad (1)$$

where

S = sedimentation coefficient,

η = viscosity,

ρ_s = density of a particle (virus, etc.),

ρ_m = density of the solution stratified,

R = radial distance from axis of centrifuge bowl (rotor) to the extremity of the cylindrical volume which contained the fluid volume represented by the sample withdrawn into container i,

$\omega = 2\pi(\text{rpm})/60$,

t = time (sec) of effective centrifugation, including corrections for acceleration and slowing of the rotor (the equipment incorporates an integrator which records $\omega^2 t$),

$\rho_{20,w}$ = density of water at 20°C,

$\eta_{20,w}$ = viscosity of water at 20°C,

i = subscript denoting a specific portion of centrifuged solution, that is, tube, cut, or fraction.

Tabulated data of sucrose concentration vs density (at 0°C) and viscosity (at 5°C) are available. These data have been fitted, by the least-squares method, to polynomial equations. For the density, the following third-degree equation provided a very close fit:

$$\rho = 1.0 + 0.003929917x + 0.000016603218x^2 , \quad (2)$$

where ρ is density, g/ml, and x is concentration, g/g, expressed as percent. It was necessary to break the viscosity curve into ten segments to attain a satisfactory fit with a fourth-degree equation of the form:

$$\eta = A + Bx + Cx^2 + Dx^3 , \quad (3)$$

where η is viscosity, centipoise; x is sucrose concentration, g/g, expressed as weight percent; and A, B, C, D are polynomial coefficients. The limits of each curve segment, and the applicable coefficients, are tabulated in Table XIV-A-1.

The program permits the addition of data for solutions other than sucrose, up to a total of nine solutions. The following is the equation for the volume of rotor B-II:

$$V = 74 + 25.87\,[\pi R^2 - 2.88(R - 2) - 4\pi] , \quad (4)$$

where R is radius (cm) and V is volume (cc). Since the program requires calculation of the radius for a given volume, the form used is

$$R = 81.273V^2 - 74.506V - 102.082 . \quad (5)$$

The program provides for use of up to 99 different rotors. Each time a new rotor is put into production, it will be necessary only to recompile a new subroutine, incorporating the proper coefficients in arrays A, B, and C. Rotor B-V, now undergoing tests, will require such a revision in the program.

A FORTRAN deck was compiled on an IBSYS monitor. A FORTRAN glossary and listings are not included here but are available.[1]

The program is designed to accept data for a maximum of 100 tubes (cuts). If the quantity of data exceeds this value, the calculations will be completed through tube 100, and the balance of the data will be ignored. If future experimental conditions should increase the quantity of data, only minor program changes would be necessary.

[1]Can be obtained from N. G. Anderson, Biology Division.

Table XIV-A-1. Limits and Applicable Coefficients for Each Segment of the Viscosity Curve

Range of Concentration (%)	*A*	*B*	*C*	*D*
0–1	1.52	0.028458313	−0.0091426457	0.0050598586
1–15	1.5018023	0.035322959	0.0015809948	0.000037521348
15–30	0.51940283	0.21893221	−0.0095684131	0.00025830963
30–40	−32.398942	3.4653102	−0.11602272	0.0014195706
40–50	−485.38163	36.201171	−0.90605868	0.0077874755
50–55	−6,716.4824	404.22887	−8.1603287	0.055511223
55–59	7,089.3527	−300.05596	3.7849495	−0.011832235
59–62	−134,047.78	6,845.4074	−116.84542	0.6672486
62–64	−455,574.31	22,279.857	−363.78081	1.9839709
64–66	−4,172,494.9	195,551.72	−3055.7052	15.92152

3. Data Preparation

Figure XIV-A-1 shows a convenient format for presenting the run data. A new data sheet is originated for each run. Figure XIV-A-2 shows the required arrangement of the cards in the data deck. The types of information noted on the card column are shown. Detailed aspects of FORTRAN format are not included.

4. Reports of Results

The calculated sedimentation coefficients for a single cell-component density are presented on a sheet. Each sheet has appropriate experimental identification data in the headings. The results are tabulated as one, two, or three pairs of columns, depending on the quantity of information. Figure XIV-A-3 is an example of the output for two pairs of columns. A secondary listing will follow each page described above. This report (see Fig. XIV-A-4 for an example) contains identification headings and tabular correlations of run number, sucrose concentration, viscosity, density, and sedimentation coefficient.

On the sheet following the last page of output, the number of runs processed in the current job is reported as follows:

——— LOGICAL RUNS COMPUTED IN THIS JOB .

Normally this message will result when the job is terminated. The main program is designed to furnish output for 100 tubes (cuts). This is adequate for present rotor systems. Errors are also reported in the output. A general scheme of data computation is shown in Fig. XIV-A-5.

UNCLASSIFIED
ORNL-DWG 63-4256

REQUEST 3640 JOB TITLE NIH-AEC ZONAL CENTRIFUGE WRITTEN BY DATE

RUN NO. EXP. NO.	MONTH DAY	YEAR ROTOR IDENT.	ROTOR CODE	TEMP	SIDE PUMP FLOW RATE	$\omega^2 t \times 10^{-6}$	OVERLAY VOL.	CUT VOL.	SAMPLE VOL.	DEN CD	LINE VOL.	DENSITIES	SOL CD
1–8	9–16	17–24	25–32			33–40	41–48	49–56			57–64	65–72	73–80

CUT TIME	CONCENTRATION	CUT NO.	CUT TIME	CONCENTRATION	CUT NO.	CUT TIME	CONCENTRATION	CUT NO.
1 2 3 4 5 6 7 8	9 10 11 12 13 14 15 16	78 79 80	1 2 3 4 5 6 7 8	9 10 11 12 13 14 15 16	78 79 80	1 2 3 4 5 6 7 8	9 10 11 12 13 14 15 16	78 79 80
		1			3 4			
		2			3 5			
		3			3 6			
		4			3 7			
		5			3 8			
		6			3 9			
		7			4 0			
		8						
		9						
		1 0						
		1 1						
		1 2						
		1 3						
		1 4						
		1 5						
		1 6						
		1 7						
		1 8						
		1 9						
		2 0						
		2 1						
		2 2						
		2 3						
		2 4						
		2 5						
		2 6						
		2 7						
		2 8						
		2 9						
		3 0						
		3 1						
		3 2						
		3 3						

Fig. XIV-A-1. Format for Presenting Run Data.

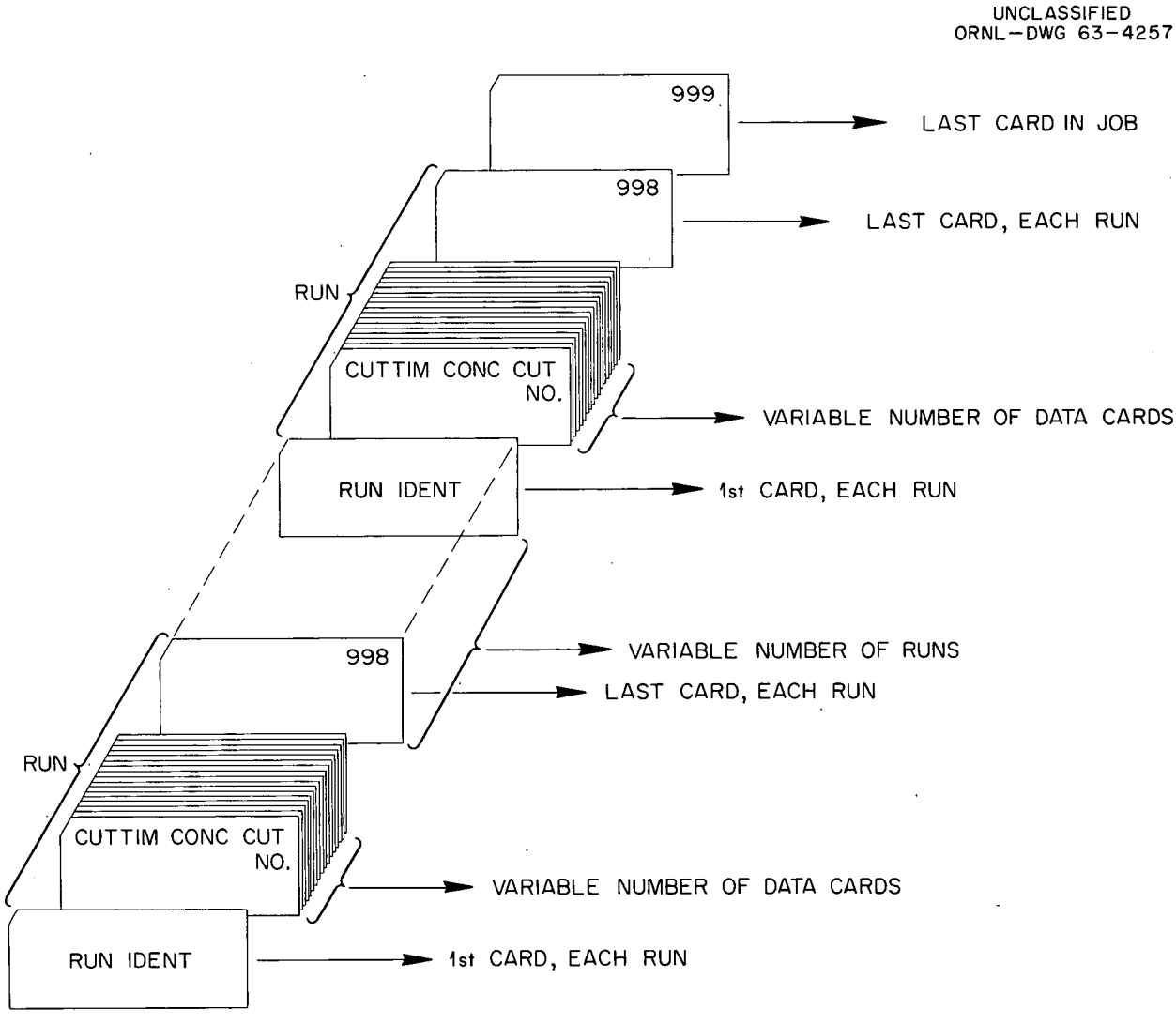

Fig. XIV-A-2. Data Deck.

UNCLASSIFIED
ORNL-DWG 63-4258

NATIONAL INSTITUTE OF HEALTH - U.S.ATOMIC ENERGY COMMISSION ZONAL CENTRIFUGE PROGRAM

EXPERIMENT NUMBER -0 RUN NUMBER 173 DATE OF RUN MARCH 28, 1963

ROTOR B-II DENSITY (1 OF 1) # 1.500

CUT	SEDIMENTATION COEFFICIENT (REF.WATER,20C)	CUT	SEDIMENTATION COEFFICIENT (REF.WATER,20C)
	-13 X10		-13 X10
13	7.014	53	552.
14	16.909	54	587.
15	26.985	55	630.
16	37.454	56	683.
17	47.889	57	745.
18	58.372	58	830.
19	69.414	59	924.
20	80.494	60	1049.
21	91.516	61	1187.
22	103.	62	1370.
23	113.		
24	124.		
25	136.		
26	147.		
27	158.		
28	169.		
29	180.		
30	192.		
31	203.		
32	215.		
33	227.		
34	239.		
35	251.		
36	263.		
37	276.		
38	290.		
39	303.		
40	316.		
41	330.		
42	344.		
43	358.		
44	372.		
45	387.		
46	403.		
47	419.		
48	435.		
49	454.		
50	474.		
51	495.		
52	521.		

Fig. XIV-A-3. Example of Output for Two Pairs of Columns.

UNCLASSIFIED
ORNL-DWG 63-4259

NATIONAL INSTITUTE OF HEALTH - U.S.ATOMIC ENERGY COMMISSION ZONAL CENTRIFUGE PROGRAM

EXPERIMENT NUMBER -0 RUN NUMBER 173 DATE OF RUN MARCH 28, 1963

ROTOR B-II DENSITY (1 OF 1) # 1.500

CUT NO.	PERCENT SUCROSE	DENSITY	VISCOSITY	SEDIMENTATION COEFFICIENT
13	8.324000	1.033868	1.927806	7.01420
14	9.700000	1.039682	2.027435	16.90856
15	11.100000	1.045668	2.139997	26.98483
16	12.800000	1.053023	2.291654	37.45424
17	13.600000	1.056518	2.368999	47.88899
18	14.500000	1.060475	2.460778	58.37168
19	16.200000	1.068022	2.653181	69.41396
20	17.000000	1.071607	2.745054	80.49420
21	17.600000	1.074310	2.816944	91.51649
22	18.200000	1.077024	2.891765	102.50126
23	18.800000	1.079751	2.969851	113.46842
24	19.500000	1.082947	3.065525	124.49971
25	20.200000	1.086159	3.166631	135.61741
26	20.800000	1.088925	3.258020	146.77777
27	21.300000	1.091240	3.337766	157.93241
28	21.900000	1.094028	3.438056	169.16581
29	22.500000	1.096828	3.543677	180.49662
30	22.800000	1.098233	3.598590	191.72754
31	23.600000	1.101993	3.752267	203.23436
32	24.300000	1.105301	3.895864	214.96989
33	24.800000	1.107674	4.003959	226.79816
34	25.300000	1.110054	4.116880	238.73372
35	26.000000	1.113402	4.283443	250.95962
36	26.600000	1.116284	4.434443	263.41349
37	27.400000	1.120145	4.648205	276.29937
38	28.100000	1.123541	4.847468	289.55648
39	28.500000	1.125489	4.966669	302.91264
40	28.800000	1.126953	5.058693	316.27851
41	29.900000	1.132348	5.416067	330.49570
42	29.900000	1.132348	5.416067	344.42255
43	30.000000	1.132840	5.450157	358.17521
44	30.300000	1.134320	5.570452	372.01170
45	31.600000	1.140765	6.043047	386.99786
46	32.300000	1.144258	6.322303	402.53228
47	32.900000	1.147266	6.578350	418.53244
48	33.800000	1.151799	6.995517	435.45623
49	35.200000	1.158905	7.736633	454.22276
50	35.900000	1.162482	8.155540	473.86558
51	36.700000	1.166591	8.678701	494.66262
52	39.400000	1.180613	10.850423	521.34737
53	41.000000	1.189037	12.502342	552.40387
54	42.200000	1.195410	14.002296	587.33496
55	44.000000	1.205060	16.708595	629.69070
56	45.900000	1.215363	20.427605	682.50159
57	47.300000	1.223031	23.918114	745.06165
58	49.600000	1.235770	31.405525	829.85003
59	50.400000	1.240243	34.884338	924.21011
60	52.300000	1.250949	45.016968	1049.33095
61	53.000000	1.254924	49.628662	1187.46042
62	54.700000	1.264645	63.772217	1369.62770

Fig. XIV-A-4. Secondary Listing Which Follows Each Sheet Showing Output.

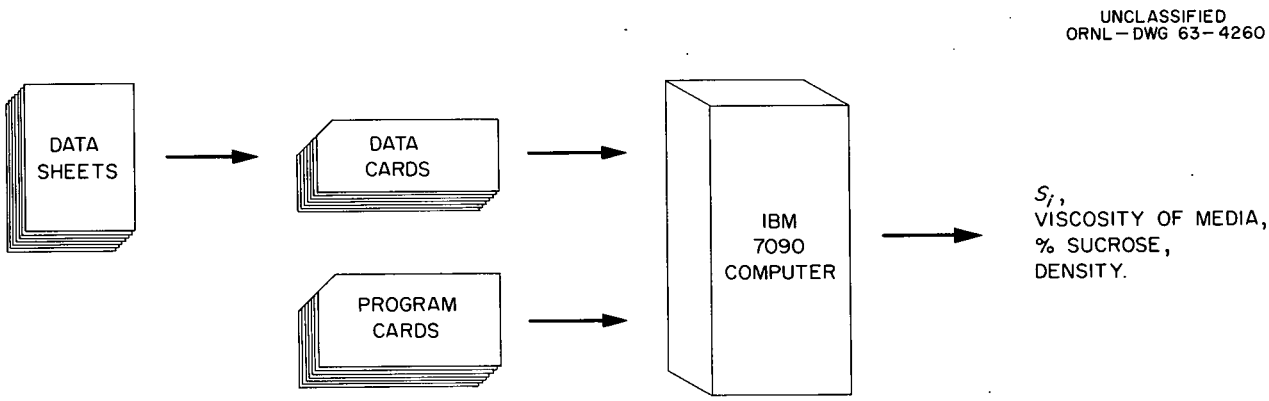

Fig. XIV-A-5. General Scheme of Data Computation.

B. CALCULATION OF DENSITY AND VISCOSITY OF SUCROSE SOLUTIONS

E. J. Barber P. B. Wood

1. General Considerations

In the calculations used in the preceding section, the density and viscosity are two of the intensive properties of the sucrose gradient which must be accurately known. Both of these intensive properties are functions of the readily measured parameters of temperature and composition of the solution at any given point in the centrifuge. Since the density and viscosity of sucrose solutions have been experimentally determined over a range of compositions and temperatures and reasonably precise tables prepared giving these or related properties as functions of the weight percent sucrose and the temperature,[2,3] it is possible to compute, by interpolation of the tables, the density and viscosity of the solution for each fraction withdrawn from the zonal ultracentrifuge. Because of the number of samples collected from even a single run of the centrifuge, this approach is impractical and means of expressing the density and the viscosity as analytical functions of the temperature and composition were sought. The analysis of the density and viscosity data are two different problems, since even the form of the functions are different and the analyses are therefore discussed separately. Both analyses are approaching completion.

2. Density Relations

Changes in the density of a solution due to a change in temperature are usually quite accurately expressed as a second-order polynomial in the change in temperature so that the density ρ at one temperature is readily calculated from the known density at another temperature, that is,

$$\rho_{t_2} = \rho_{t_1}[1 + \alpha(t_2 - t_1) + \beta(t_2 - t_1)^2] \qquad (1)$$

or

$$\rho_{t_2} = \rho_{t_1} + \alpha\rho_{t_1}(t_2 - t_1) + \beta\rho_{t_1}(t_2 - t_1)^2 .$$

Since the temperature range of interest includes 0°C and accurate density data are available at that temperature, we can let t_1 = 0°C and t_2 become t°C and as an applicable equation for any given composition as a function of temperature, we would have

$$\rho = A_1 + A_2 t + A_3 t^2 , \qquad (2)$$

provided t does not become too large.

[2]C. F. Snyder and L. D. Hammond, *Weights Per United States Gallon and Weights Per Cubic Foot of Sugar Solutions*, Circular of the National Bureau of Standards C-457, Dec. 5, 1946.

[3]J. F. Swindells *et al.*, *Viscosities of Sucrose Solutions at Various Temperature: Tables of Recalculated Values*, Supplement to National Bureau of Standards Circular 440, July 31, 1958.

In the particular case of sucrose solutions, one also notes that the molecular weight of sucrose is 342.3 as compared to a molecular weight of 18.032 for water. Since the density of sugar is only about 50% greater than that of water, a plot of the density of sucrose solutions of varying compositions at a given temperature vs compositions in terms of weight fraction may, and does in this case, show only small deviations from linearity. This means that at constant temperature, density is probably accurately expressed as a function of the weight fraction by the second-order polynomial

$$\rho = C_1 + C_2X + C_3X^2 , \qquad (3)$$

where ρ is the density of solution of composition X, X is the weight fraction of sucrose, and C_1, C_2, and C_3 are temperature-dependent constants. The constant C_1 can be interpreted as the density of water at the given temperature.

Combination of the relation in Eq. (2) with that in (3) suggests that over the temperature range for which data are available, an equation of the following form would be sufficiently accurate:

$$\rho = (B_1 + B_2 t + B_3 t^2) + (B_4 + B_5 t + B_6 t^2)X + (B_7 + B_8 t + B_9 t^2)X^2 , \qquad (4)$$

where ρ is the density of a sucrose solution, t is the temperature in °C, X is the weight fraction of sucrose, and the B_i are constants valid over the temperature and composition ranges for which data are available.

From the data previously reported[1] covering the temperature range of 0 to 30°C, the set of constants listed in Table XIV-B-1 gives an equation with a maximum error of about 7 parts in 10,000.

The equation in Table XIV-B-1 is sufficiently accurate over the temperature range of the data, but it cannot be extrapolated with any reliability. An equation giving reasonable accuracy to 50°C is needed. A reference which gives the accurate densities of sucrose solutions up to 60°C has been found;[4] but as yet the data which it contains have not been obtained. The available data have therefore been examined to see if any reliable method for extrapolation exists. The density of any binary solution at a given temperature may be calculated by the relation

$$\rho = \frac{xM_1 + (1 - x)M_2}{x\overline{V}_1 + (1 - x)\overline{V}_2} , \qquad (5)$$

where x is the mole fraction of component 1:

$$\frac{X_1/M_1}{X_1/M_1 + [(1 - X_1)/M_2]} ,$$

M_1 and M_2 are the molecular weights of components 1 and 2, $\overline{V}_1$ and $\overline{V}_2$ are the partial molar volumes of components 1 and 2, and X_1 is the weight fraction of component 1.

The partial molar volumes $\overline{V}_1$ and $\overline{V}_2$ may also be functions of the composition. Often the molar volumes V_1 and V_2 may be substituted with essentially no loss in accuracy, and the solutions are said to be ideal. Since the molecular weight of one total mole is always given by the expression,

Table XIV-B-1. Constants for Use in Expressing Density as a Function of Concentration and Temperature[a]

Constant	Value
B_1	1.0003698
B_2	3.9680504×10^{-5}
B_3	$-5.8513271 \times 10^{-6}$
B_4	0.38982371
B_5	$-1.0578919 \times 10^{-3}$
B_6	1.2392833×10^{-5}
B_7	0.17097594
B_8	4.7530081×10^{-4}
B_9	$-8.9239737 \times 10^{-6}$

[a]Density expressed in g/ml, concentration as weight fraction sucrose, temperature as °C, constants valid over temperature range of 0 to 30°C and composition range of 0.00 to 0.75 weight fraction sucrose.

[4]Plato, *Wiss. Abhandl. Kaiserlichen-Normal-Eichung-Kommission* **2**, pp 140–53 (1900).

$xM_1 + (1 - x)M_2$, the actual molar volume of the sucrose solution could be calculated from the density by the relation

$$V_x = \frac{xM_1 + (1 - x)M_2}{\rho_x}, \qquad (6)$$

where V_x is the molar volume at mole fraction x and ρ_x is the experimental density at the same mole fraction. A plot, V_x against x at a given temperature, was linear within the plotting error so that sucrose solutions may be said to be nearly ideal and the following equation may be applied with reasonable accuracy:

$$\rho = \frac{xM_1 + (1 - x)M_2}{xV_1 + (1 - x)V_2}, \qquad (7)$$

when ρ is the density of sucrose solution, x is the mole fraction sucrose, M_1 and V_1 are the molecular weight and molar volume of sucrose, and M_2 and V_2 are the molecular weight and molar volume of water.

Now we note that V_1 and V_2 are both expressible as second-order polynomials in t, where t is in °C, and that the data for the molar volume of water are accurately known over the whole temperature range of interest[5] so that V_2 can be determined independently of the set of data for the density of sucrose solutions. Thus the data on the density of sucrose solutions can be used to determine the theoretical molar volume of liquid sucrose as a function of temperature. Since the curvature will be small, the density equation will have the form

$$\rho = \frac{xM_1 + (1 - x)M_2}{x(B_1 + B_2t + B_3t^2) + (1 - x)(A_1 + A_2t + A_3t^2)}, \qquad (8)$$

where $V_1 = B_1 + B_2t + B_3t^2$; $V_2 = A_1 + A_2t + A_3t^2$; B_1, B_2, and B_3 are constants determined from the sucrose solution data; A_1, A_2, and A_3 are constants determined from the data on pure water; and the other symbols have the meanings given before.

The constants in Eq. (8) are given in Table XIV-B-2. Using these constants, the maximum error in the range of the data between 0 and 30°C and 0 to 70 wt % sucrose is 4 parts in 1000. It is believed that this equation will suffer very little loss in accuracy in being extrapolated to 50°C, particularly because the ideality of sucrose solutions improves with increasing temperature and the relation for the molar volume of liquid sucrose shows but little deviation from linear dependence on the temperature.

Table XIV-B-2. Constants for Use in Expressing Density as a Function of Mole Fraction of Sucrose

Constant	Value
A_1	18.027525
A_2	4.8318329×10^{-4}
A_3	7.7830857×10^{-5}
M_1	342.30
M_2	18.032
B_1	212.57059
B_2	0.13371672
B_3	$-2.9276449 \times 10^{-4}$

3. Viscosity Relations

The viscosity data chosen for fitting are those of the National Bureau of Standards.[2] These data are tabulated as functions of composition at 1 wt % intervals from 20 to 75 wt %. Data between 0 and 20 wt % were calculated at 5°C intervals over the temperature range of 0 to 80°C, using an equation of the form

$$\ln \frac{n}{n_0^T} = A \frac{X}{1 - X} + BX^2, \qquad (9)$$

where n is the viscosity of sucrose solution at a given temperature, n_0^T is the viscosity of pure water at the given temperature, X is the weight fraction of sucrose, and A and B are temperature dependent constants. This equation was developed originally by the Bureau of Standards[2] for the data at 20°C. Values of A and B were computed from the viscosity data for pure water and the data for solutions containing 20 and 30 wt % sucrose at the desired temperature intervals.

[5] C. D. Hodgman (ed.), p 1630, *Handbook of Chemistry and Physics, Twenty-Eighth Ed.*, Chemical Rubber Publishing Co., Cleveland, Ohio, 1944.

This equation cannot be extrapolated to higher sucrose concentrations with any accuracy. The viscosity data tabulated in Tables 131 and 132 of the National Bureau have been supplemented by the data for pure water and values calculated at 5, 10, and 15 wt % sucrose at each 5°C interval using equations of this form.

In fitting the viscosity data, it is recognized that water is an associated liquid containing clusters of molecules with a high degree of structural order and that sucrose itself is capable of forming hydrogen bonds with the water. Since varying the amounts of sucrose may be expected to affect the structural arrangement of the solution more than varying the temperature, an equation was sought which would accurately describe the change of the viscosity with temperature at constant composition. Reasoning that one of the more successful viscosity treatments is the "hole" theory of Eyring and associates[6] and noting the analogy between the number of "holes" per unit volume and the vapor pressure, the Antoine equation, so successfully used with vapor pressure data, was tried. This equation as related to viscosity has the form

$$\log n = A + \frac{B}{t + C}, \tag{10}$$

where n is the viscosity at a given composition, t is the temperature in °C, and A, B, and C are composition-dependent constants. This equation may be more familiar in the form

$$\ln \frac{n}{n_0} = \frac{\Delta H^*}{R(T - T_0)}, \tag{11}$$

where

$$\ln n_0 = 2.303A,$$
$$\Delta H^*/R = 2.303B,$$
$$T_0 = 273.16 - C,$$

n_0 is the limiting viscosity, ΔH^* is the heat of activation for viscous flow, R is the gas constant, and T_0 is a temperature correction which fixes the virial coefficients, α, β, γ, etc. in the expression

$$\frac{\Delta H^*}{RT}\left(1 + \frac{\alpha}{T} + \frac{\beta}{T^2} + \frac{\gamma}{T^3} + \ldots\right). \tag{12}$$

When this evaluation is carried out, constants A, B, and C are found at any given composition such that the viscosity data as a function of the temperature are reproduced to about 3 parts in 1000. It is now necessary to determine A, B, and C as functions of the composition. The Antoine constant C has been shown to be fitted when plotted as a function of the mole fraction by the right negative leg of a hyperbola having the equation

$$C = 146.06635 - 25.251728 \times \left[1 + \left(\frac{X}{10.070674842}\right)^2\right]^{1/2}, \tag{13}$$

where X is the mole fraction and C has the units of degrees in the Centigrade or Kelvin scale.

Substitution of this equation for C in Eq. (10) for the various compositions studied results in an insignificant loss in accuracy so that evaluation of A and B as functions of mole fraction is now in progress. These constants plot as smooth functions of the mole fraction sucrose but contain some features which are difficult to describe analytically using any simple function. Preliminary study indicates that these constants can be expressed in terms of polynomials provided one polynomial expression is used to describe the values from 0 to about 55 wt % sucrose and a second is used over the range of 45 to 75 wt % sucrose. Expressed in terms of mole fraction sucrose, these ranges are 0.00 to 0.06 and 0.04 to 0.14 respectively. It is believed that this approach will yield analytical expressions with the desired accuracy of 1% or better.

Attempts to analyze the A constant in terms of the limiting viscosity concept, using the relations that the reciprocal of the viscosity is the fluidity and that the molar fluidities are additive according to the mole fraction rule, did not result in anything easier to treat analytically than is the A constant as a function of mole fraction itself. Also attempts to handle the B constant in terms of molar heats of activation using the additivity rule were similarly unfruitful.

[6] S. Glasstone, K. J. Laidler, and H. Eyring, *The Theory of Rate Processes*, McGraw-Hill, New York, 1941.

XV. Centrifuge Instrumentation

R. H. Stevens M. J. Bartkus

A. REQUIREMENTS

The instrumentation complex required for zonal-centrifuge operation is divided into three basic systems. These are (1) the controls and indicators for actual centrifuge operation, (2) the speed-sensing system for determining $\int \omega^2 \, dt$ at any time during the centrifuge run, and (3) the analytical monitor for determining the distribution of particles in the gradient recovered from the centrifuge. For work with potentially hazardous materials it is desirable to mount as much of this complex as possible away from the centrifuge. During the present report period a complete prototype has been constructed and extensively tested.

B. INSTRUMENTATION

Instruments associated with the modified Beckman Spinco L centrifuge which uses the B-II rotor are shown in Fig. XV-B-1. Mounted in the centrifuge cabinet is the drive motor, heating and cooling system vacuum pump, thermister rotor temperature sensor, thermocouple environmental pressure sensor, a proximity type H1 speed sensor, and a mechanical tachometer. A Beckman DU spectrophotometer, located in the glove box, is used to measure the ultraviolet absorbance of the density gradient of the centrifuge effluent stream. The remaining analytical and control instruments were packaged in two cabinets which are remote from the centrifuge.

The analytical cabinet contains a Gilford model 205 light stabilizer which powers the hydrogen lamp used in the spectrophotometer. A Gilford model 220 optical-density converter, also connected to the spectrophotometer, produces a dc output voltage proportional to the uv absorbance which drives a Brown "Electronik" 10-mv absorbance recorder. A Sola type CVH-1 constant-voltage transformer supplies power for the analytical instruments.

The rotor speed control, indicators of temperature and pressure in the centrifuge, a Bentley E15 power supply, and a Bentley D152 amplifier have been assembled on a control panel in the control cabinet. Also mounted in this cabinet is a Hewlett Packard model 500BR frequency meter, which senses the rotor speed signal from the Bentley amplifier and provides a dc output voltage proportional to speed. This voltage drives a Leeds and Northrup model H "Speedomax" indicator, which was modified by the addition of a squaring circuit. The squaring circuit output is electronically integrated in the Royson "Lectrocount" integrator. The Royson provides a digital indication of the time integral of the square of the rotor's angular velocity, for example,

$$\int_{t=t_0}^{t=t_1} \omega^2 \, dt \, .$$

Additional instrumentation required for driving a C-II rotor includes a Hewlett Packard model 200 ABR audio-frequency (af) generator, a phase-splitting control panel, and two Bogen model MO 100 booster amplifiers. The Royson "Lectrocount" was modified to increase the integrating rate because the frequency meter output was reduced. A dual scale on the L. and N. "Speedomax" model H indicator facilitates reading speed of either the B-II or C-II rotor directly.

UNCLASSIFIED
PHOTO 62578

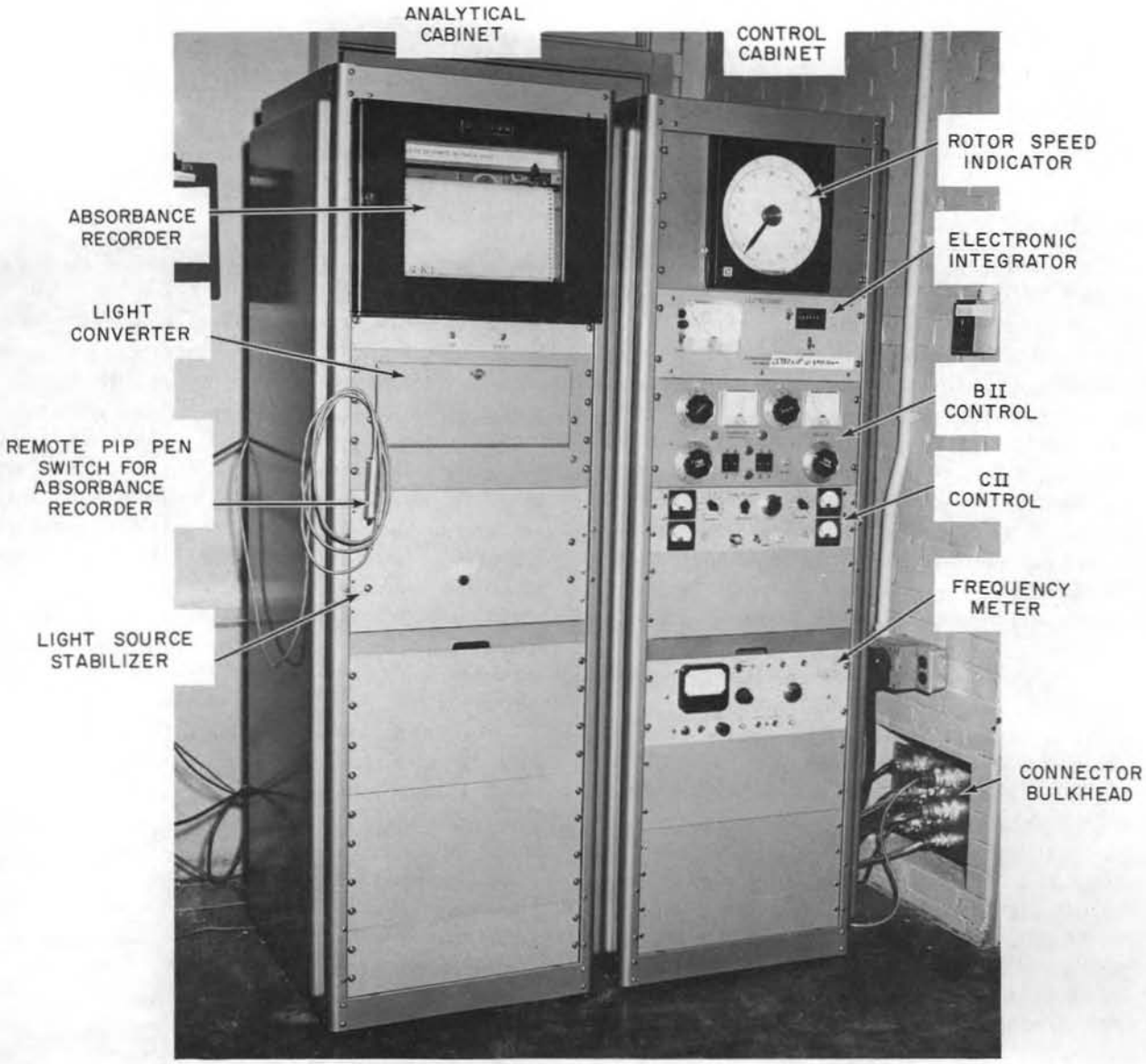

Fig. XV-B-1. Analytical and Control Instruments for B-II and C-II Rotor Systems. The B-II containment system shown in Fig. XII-B-1 is in an adjoining room.

XVI. Electron Microscopy

W. W. Harris

Biological monitoring methods for viral systems depend upon plaque, serological, or live-animal tests. Plaque testing requires several hours, usually overnight. Serological methods vary in time required for positive identification, while bioassays require weeks to months for completion. None of these methods determines the total number of viral particles separated, only the infectivity. Electron microscopy is a physical method, when the particles are sufficiently concentrated, for rapid detection and identification of known virus particles. The method can be semiquantitative for the number of particles present but gives no information about virulence.

During this period, electron microscopy was used to monitor 16 zonal-centrifuge runs and for complete surveys of two of these runs. Positive identifications were obtained within an hour or two after withdrawal from the centrifuge for T2 and T3 phages, types 2 and 5 adenovirus, and the Rauscher agent (Fig. XVI-A-1). In several runs, information about stability of the viral particles to centrifuging conditions was obtained by comparison of particle morphology in relation to pH or to gradient composition.

Two of the zonal-centrifuge runs of this period were attempts to isolate a suspected viral particle associated with the ORNL myeloid leukemia of RF/UP mice. Although a viral particle has been observed in infected tissue,[1] its morphology in free suspension is unknown. Several virus-like particles were observed after four days of examination, and one or two such particles were observed after several more days of examination of samples from laboratory preparations of tissue. This number of observations is insufficient for any conclusion to be made about the viral agent. The tailed particle observed was seen in the fraction just preceding the mitochondria peak and resembles a Rauscher particle.[2]

The sharpness of separations expected of the zonal centrifuge systems makes consideration of detailed microscopy of entire peaks with the possibility of detecting heretofore unobserved morphological differences necessary. There are many examples in the literature of discrepancies in virus sizes as measured from tissue cross sections and partially separated particles. These discrepancies have been attributed to alterations of the particles by differences in environment.

The negative staining method of Brenner and Horne[3] and the manipulative techniques of the Laboratory of Viral Oncology of the National Cancer Institute[4] were used throughout this period. The limit of detection was 10^4 to 10^5 particles per ml. By centrifuging the entire sample received from the zonal centrifuge onto a microscope specimen grid, a gain in sensitivity of several orders of magnitude is expected using a Sharp rotor and a Spinco centrifuge.

Although specimen techniques used for this period have been adequate for identification and morphological examination, separate study of environmental factors such as pH, ion types, and tonicities will be made for each new zonal biophysical separation. For viral systems such as RS and polio, additional morphological examinations requiring treatment with detergents and/or enzymes to establish the structure of the particle core will be undertaken. By use of more quantitative methods, comparisons between particle counts and infectivity will be made for some of the respiratory viruses under study.

[1] D. F. Parsons *et al.*, *Cancer Res.* **22**, 728 (1962).

[2] R. F. Zeigel and F. J. Rauscher, *J. Natl. Cancer Inst.* **30** (1963).

[3] S. Brenner and R. W. Horne, *Biochim. Biophys. Acta* **34**, 103 (1959).

[4] Visit to NIH by T. W. Bartlett and W. W. Harris; oral communication, A. J. Dalton, Mar. 28, 1962.

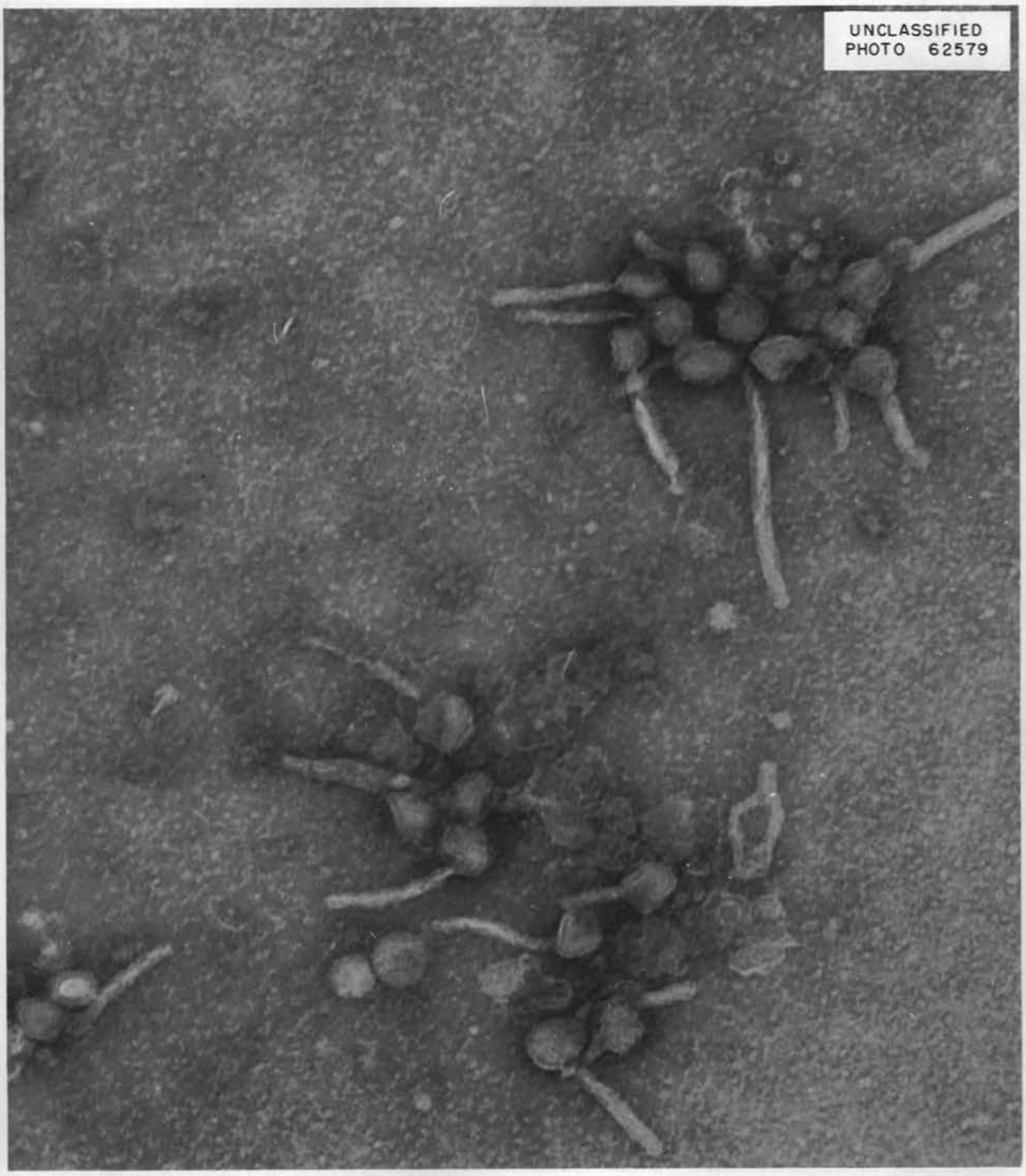

Fig. XVI-A-1. Electron Micrograph of Rauscher Virus Particles. 150,000X.

XVII. Ancillary Studies

A. STUDIES ON SYNCHRONIZED CELL DIVISION

G. M. Padilla T. W. James R. H. Stevens

Cell components have generally been isolated from tissues which contain more than one cell type. In addition, cells of the same type may be in quite different physiological states in different parts of the tissue. It would be desirable to begin all fractionation with homogeneous cell populations with all cells in the same stage of the cell cycle. This approach has the advantage of also providing means for studying changes which may occur during certain portions of the cell cycle. The problem of synchronizing cell division and growth in large populations of cells is therefore a central one in the present program. While many formidable technical obstacles remain, the most difficult single problem, that of continuous cell counting under sterile conditions, has now been solved.

The engineering design of a fully automated pilot-plant-size system to synchronize the growth of large numbers of cells is shown in Fig. XVII-A-1. The functional requirements for this system have been described.[1]

The cell synchronizer in use was described in a more recent report.[2] This unit consists of a 5-liter water-jacketed culture vessel programed with a repetitive temperature cycle (17.5 hr at 14.5°C and 6.5 hr at 28.5°C), which induces cell-division synchrony in the colorless flagellate *Astasia longa*.[3,4] A cell-density monitor has been developed which together with potentiometric electrodes (e.g., Oxygen Electrode, Beckman) permits one to determine continuously the pattern of cell-division synchrony and changes in the respiratory activity of the cells. The results of these investigations are presented in this report. In addition, alternate techniques for continuous cell counting and biochemical assays are being developed and shall be reported later.

1. Respiratory Activity of Synchronized Cells

The implementation of cell-division synchrony and design of culture apparatus, probes, in-line assays, and other continuous monitoring devices, is based on the proposition that a synchronized culture is an entity whose attributes and physiological functions must be examined concomitantly with the occurring process of cell division. This approach will allow the initial determination of the existence of an event that may be uniquely placed in the schedule that is called the cell cycle. If the culture vessel is designed large enough, ample quantities of synchronized cells are readily available for further studies by use of routine biochemical and biophysical techniques.

The cellular function that is being initially examined in relation to the synchronized cell cycle is the respiratory activity. The continuous measurement of oxygen tensions has become possible since the development of oxygen electrodes that retain their potentiometric function for considerable periods of time. Such an electrode has been incorporated in the design of the

[1] T. W. James and R. H. Stevens, *Joint NIH-AEC Zonal Centrifuge Development Program Semiann. Rept. Dec. 31, 1962*, ORNL-3415, p 86.

[2] T. W. James, *Biol. Div. Semiann. Progr. Rept. Feb. 15, 1963*, ORNL-3427, p 104.

[3] G. M. Padilla and T. W. James, *Exptl. Cell Res.* **20**, 401 (1960).

[4] J. J. Blum and G. M. Padilla, *Exptl. Cell Res.* **28**, 512 (1962).

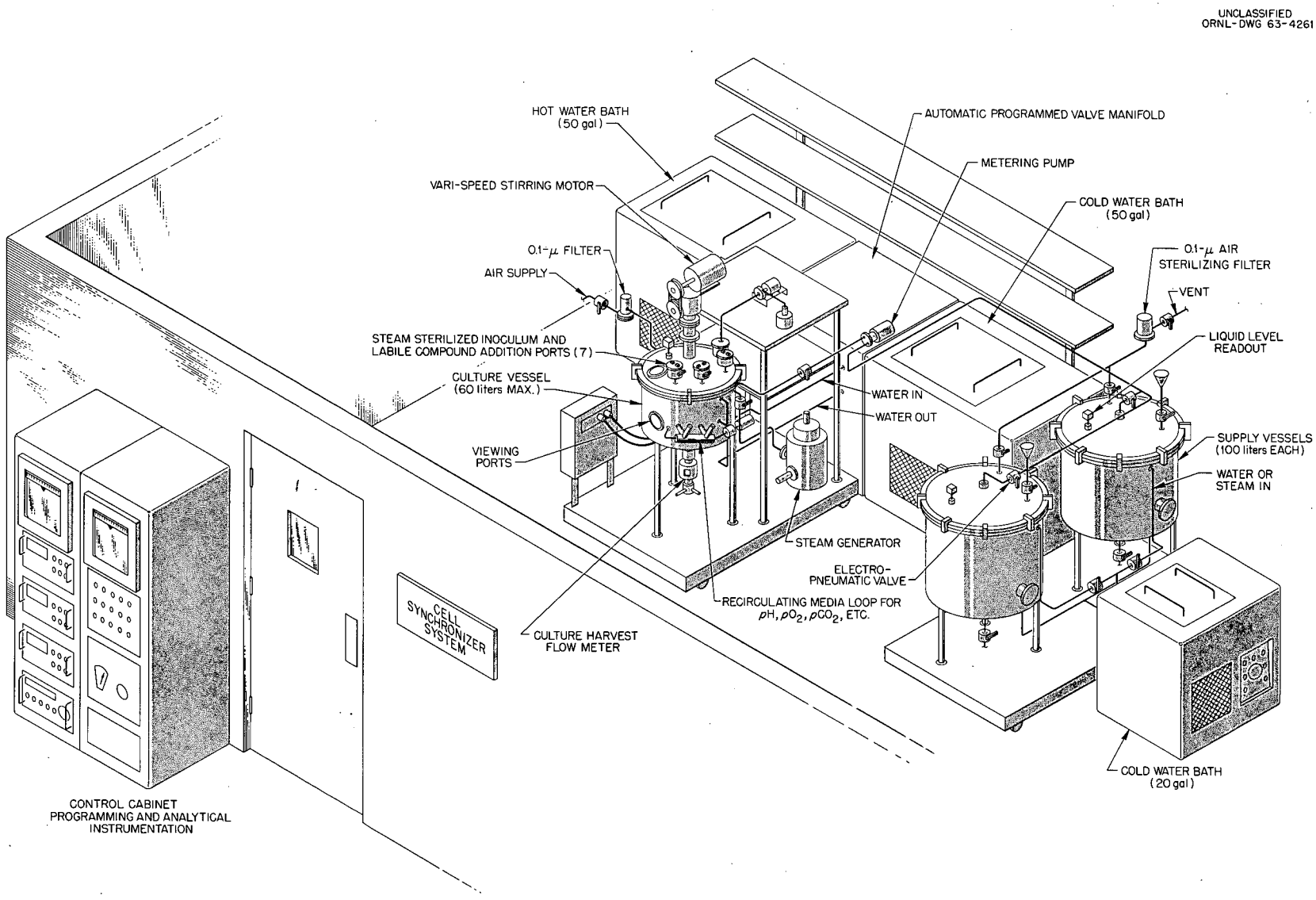

Fig. XVII-A-1. Conceptual Design of Cell Synchronizer System.

cell synchronizer. Figure XVII-A-2 illustrates a typical experiment in which changes in the oxygen tension in the medium of synchronously dividing *Astasia* have been recorded.

During the cold period (14.5°C) the oxygen tension decreases very slowly from approximately 95 to 65 mm Hg. During this interval the cell density remains virtually constant at about 120,000 cells/ml. As soon as the warm period begins (28.5°C), there is a rapid decrease in the level of dissolved oxygen to a partial pressure of 7 mm Hg. This rapid decrease occurs in the predivision period, which is coincident with the initial phases of mitosis[4] and reflects increased oxygen consumption by the cells. A slight decrease occurs throughout the burst of division, but at this analyzer setting it is hardly noticeable.

The formulation

$$\frac{dC}{dt} = \frac{dD}{dt} + \frac{dO_2}{dt}$$

relates the rate of oxygen utilization by the entire culture (dC/dt) to the rate of diffusion of oxygen (dD/dt) into a culture of a given volume, stirring rate, and at a given temperature, oxygen tension, etc. The rate of oxygen utilization (dO_2/dt) by

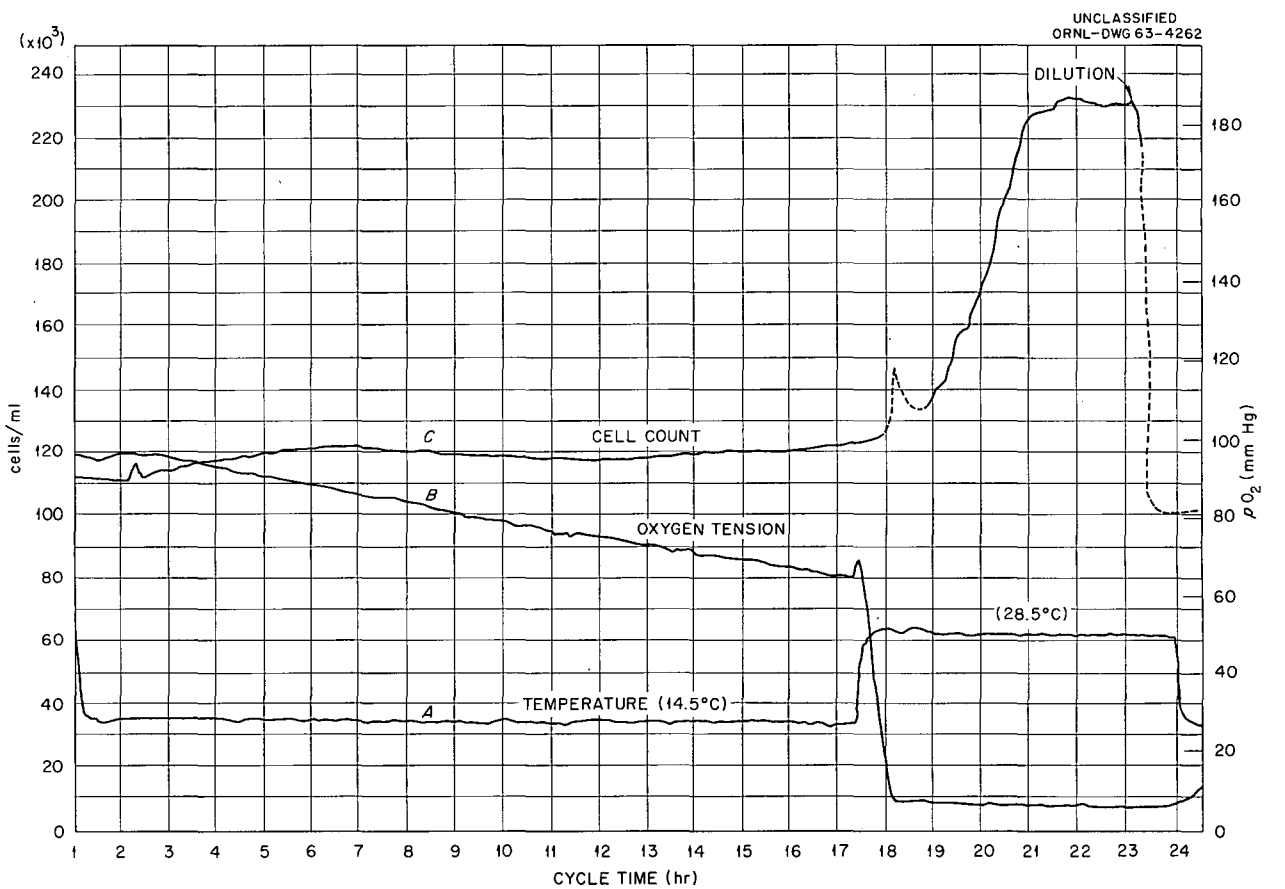

Fig. XVII-A-2. Continuous Recordings of a Synchronized Burst of Division of the Flagellate *Astasia longa*. Three tracings are shown: (*A*) temperature record showing the 24-hr temperature cycle (17.5 hr at 14.5°C and 6.5 hr at 28.5°C); (*B*) dissolved oxygen content of the medium measured with an oxygen electrode and expressed on the right ordinate in mm Hg for the partial pressure of O_2; and (*C*) cell density recording as measured by a continuous-flow Coulter counter and given on the left ordinate in cells/ml.

the cells at any time may be derived by this relation. In essence, the entire culture is treated as a large-scale respirometer, differing from the conventional type in that the cells respire *ad libitum* and are permitted to grow. Figure XVII-A-3 shows the data derived in this manner. It is clear that the maximum rate of oxygen utilization occurs at the predivision period with a constant rate through the burst of cytokinesis (there is an apparent decrease by virtue of the doubling in cell number). The figure also shows that cell division occurs at low oxygen tensions and that after it is completed (from the 21st to the 23d hr of the cycle) the rate of respiration is reduced to a level comparable with that of cells in the cold period. This rate is, in fact, considerably lower than that found for exponentially dividing cells at 28.5°C (i.e., QO_2 of 60).[5]

These results indicate that with temperature-induced synchrony, where a repetitive temperature cycle of this kind is used, there are periods of maximum and minimum respiratory activity, reflecting or possibly contributing to the synchronization process. They also emphasize the need to examine further the energetics of cell division.

2. Other Investigations

The relation that exists between the nature of the medium and cell-division synchrony are being examined. In particular, the effects of varying the concentration of reduced sulfur compounds on the pattern of synchrony are now under scrutiny. This work rests on an earlier demonstration that compounds such as mercaptoacetic acid (thioglycolic acid) are required for continued cell-division synchrony in *Astasia* grown on a chemically defined medium.[6] It is hoped that by using labeled intermediates seen in the synthetic pathways of the sulfur amino acids, an insight will be gained into the exact biochemical role that these compounds have in cell division.

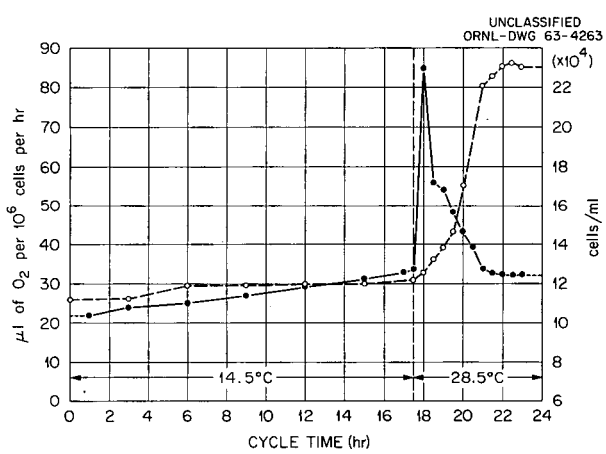

Fig. XVII-A-3. Respiratory Activity of Synchronously Dividing *Astasia longa*. Changes in QO_2 (expressed on the left ordinate in μl per 10^6 cells per hr) are indicated by the solid line. The changes in population density are given on the right ordinate in cells/ml and are indicated by the broken line.

B. AUTOMATIC CARBOHYDRATE ANALYZER

J. G. Green N. G. Anderson

1. General Considerations

A device for the separation and evaluation of saccharidic components is being developed to assist in the evaluation of materials obtained from the zonal ultracentrifuge and to facilitate the examination of naturally occurring carbohydrates.

Although sugars do not exist normally as charged species, it is known that they interact with certain ions, such as borate, to yield negatively charged complexes. Khym and Zill[7] utilized this principle to separate several sugars by ion exchange using an anionic exchange resin in the borate form and eluting with potassium tetraborate solutions. Subsequently, similar separations have been performed by Hallén[8] using manual effluent evaluation and by Syamananda *et al.*[9] employing a Technicon[10] autoanalyzer system to evaluate the effluent. Jones *et al.*[11] effected separation

[5] B. W. Wilson and T. W. James, *Exptl. Cell Res.*, in press.

[6] G. M. Padilla and T. W. James, "Continuous Synchronous Cultures of Protozoa" in *Methods in Cell Physiology* (ed. by D. M. Prescott), vol I, Academic Press, New York, in press.

[7] J. X. Khym and L. P. Zill, *J. Am. Chem. Soc.* **74**, 2090 (1952).

[8] A. Hallén, *Acta Chem. Scand.* **14**, 2249 (1960).

[9] R. Syamananda, R. C. Staples, and R. J. Block, in press.

[10] Technicon Controls, Inc., Chauncey, N.Y.

[11] J. K. N. Jones, R. A. Wall, and A. V. Pittet, *Can. J. Chem.* **38**, 2285, 2290 (1960).

of mono- and oligosaccharides on cationic exchange resins in neutral salt forms, and numerous separations of sugars by adsorption chromatography have appeared in the literature.

Preliminary reports concerning development of the present instrument have appeared.[12] The essential components of the apparatus are depicted schematically in Fig. XVII-B-1, and a photograph of the machine is shown in Fig. XVII-B-2. A mixture of sugars as borate complexes is separated on Dowex 1-X8 anion exchange resin in the borate form by elution with a linear sodium tetraborate gradient. The column effluent is processed to yield a colored stream, which is monitored by a spectrophotometer, and the absorbance of the stream is recorded to give a permanent record of the analysis.

[12]J. G. Green and N. G. Anderson, *Biol. Div. Semiann. Progr. Rept. Aug. 14, 1962*, ORNL-3352, p 128; *Biol. Div. Semiann. Progr. Rept. Feb. 15, 1963*, ORNL-3427, p 118.

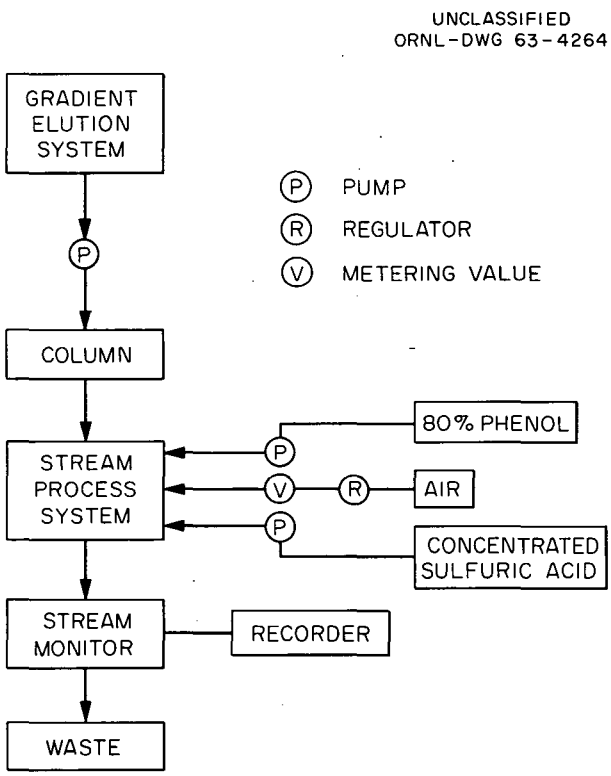

Fig. XVII-B-1. Diagrammatic Representation of Carbohydrate Analyzer.

2. Materials and Design

Standard Solutions. – Standard solutions of the individual sugars and of a mixture of all the sugars at the same concentration are used. These solutions contain arabinose, cellobiose, fructose, galactose, glucose, lactose, maltose, raffinose, rhamnose, ribose, sorbose, sucrose, and xylose in a concentration of 5 μM per ml. Mannose was added later; lactose was chosen as an internal standard.

Column. – Initially, jacketed glass columns measuring 0.9 × 150 cm and 0.9 × 60 cm fitted with ball-and-socket joints were used. These columns were not suitable for pressures in excess of 80 psi. To evaluate the performance of very fine resins, jacketed columns employing heavy-walled borosilicate glass tubing were fabricated. The fitting used at the base of the column has been modified to support the resin and to minimize dead space by using a 5-μ porosity-sintered, stainless steel disk in the snubber fitting. These columns have been operated at 160 psi and tested to 200 psi with no evidence of failure.

In the present experimentation, Dowex 1-X8 (ref 13) has been used; however, 10% cross-linked resin has yielded essentially similar resolution. Somewhat higher resolution has been obtained with a 4% cross-linked resin, but the behavior of the resin under pressures in excess of 20 psi has not been evaluated. Trials with Dowex 2-X10 yielded unsatisfactory resolution, for nearly all the sample placed on the column eluted early as a single skewed peak.

The size of the resin particles greatly influences the resolution obtained. Finer resins yield decreased eluted bandwidth but require increased pressure to maintain a specific flow rate. Following the development of the 200-psi columns, experimentation is under way to evaluate more exactly the influence of resin particle size on column resolution in this system.

Resolving capability of the resin is affected by the temperature at which the elution is performed. In this system, the width of an eluted band decreases with temperature increase in the range from ambient to 55°C. Little improvement in resolution is obtained with further temperature

[13]Bio-Rad Laboratories, 32nd and Griffin, Richmond, Calif.

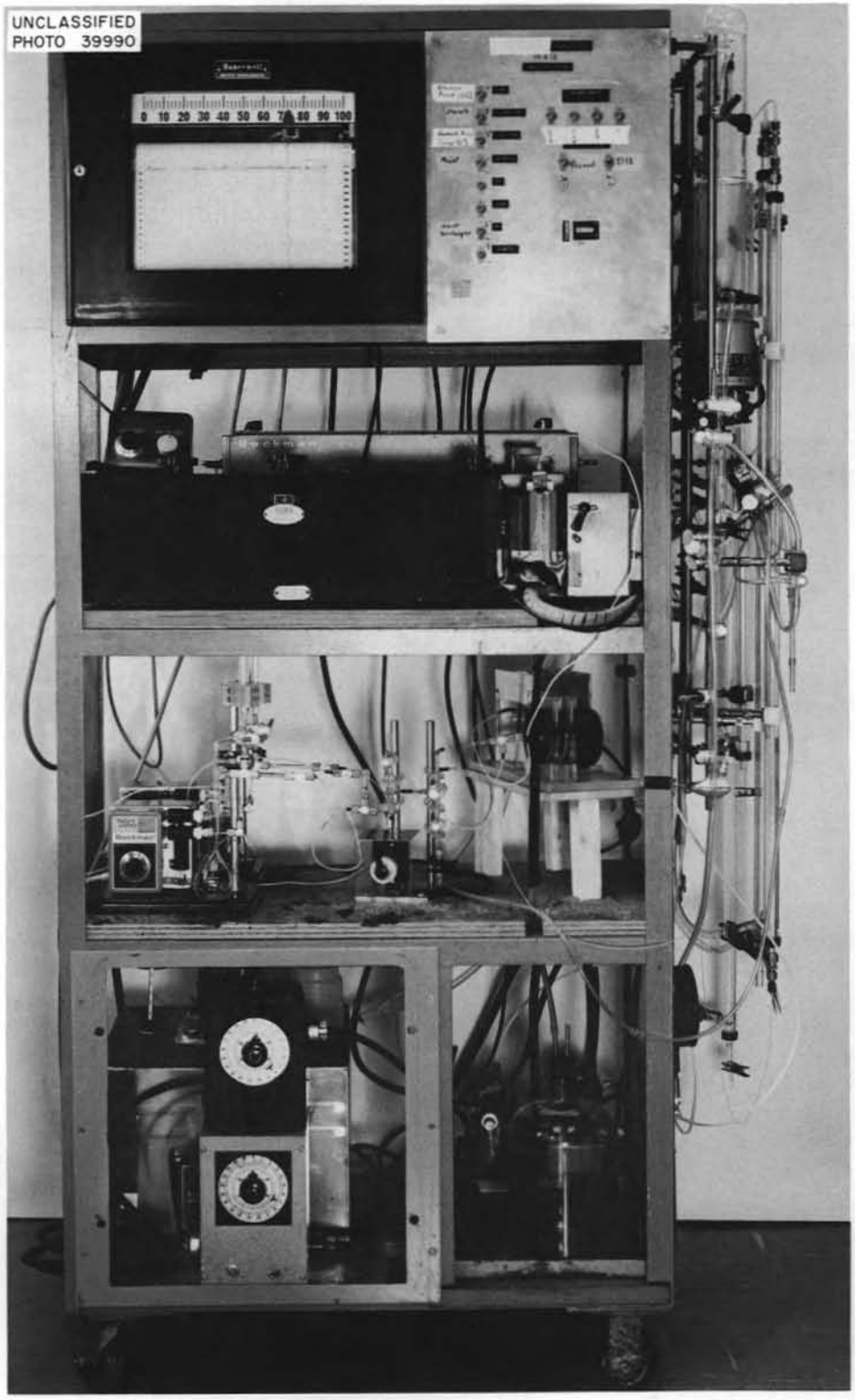

Fig. XVII-B-2. Photograph of Assembled Carbohydrate Analyzer.

increase, and at temperatures in excess of 65°C some sugars, notably fructose, appear to be partially degraded during passage through the column. Routinely, separations are performed at 50°C or, for increased resolution, at 55°C where resolution is nearly optimal and degradative losses are inconsequential.

The resin is prepared for use by washing in sequence with 1 *N* hydrochloric acid, 1 *N* sodium hydroxide, water, and the borate eluting solution. Satisfactory results have been obtained by washing the hydroxide form of the resin with 0.5 *M* boric acid and suspending the resin in the borate eluting solution. The resin in a 30% slurry is packed in the column under air pressure and equilibrated several hours with the starting eluting medium prior to use.

Elution System. – An elution system using a borate salt was chosen to permit reuse of a packed column following a simple equilibration with the initial eluting solution. Sodium tetraborate has been used in the present system, and boric acid has been employed to reduce the pH of the solution to the range of 8.65 to 8.80, which yields the best separations. In practice, a linear concentration gradient with a starting concentration of 11.7 g of sodium tetraborate and 2.1 g of boric acid per liter grading to a final concentration of 38.9 g of the salt and 7.0 g of the acid per liter has given excellent separation. The total volume of solution used may be varied over a wide range to yield any desired degree of separation or to fit a specific problem.

To prevent the formation of air bubbles in the lower part of a column, especially at elevated pressure and temperature, it has been necessary to deaerate the eluting solution before passage to the column. Deaeration is accomplished by warming the eluting medium in the terminal gradient cylinder through jacketing of the cylinder. Water from the 50°C circulating bath is passed through the water jacket of the column to the water jacket of the final cylinder and back to the bath. The eluting solution is delivered from the terminal gradient cylinder to the column by a Milton Roy Minipump.[14] The pressure at the top of the column can be read from a pressure gage inserted in the line between the pump and the column.

Stream Processing System. – Since carbohydrates do not possess characteristic uniform spectral absorption bands and because current automatic polarimetric, and refractometric instruments lack sufficient sensitivity to monitor dilute column effluents, a colorimetric procedure was chosen to monitor the column eluate. The phenol–sulfuric acid method[15] has been adapted to the present process. It is suitable for all carbohydrates and yields maximal absorption at 485 to 490 mμ for hexoses and di- and oligosaccharides, at 480 mμ for pentoses and at a lower wavelength for glycerol.

Eighty-percent phenol and concentrated sulfuric acid are dispensed by solution metering pumps. To render the pump suitable for metering the acid, it was necessary to use Teflon-coated valve diaphragms supplied in kit form by the manufacturer and to replace the valve and cylinder retainers with parts fabricated from iron-filled Teflon. As shown in Fig. XVII-B-3, pulsation-free flow from the piston pump is obtained by having the pump deliver through a glass check valve to an air dome. The latter delivers the fluid through a capillary of suitable bore and length to the mixer. Thus, pulsation-free flow is obtained, and the check valve isolates back pressure of the system from the pump except during the delivery portion of the piston stroke.

In the automated system employed here, the phenol and acid are mixed before addition of the column effluent to preserve resolution obtained from the column. The mixing module, shown in Fig. XVII-B-4, consists of a stream isolating chamber, a mixing chamber, a reservoir and air trap, and a stream segmenting manifold. The reagents are stirred by a Teflon-coated, magnetically driven stirring bar. The isolation chamber interposes an air gap between the phenol and acid streams, preventing line plugging by dehydration of the phenol following accidental contact of the reagents. Some air is liberated during mixing of the reagents but is trapped within the reservoir dome. The mixed reagent stream is segmented with air at a three-way Teflon stopcock. The air is reduced from line pressure to 5 psi by an acetylene regulator and metered by an integral metering valve in the lower

[14] Milton Roy Co., 1300 East Mermaid Lane, Philadelphia, Pa.

[15] M. Dubois *et al.*, *Anal. Chem.* **28**, 350 (1956).

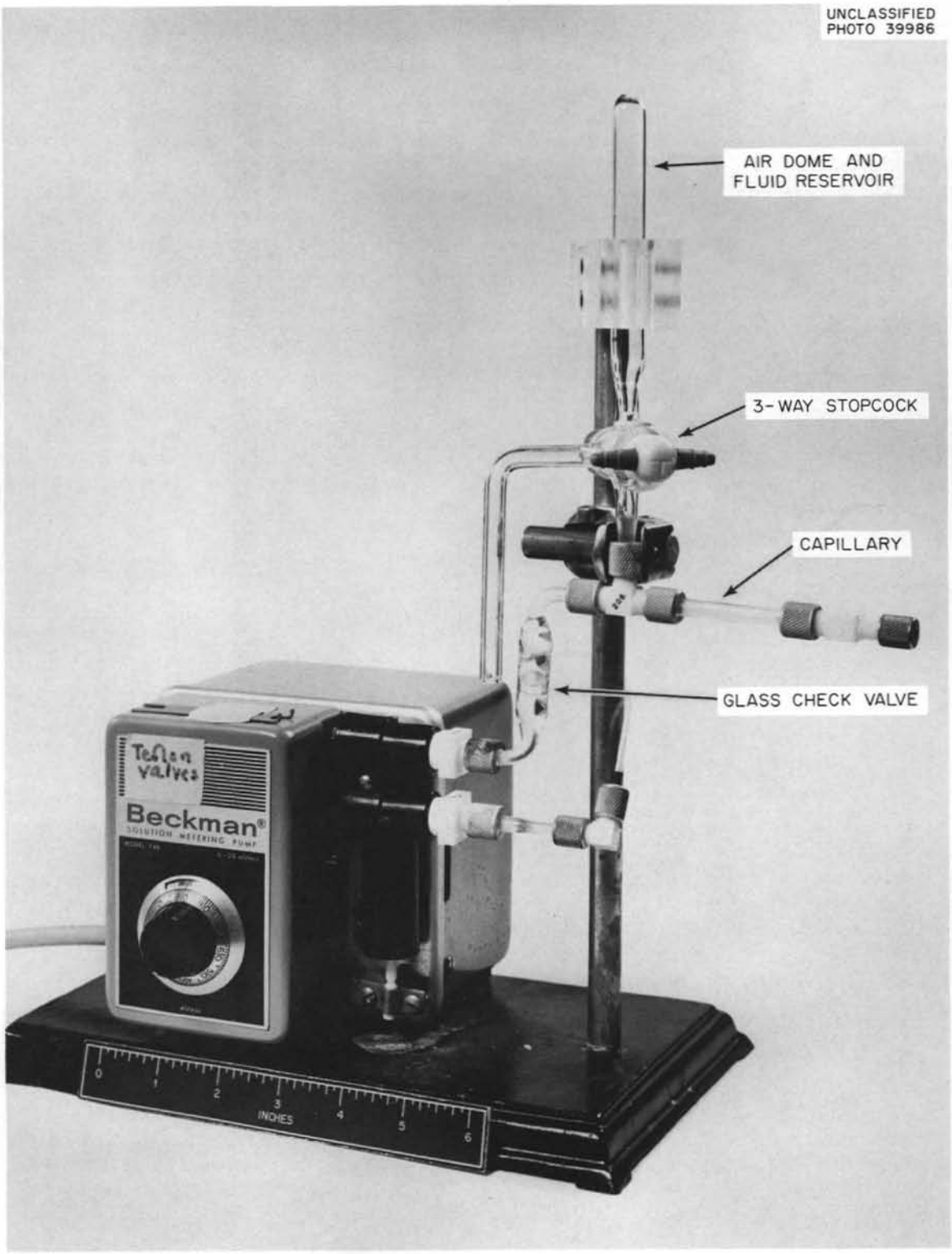

Fig. XVII-B-3. Application of Beckman Solution Metering Pump to Pulsation-Free Flows on Carbohydrate Analyzer.

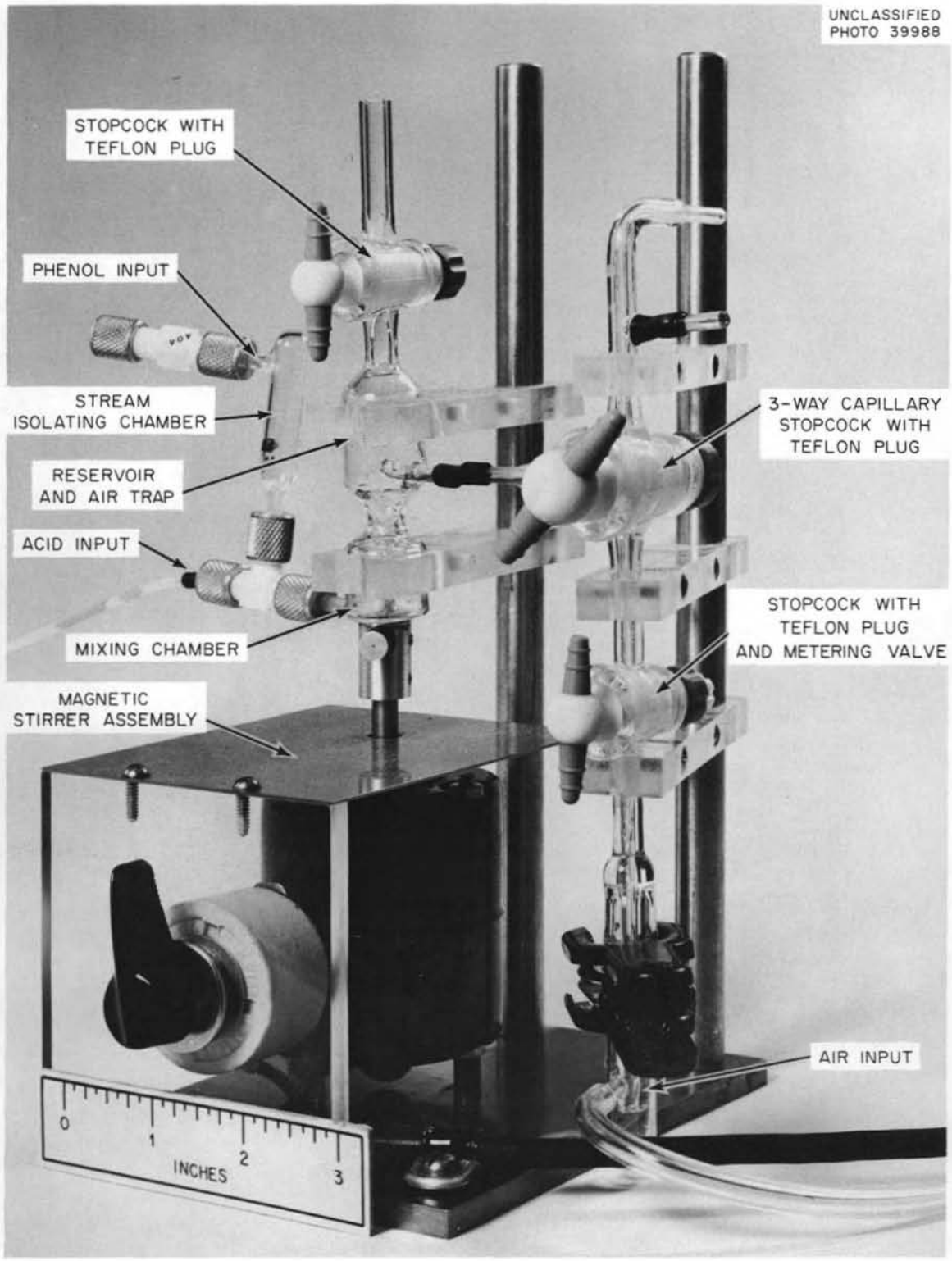

Fig. XVII-B-4. Mixing Module.

stopcock in Fig. XVII-B-4. The size of the segmenting air bubble is determined by the size of the bore of the Teflon plug in the three-way stopcock.

The uniformly segmented reagent stream is conducted to a heat exchanger where the heat of mixing of the aqueous column effluent and the reagent stream causes color development to occur. The heat exchanger shown in Fig. XVII-B-5 consists of four borosilicate glass coils contained in a box fabricated of aluminum and methyl methacrylate plastic.

It is possible to selectively air purge the stream-processing system from the reservoir dome at each pump to the flow cell, a procedure which would be difficult and perhaps hazardous to perform with water.

Flow Rates. – Suitable elution flow rates vary with the diameter of the column employed, but, in general, flow rates of 0.65, 1.26, and 1.76 ml/min have been used with the $^3/_8$-in., $^1/_2$-in., and 0.9-cm columns respectively. In most applications, the acid is dispensed at 4.20 ml/min and the 80% phenol at 1.0 ml/min. Color intensity of the monitored stream appears to be independent of the effluent flow rate at these volumes. In the proportions dispensed, the mixed reagent yields maximal immediate color development for 35 min after mixing; therefore, the 8-ml holdup volume of the mixer does not result in a reduction of the color intensity.

Stream Monitoring and Readout. – The stream from the heat exchanger is conducted to a 10-mm Technicon flow cell mounted in a Beckman DU

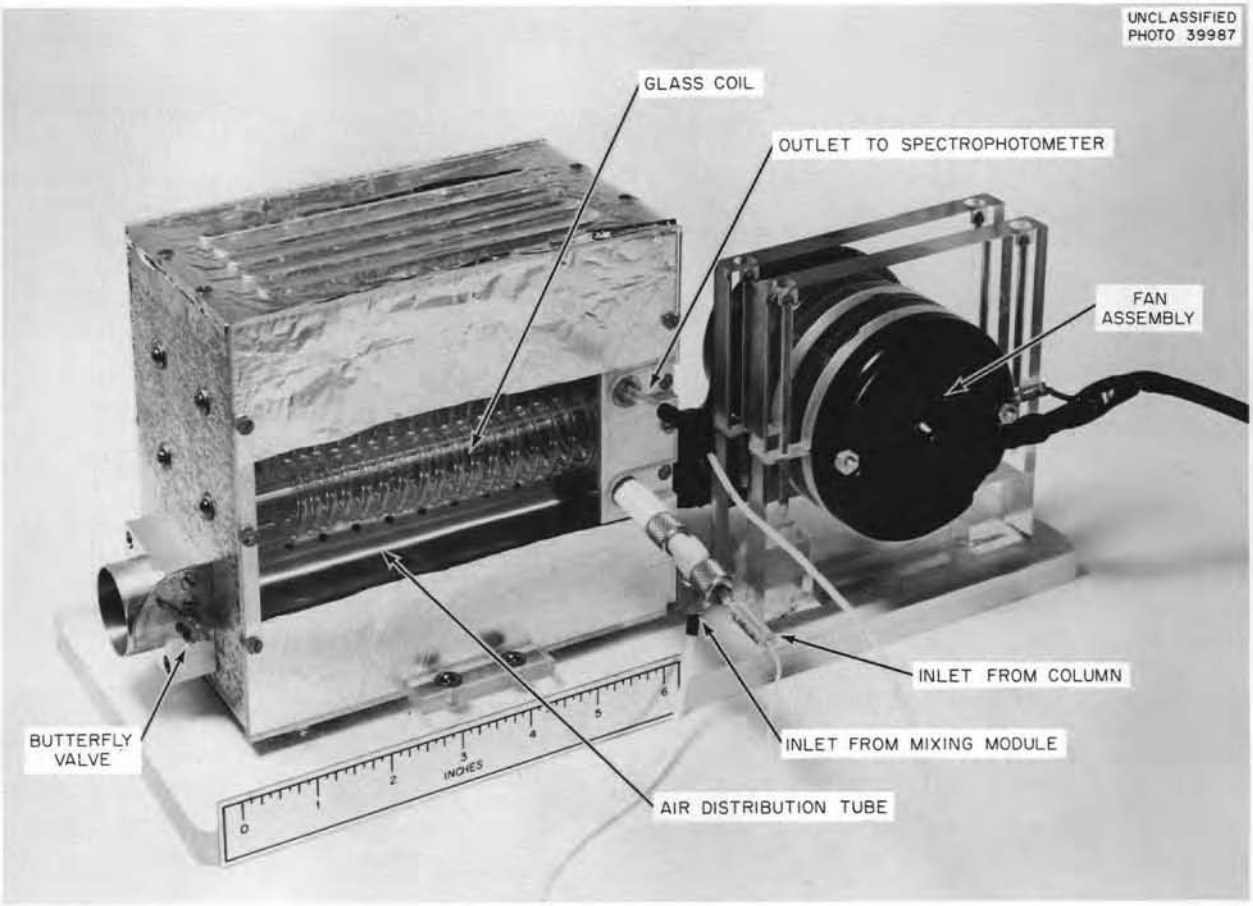

Fig. XVII-B-5. Photo of Heat Exchanger.

spectrophotometer adapted for continuous recording. The cell is spring-mounted in a cell compartment fabricated in two halves from polyvinyl chloride, is adjustable vertically and laterally, and is isolated from the spectrophotometer by cemented glass windows. The stream is drained vertically downward to a waste vessel from the cell. The spectrophotometer output is recorded on semilog paper by a 10-mv potentiometric single-pen recorder. Gaussian curves are obtained, and preliminary investigation indicates that the quantity of an eluted sugar is proportional to the area of the recorded curve.

3. Performance

The data in Fig. XVII-B-6 and XVII-B-7 indicate that in its present form the analyzer is a serviceable research tool. However, technical refinements in the stream-processing and monitoring systems are contemplated, and investigation of the effects of resin size and column dimensions on resolution is being conducted. In addition, experimental studies on separation of phosphorylated intermediates by ion exchange and of carbohydrate polymers by molecular sieving are planned.

No well-established procedures comparable with nucleotide fractionation techniques have been derived for the naturally occurring carbohydrates; therefore, sample preparation techniques such as alcohol extraction and precipitation, acid and alkaline extraction, and hydrolytic procedures require further study, which will be facilitated by the analyzer.

The analyzer will be a valuable complement to research activity in investigation of cell constituents, food and drug monitoring, quality control, and other areas.

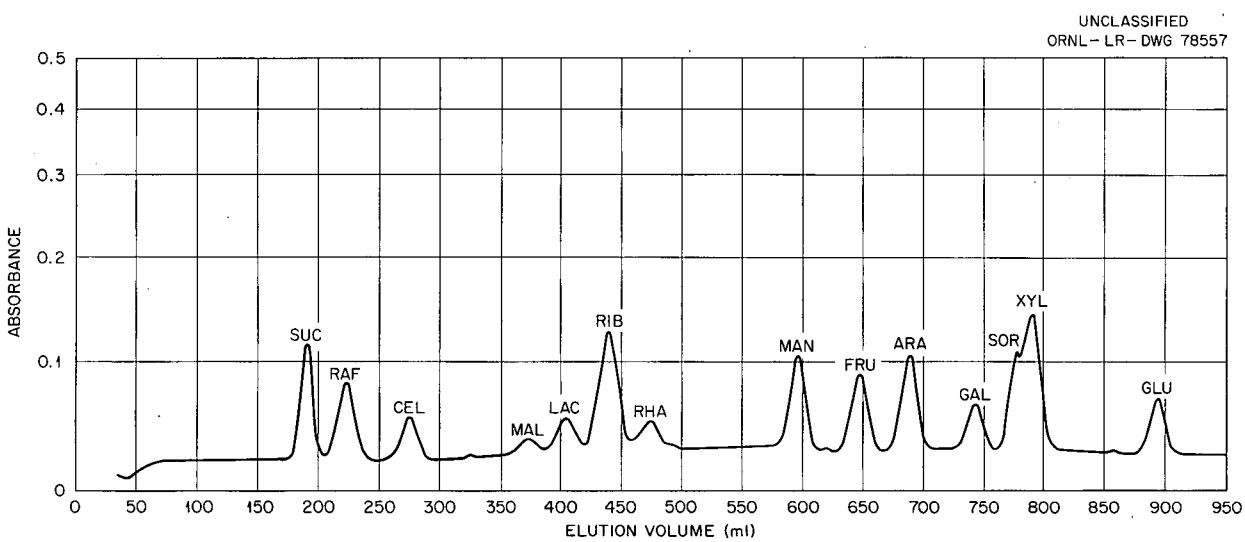

Fig. XVII-B-6. Separation of a Standard Mixture on a Long Column. Mixture contains 150 μg of each of 14 sugars on Dowex 1-X8 in a column 0.9 × 150 cm.

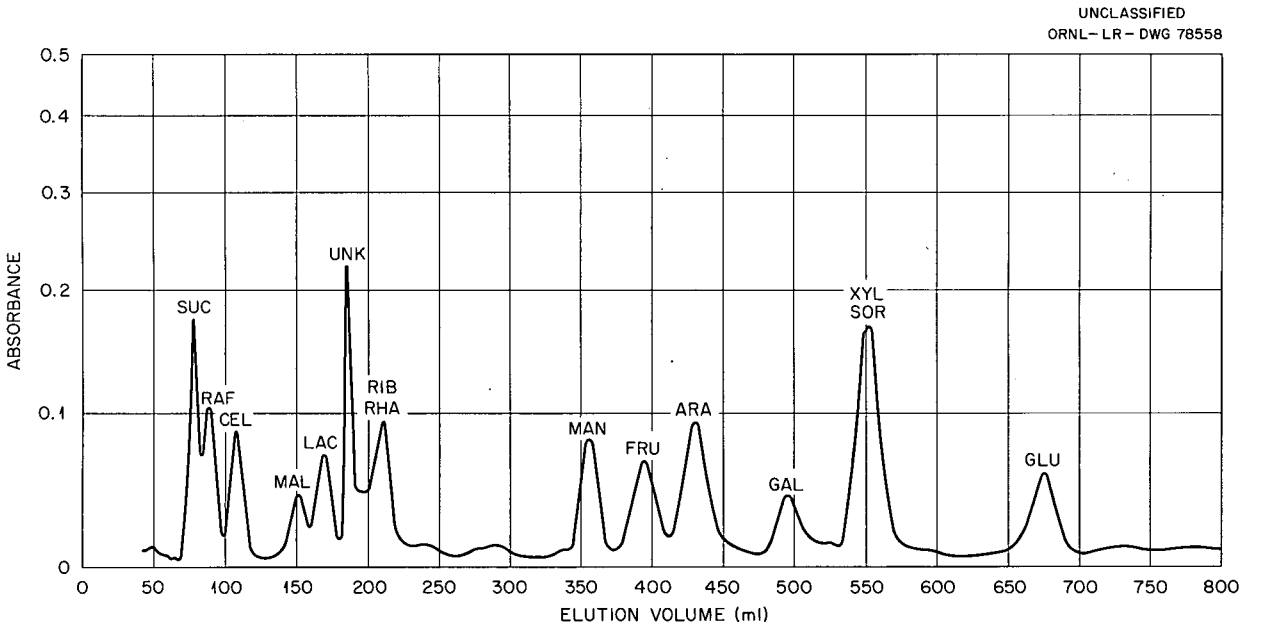

Fig. XVII-B-7. Separation of a Standard Mixture on a Medium-Length Column. Mixture contains 150 μg of each of 14 sugars on Dowex 1-X8 in a column 0.9 × 60 cm.

C. FLAME IONIZATION ANALYZER FOR DETERMINING TOTAL CARBON IN LIQUID STREAMS OR SOLID SAMPLES

N. G. Anderson R. H. Stevens

1. General Considerations

A general method for determining total carbon at the picogram (10^{-12} g) level in liquid streams or in solid samples would find numerous applications. Cells and large subcellular particles could be individually analyzed and counted if replicate determinations could be made. Ion exchange columns could be monitored and miniaturized to the point where very tiny samples could be analyzed. In addition, the difficulties associated with wet chemistry systems for analyzing column effluents would be eliminated. With these considerations in mind, the possibility of introducing solid samples into a hydrogen-flame ionization detector have been investigated. To analyze liquid streams, methods for evaporating solutes onto the transport wire have been investigated.

2. Experimental Prototype

Duplicate samples of 8×10^{-13} g of carbon (palmitic acid) were deposited on a 0.005-in.-diam platinum-rhodium wire, by evaporation of a 0.1-μl droplet of acid in ethanol, and transported through the detector flame (Figs. XVII-C-1 and -2). Nearly identical pulses were recorded. Larger samples of 10, 100, and 1000 picograms of palmitic acid were also detected, but the response of the system was not linear. The cause of the nonlinearity has not yet been determined. Samples of discrete particulate matter, namely, the protozoan *Astasia longa* and ragweed pollen, were also detected as individual particles with satisfactory separation of pulses. The deposition of samples onto the wire is the area of greatest immediate concern since consistent samples of known weight are required to optimize the detector operation. At present, the placement of solutes on the wire is accomplished by hanging a drop of solution of known volume from the wire and allowing it to evaporate. A 2-μl drop of ethanol is about the largest volume that can be suspended in this manner. Solutions of particulate matter, for example, pollen or *Astasia*, can be sampled continuously by passing the wire through a larger

Fig. XVII-C-1. General View of Prototype Flame Ionization Analyzer. Hydrogen generator system, left; hood containing flame ionization chamber, center; amplifier and recorder, right.

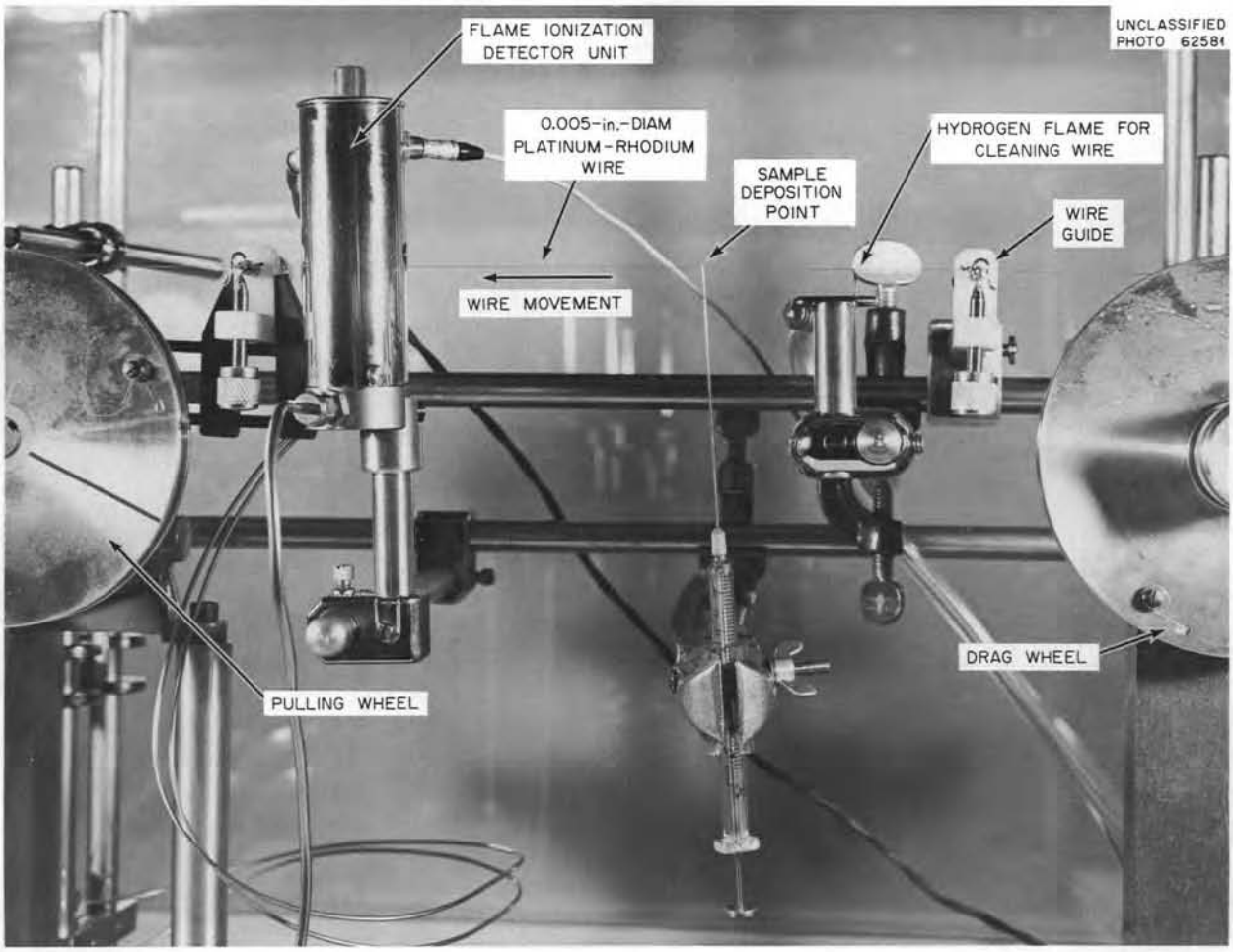

Fig. XVII-C-2. Flame Ionization Detector for Solid Organic Samples.

drop which is fed from a syringe to overcome evaporation losses. The particles adhere to the wire in an apparently random manner. Initial tests have indicated that this latter technique does not result in solute pickup for materials in true solution. The use of inorganic coatings on the wire to present a more hydrophilic surface for better adherence of the solution is planned. A continuous sample deposition method is highly desirable for applications that involve the analysis of discharges from continuous microprocesses.

The effects of size, material, placement in the flame, speed of the wire, and the influence of the wire in the ionization chamber are to be investigated.

D. HIGH-PRESSURE ION EXCHANGE CHROMATOGRAPHY

C. L. Burger H. P. Barringer

The theory of chromatography on ion exchange beads suggests that the resolution obtainable with a given mixture of solutes and a particular ion exchange material is a function of the diameter of the resin beads, the cross section of the column, and the flow rate. The limiting factor is the rate of diffusion of the solute into and out of the resin bead. As bead size is diminished, the pressures required to pump fluid through a column of given length increase sharply. This effect can be partially offset by increasing

the temperature, providing no deleterious effects are produced on the materials to be separated.

To obtain maximum resolution the behavior of ion exchange columns is examined when they are operated at very high pressure, with very small (about 1 to 5 μ) resin particles, in columns with a very small diameter. The diameter will be limited by the capacity of the resin and the sensitivity of the detection system used to monitor the column. As is discussed in the preceding section, preliminary studies on a system for determining total carbon in streams at the picogram level are now under way.

Where maximum resolution is not required it is evident that high-pressure chromatographic systems can be used to minimize the time required for analysis. It should be noted that labile compounds such as ATP can be chromatographed successfully at temperatures as high as 60° provided the separation is carried out in a few minutes.[16]

Pumps, valves, and supporting equipment are being procured to build a continuous-flow, 60,000-psi pressure system. The pump shown in Fig. XVII-D-1 will deliver a sodium acetate gradient through a resin column reinforced by a sintered metal filter on the bottom end. Since the sodium acetate is pumped directly onto the resin, the air-driven piston-pump rod seal will have a shortened life, which the vendor estimates will be approximately 100 hr at 60,000 psi, with successively longer life at reduced pressures.

The column is to be designed so that the sample can be added directly to the column surface for effective processing. The column will be formed from a section of $\frac{1}{4}$-in.-OD by $\frac{3}{32}$-in.-ID stainless steel tubing approximately 2 ft long. Packing the column to remove all voids may require the fabrication of special equipment.

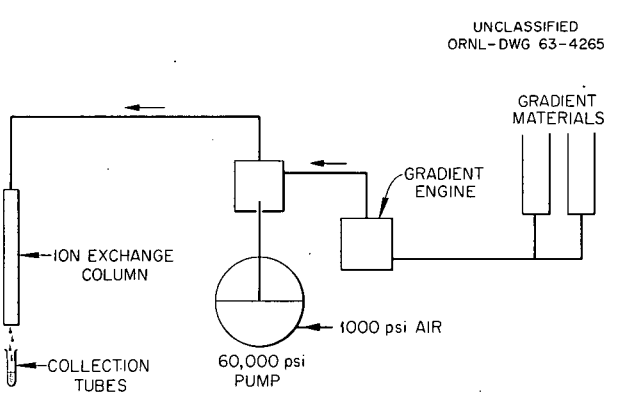

Fig. XVII-D-1. Schematic Diagram of High-Pressure Ion Exchange Column.

E. ANALYSIS OF PARTICULATE MATERIAL FROM NATURAL WATER

W. T. Lammers

The problems involved in fractionating and analyzing the contents of natural water are similar in theory to those used for fractionating and analyzing subcellular components. Many of the centrifuge systems developed under this program are applicable to the problem of separating organic from inorganic material in river water, and to the further separation of organic particles on the basis of sedimentation rate or density. Since the advent of the use of organic pesticides, especially chlorinated hydrocarbons, and radionuclides in research and industry, the incidence of such contaminants in the human environment has increased manyfold. It is of vital interest that methods be developed to elucidate contaminant uptake by, and distribution among, the various fractions that are found in natural water. At present an investigation of radionuclide distribution among the various fractions of natural water from the Clinch River is being conducted,[17] and the theories and methods already devised may now be applied to investigations of organic-pesticide distributions in waters that will be used ultimately for human consumption.[18]

Proportional-flow water samples are collected on a statistically planned schedule from selected sites along the Clinch River so that samples, representing water masses of known history, are available with differing times of contact with radionuclides. An initial continuous-flow centrifugation is used to separate noncolloidal particulate material from colloids and solutes. The

[16] A. A. Barber *et al.*, *Federation Proc.* **20**, 354 (1961).

[17] W. T. Lammers, *Limnology and Oceanography* **7**, 224 (1962); *Science* **139**, 1298 (1963); paper to be published in *Proceedings of the XV International Congress of Limnology, Madison, Wis., Aug. 19–25, 1962.*

[18] W. T. Lammers, p 78 in *Status Report No. 3 on Clinch River Study* (ed. by R. J. Morton), ORNL-3370 (1962).

noncolloidal particulate material, containing both organic and inorganic material, is resuspended and separated into organic and inorganic fractions by density gradient centrifugation, isolated, and prepared for radionuclide analysis. Aliquots of the original raw-water sample and of the supernatant water (colloids and solutes) from the continuous-flow centrifugation, were reduced to a 10-ml volume under vacuum at 35°C and also prepared for a radionuclide analysis.[17]

Since the river discharge (dilution factor) as well as the time of travel (time of contact) of the sampled water mass is known, the radionuclide analysis results can be expressed as the total amounts of the various radionuclides moving past the sampling sites at the time of sampling as well as the distribution of the various radionuclides among the isolated fractions. When the field studies are completed, the results will be subjected to statistical analysis to help in determining the ultimate fate of radionuclides discharged at ORNL into the Clinch River so that an estimate of the actual and potential hazard may be made.[18]

Samples of natural water may be quantitatively separated and isolated into four fractions: (1) noncolloidal organic, (2) noncolloidal inorganic, (3) colloids and solutes, and (4) pure water. These methods have been standardized, and investigation has begun of means of isolating the various homogeneous groups in the colloidal range found in the supernatant water from the continuous-flow centrifugation. Such a quantitatively reproducible system of fractionation and analysis of natural water will permit the determination of any contaminant's uptake by, and distribution among, the various fractions of natural water by modification of the end analytical methods (radioactivity determination or pesticide analysis) to suit the contaminant under investigation.

F. RATE-ZONAL SEPARATION OF LARGE PARTICULATES FROM BACTERIAL PROTOPLASTS

G. B. Cline W. D. Fisher

Rate-zonal separation in sucrose gradients in the B-II or B-IV rotor systems[19,20] of water lysates of *E. coli* protoplasts reveals a component in the leading heavy peak which contains particles of ribosomal dimensions. Since aggregated ribosomes have been found to be the site of protein synthesis in rabbit reticulocytes,[21] it seemed of interest to analyze the components of the leading peak more critically to determine whether or not aggregated ribosomal clumps were present in *E. coli* which could be shown to be active in protein synthesis.

The results of several experiments using the analytical ultracentrifuge show that there are particulates in the water lysate of protoplasts which have sedimentation coefficients ranging from 150-S to 1200-S and have a 280:260 mμ ratio of 0.6. Lysates of protoplasts induced for β-galactosidase show that the enzyme distribution is coincident with both the soluble as well as the leading peak (Fig. XVII-F-1).

Low-resolution electron micrographs of the leading peak show particles containing organized ribosomes as well as protoplast ghosts and so-called "lipid granules."[22]

The relation between the ordering of the ribosomes on the surface of membranes and protein synthesis deserves careful attention since the organization of ribosomes into polysomes has been shown to be important in other systems. In the *E. coli* materials prepared by methods involving high shearing fields, DNA molecules are broken and complex ordered macromolecular structures would be disrupted. It is essential, therefore, to develop extremely gentle methods for disassembling cell structures which would preserve as many of the relations existing in the intact cell as possible. *E. coli* infected with T2 bacteriophage has also been studied to determine whether the ordering of ribosomes on the cell membrane is characteristic only of β-galactosidase-induced protoplasts. After lysis the phage and large particulate material were separated from the free ribosomes and soluble substances by zonal centrifugation under conditions identical to those shown in Fig. XVII-F-1. An electron micrograph showing organized

---

[19] N. G. Anderson and C. L. Burger, *Science* **136**, 646–48 (1962).

[20] N. G. Anderson, *J. Phys. Chem.* **66**, 1984–89 (1962).

[21] P. A. Marks, E. R. Burks, and D. Schlessinger, *Proc. Natl. Acad. Sci. U.S.* **48**, 2163 (1962).

[22] C. Weibull, *J. Bacteriol.* **66**, 696 (1953).

ribosomes in gradient fraction 33 is shown in Fig. XVII-F-2. These structures are therefore not characteristic only of β-galactosidase-induced cells. Since the higher levels of cell organization may be important in the control of synthetic activities, it is important to attempt the isolation of the fragments showing the organized ribosomal arrays. Fractionation of both the leading heavy fraction and the leading edge of the soluble peak observed from protoplast lysates is being explored by rate-zonal centrifugation and isopycnic banding in CsCl using the new methods for CsCl centrifugation previously discussed in this report.

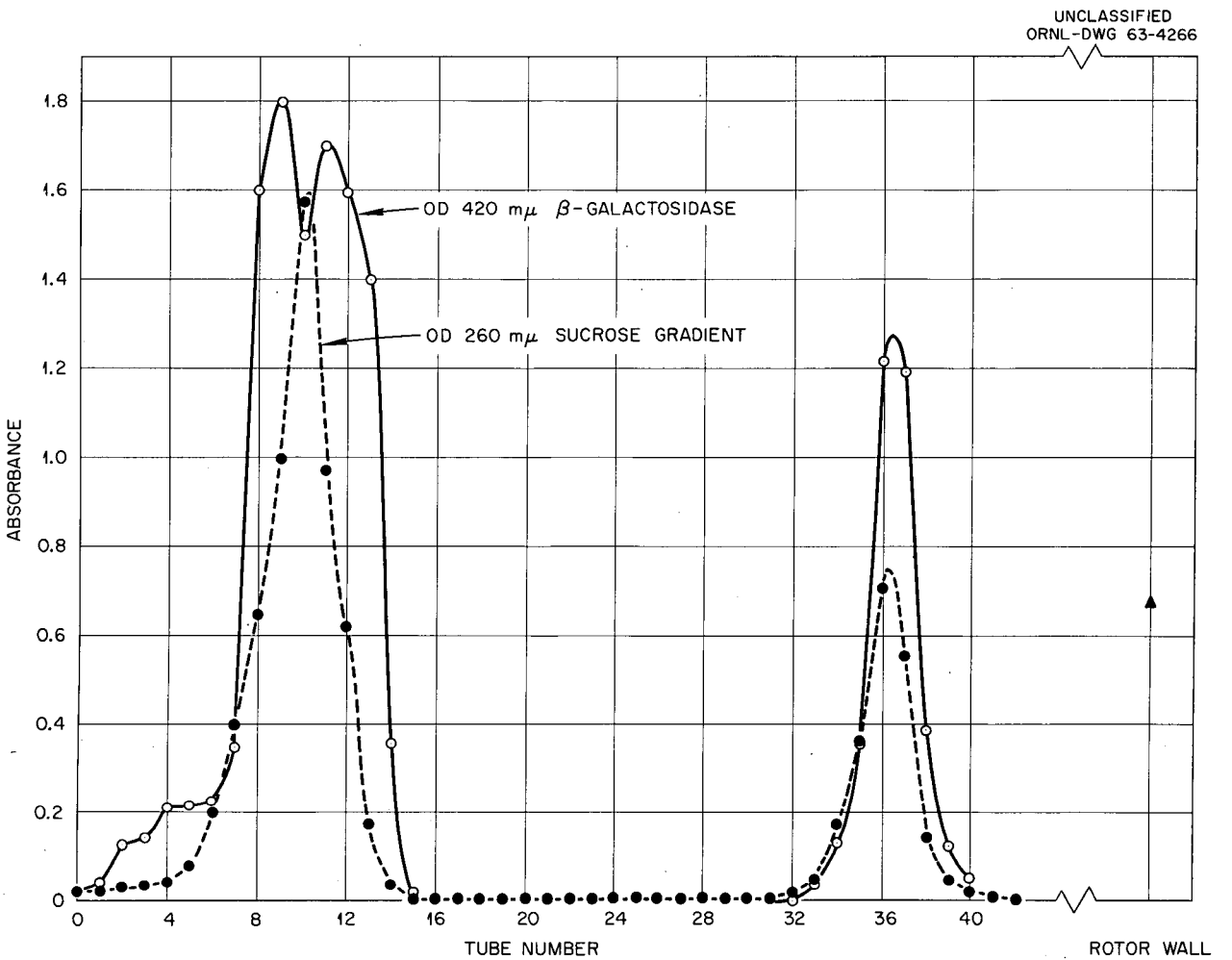

Fig. XVII-F-1. β-Galactosidase Distribution of Lysate from Induced *E. coli* Protoplasts.

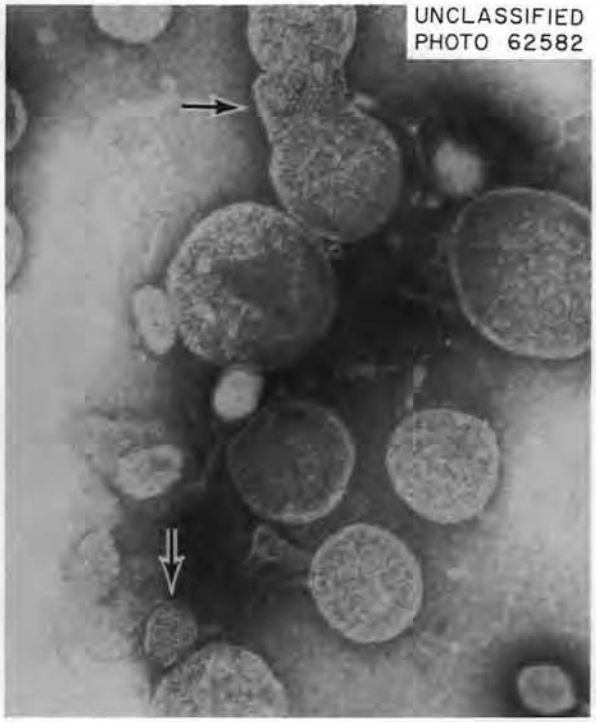

Fig. XVII-F-2. Particles Containing Organized Ribosomes in Lysates of T2 Infected *E. coli*. Negatively stained with phosphotungstate. 80,000X.

G. PROTEIN SYNTHESIS ON RIBOSOMES

G. B. Cline A. W. Prestayko W. D. Fisher

1. Problems of Ribosome Isolation

The B-II and B-IV rotor systems, when operated at their maximum speed of 40,000 rpm, are designed to separate quantities of ribosomes and ribosomal subunits from cell extracts in $1\frac{1}{2}$ to 2 hr of centrifugation. In a previous report[23] the separation of ribosomes which had been previously separated from the majority of soluble materials of the cell by preparative ultracentrifugation was demonstrated. Prepacking of ribosomes lengthens the time interval between initial cell disruption and final separation of the particles in a density gradient and is known to alter the physical properties of the particles.

It is essential to know whether or not rapidly prepared, broken cell suspensions may be introduced directly into the B-II or B-V rotors and whether or not the amount of material which may be introduced in a narrow starting zone will be sufficient to observe on a uv run monitor and for subsequent biochemical analysis. If rapid separation of ribosomal particulates from the original homogenate can be achieved, the artifacts associated with presedimentation and prolonged incubation may be minimized. More important, pulse-labeling experiments to follow protein synthesis on these subcellular particles may be initiated. The experiments reported here were performed before the new B-II and B-IV upper bearing systems, which make possible operation to 40,000 rpm, became available.

2. Separation of Ribosomes

The work described here is part of a program to investigate the role of ribosomal particles isolated by zonal ultracentrifugation in protein synthesis. Ribosomes from log phase cultures of *E. coli* and from isolated rat thymus nuclei have been separated in sucrose density gradients, as shown in Figs. XVII-G-1 and XVII-G-2. The *E. coli* cells were induced for β-*d*-galactosidase, disrupted in a constant-pressure French press at 14,000 psi, and loaded into the B-V rotor at 5°C. Figure XVII-G-1 shows the absorbance of the effluent gradient stream at 260, 280, and 415 mμ and the distribution of β-galactosidase. This demonstrates the feasibility of such direct separations. Pulse-labeling studies of induced enzyme synthesis are in progress. Figure XVII-G-2 shows the uv run monitor chart for the rat thymus nuclear ribosomes. The S_{20} values were extrapolated from comparable analytical ultracentrifuge runs since the computer program for the determination of sedimentation coefficients with the B-V rotor is not complete. Results of *in vitro* studies on the composition and enzyme complement of nuclear ribosomes and their protein-synthesizing capabilities will be included in a subsequent report.

[23] N. G. Anderson, *Joint NIH-AEC Zonal Centrifuge Development Program Semiann. Rept. Dec. 31, 1962*, ORNL-3415, p 48.

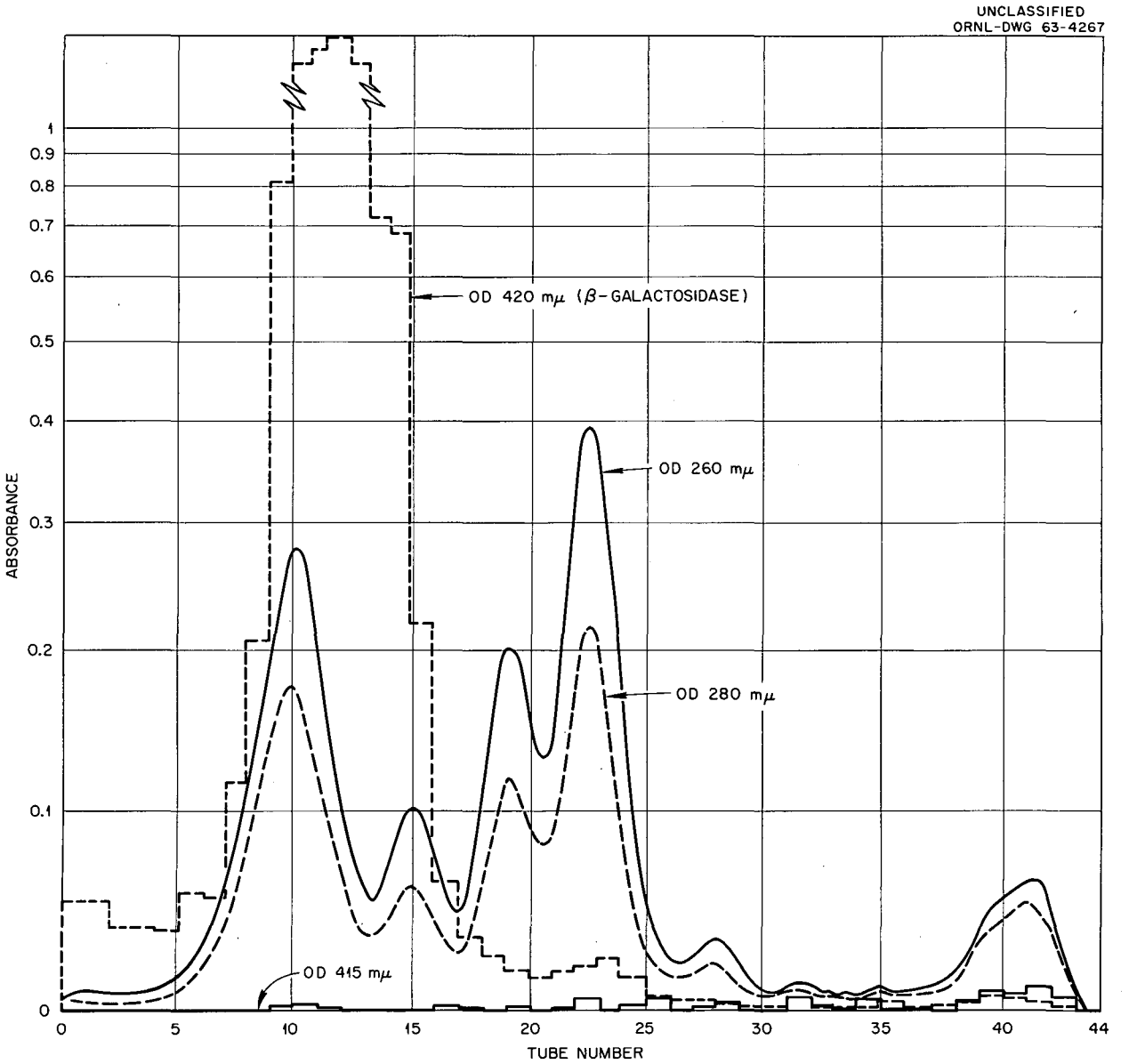

Fig. XVII-G-1. Separation of Ribosomes from β-Galactosidase-Induced *E. coli*. Absorbance at 260 mμ was determined by the centrifuge run monitor, from which 280 and 415 mμ absorbancies were obtained from the collected fractions. β-Galactosidase (420 mμ) was determined using *o*-nitrophenyl-*d*-galactopyranoside as the substrate. The rotor was loaded and unloaded at 3000 rpm and run for 5 hr at 25,000 rpm. The sucrose density gradient extended from 10 to 30% with a 55% (w/w) cushion.

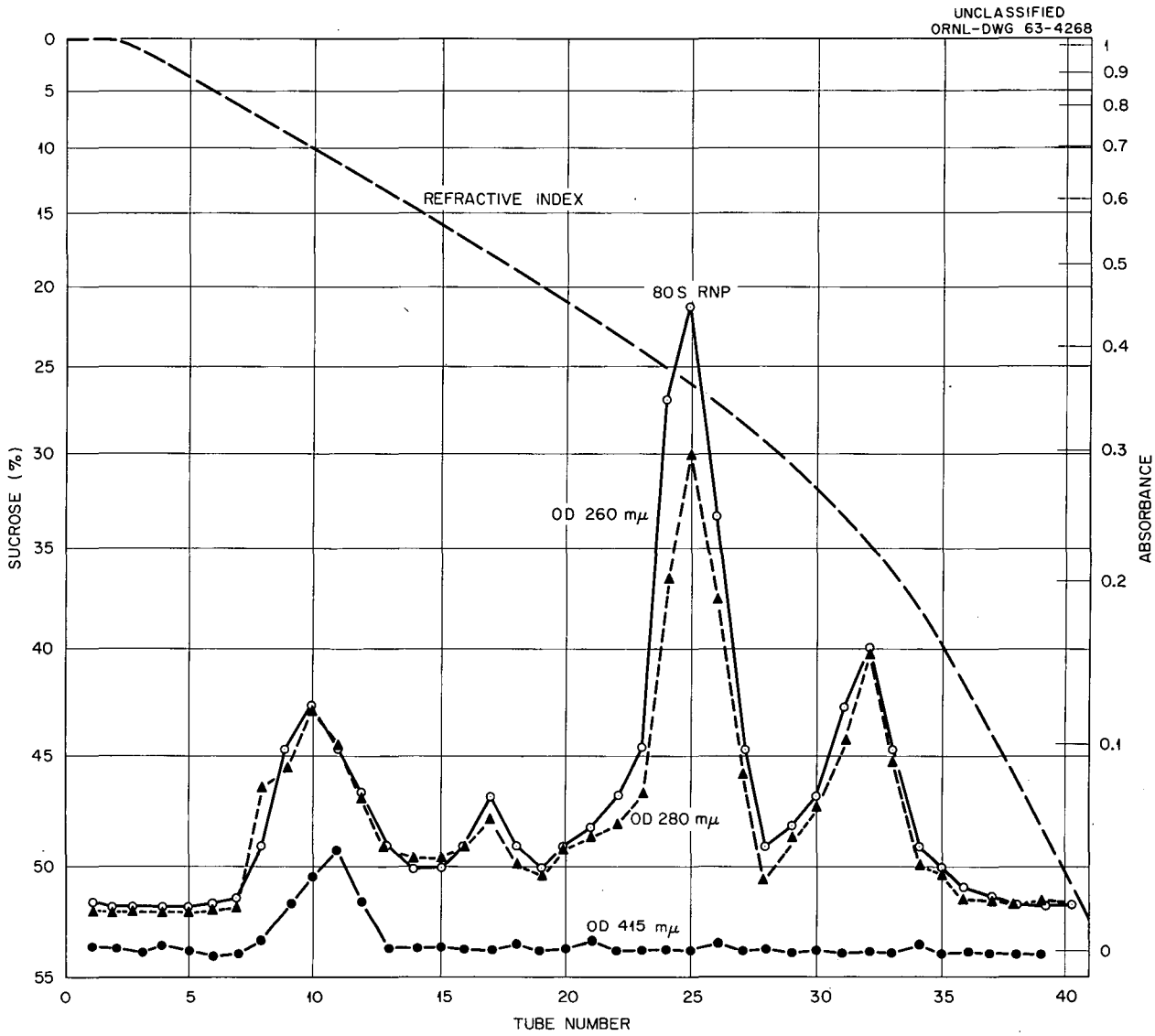

Fig. XVII-G-2. Separation of Nuclear Ribosomes from 5 g of Isolated Rat Thymus Nuclei in the B-V Rotor in a 10 to 30% Sucrose Gradient. Plots at 260, 280, and 415 mμ show absorbance of rotor effluent stream. Refractive index was automatically recorded.

H. AUTOMATED NUCLEOTIDE ANALYZER

C. L. Burger

An automated system has been developed to determine quantitatively nucleotides, nucleosides, and bases in tissue extracts. The system described here was designed and built at ORNL.

Details of construction, including flow cells, have been described.[24] A reference cell has been added to prevent the rising shift in baseline which normally occurs as the analysis proceeds. It has larger tubing than normally used and is inserted in the system between the gradient cylinders and pump.

The classical approach to the problem of column chromatography was pH elution. The system in use here employs a gradient of increasing molarity of sodium acetate (0.15 to 3.0 *M*) at pH 4.4. A diagrammatic representation of the system is shown in Fig. XVII-H-1. A typical gradient for a tissue analysis is 700 ml of 3.0 *M* sodium acetate (NaOAc) grading linearly into 700 ml of 0.15 *M* NaOAc, with 3.0 *M* acetate following to complete the run.

The water-jacketed columns are about 160 cm long and 0.9 cm wide. Temperatures are normally 40°C and are maintained by a circulating water bath.

[24]N. G. Anderson *et al.*, "Analytical Techniques for Cell Fractions. III. Nucleotides and Related Compounds," to be published in *Anal. Biochem.*; N. G. Anderson, *Anal. Biochem.* **4**, 269–83 (1962); N. G. Anderson, *Anal. Chem.* **33**, 970–71 (1961).

UNCLASSIFIED
ORNL–DWG 63–4269

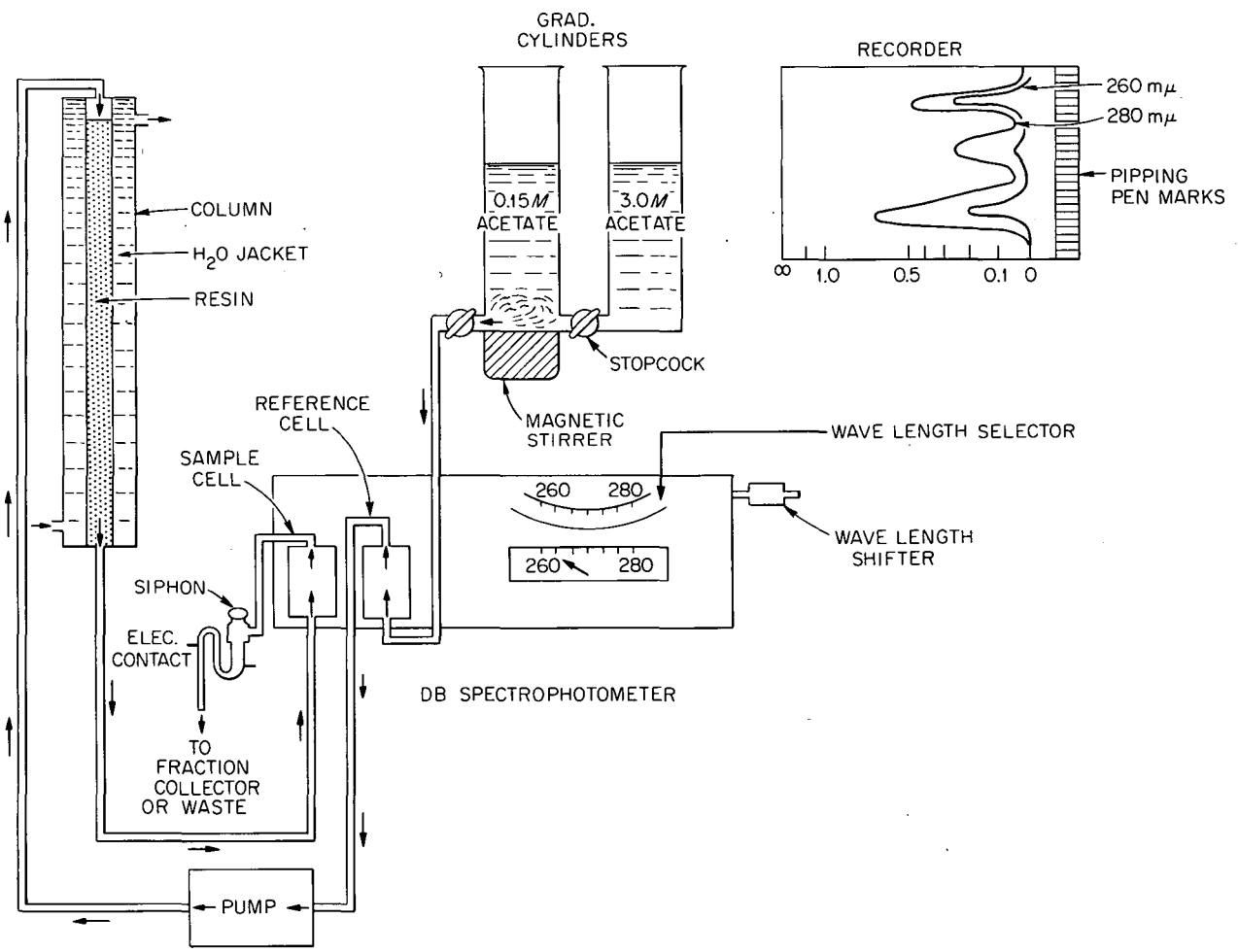

Fig. XVII-H-1. Schematic Diagram of Nucleotide Analyzer.

Samples ranging from a fraction of 1 ml up to 5 ml have been used without appreciable skewing of the peaks obtained. The resolution of the system (as measured by width at half-height) is excellent. To place a sample on the column, the buffer above the resin bed is removed and the sample is carefully pipetted to the top of the resin and forced into the column bed by compressed air. A small portion of the lower-molarity buffer is similarly added, and the column is then filled with the same starting buffer, at which time the pump and gradient are started.

Normally, a Milton Roy Minipump is set at 33.3% stroke for the first 3.25 hr, at which time it is changed automatically by a solenoid to 50% stroke for the remainder of the run.

The column effluent passes through a 1-cm path cell (or a 0.2 cm if required) and absorbancy is measured automatically at 260 mμ and 280 mμ using a Beckman double-beam spectrophotometer provided with a wave-shifting mechanism developed for this purpose. A 12-point Honeywell recorder provides a continuous record of the peaks thus obtained.

The column effluent then passes through an automatic siphon. Each time a given volume (4.065 ml) passes through the siphon, a pulse is sent through a relay, which triggers a pipping pen on the recorder so that a continuous record of volume is also available (see Fig. XVII-H-2).

The elution of all components from the column when tissue extracts are run requires about 31 hr. Since the chart speed is constant, the amount of material (in millimoles) represented by each peak on the chromatogram can be calculated.

The system thus provides both quantitative and qualitative information. A substance is recognized by its 280 : 260 ratio and quantity is measured by area beneath the peaks. The above relation is originally determined by comparison with known amounts of standards used in other runs.

A chromatogram of a rat liver extract is shown in Fig. XVII-H-3. Excellent results also have been obtained with acid-soluble nucleotides from rat thymus and gut and from *Astasia longa*, a colorless flagellate, in different stages of synchronous growth.

A cationic exchange resin (Dowex 1-X8) is used in this system. Differences between batches of resin have been traced to water and divinylbenzene content, the latter used to cross-link the copolymer beads of polystyrene. After testing all batches of the Dowex 1-X8 manufactured by Dow during a six-month period, the requisite characteristics of the resin were determined, and a pilot-plant batch of several hundred pounds was obtained.

Regeneration of the resin in the column is normally performed after a tissue analysis by pumping 3.0 *M* acetate through the resin bed for 1 hr, followed by 0.15 *M* acetate for 3 hr.

If the system is kept in continuous operation, shorter times are required for regeneration. After a period of disuse, the column may require several

UNCLASSIFIED
ORNL-DWG 63-4941

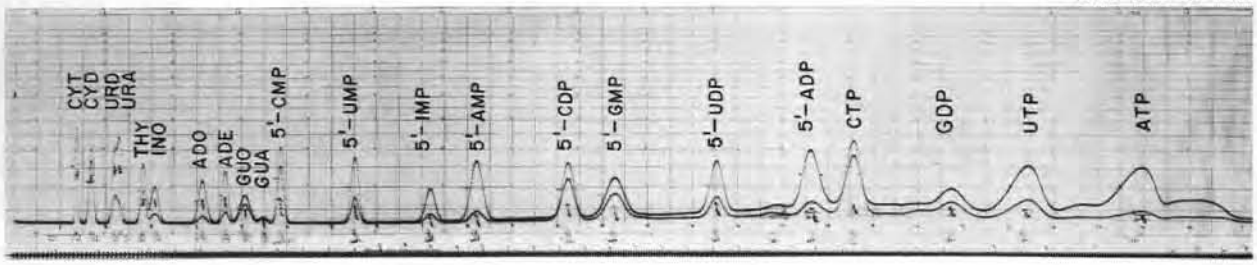

Fig. XVII-H-2. Acid Soluble Nucleotides, Nucleosides, and Base Standards. First ten peaks represent 2 micromoles, except for guanine which is 1.0 micromole. Other peaks contain 5 micromoles of material. A 0.2-cm light path cell was used in DB spectrophotometer. Gradient: 600 ml of 0.15 *M* NaOAc (sodium acetate), and 600 ml of 3.0 *M* NaOAc. Trinucleotides normally run on short column. Abbreviations on the figure are those of the *Journal of Biological Chemistry*.

UNCLASSIFIED
ORNL-DWG 63-4942

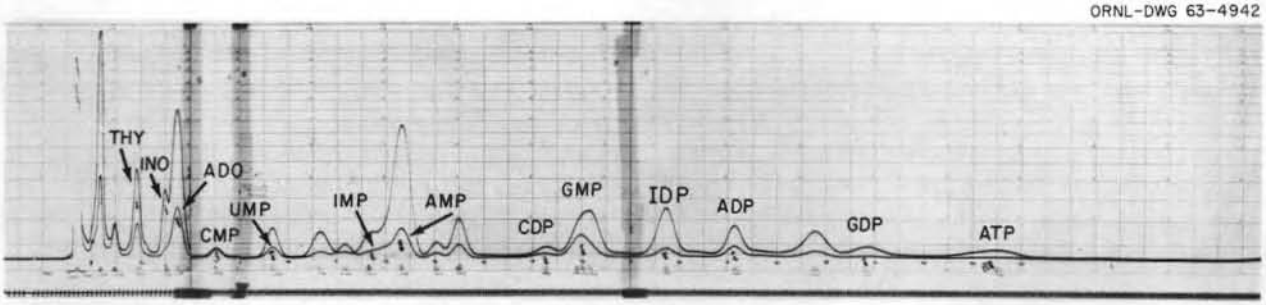

Fig. XVII-H-3. Chromatogram of Perchloric Acid-Extracted Fraction of Rat Liver. Resin, Dowex 1-X8; temperature, 40°C; sample, 404 optical density units at 260 mμ, 1-cm light path. Absorbancy measured at 260 and 280 mμ. Gradient, 700 ml of 3.0 *M* NaOAc grading linearly into 0.15 *M* NaOAc; finish run with 3.0 *M* NaOAc. DB spectrophotometer flow cell 0.2-cm light path.

hours to reach equilibrium. Whether this is due to leaching of the resin is not known.

On the assumption that narrower columns and higher pressures would permit more rapid analyses with equally good resolution, a narrower glass column capable of withstanding 200 psi was used. Here, gradients of 250 ml of each buffer proved sufficient, and total analysis time for a tissue was reduced from 31 to 10 hr. Another test system involved the use of a stainless steel column of $^1/_{16}$ in. ID and 3 ft in length attached to a French pressure cell and packed with resin using 3000 psi. Preliminary studies at this pressure showed that a length of 2 ft was sufficient. When tested with a sample of five compounds, the results show the feasibility of using such narrow columns with higher pressures. A report of the progress of this study is found in Sec XVII-D. With such a system total analysis time may be reduced to extremely short time intervals, perhaps minutes rather than hours, with little loss in resolution. Development of this system will be noted in future reports.

INTERNAL DISTRIBUTION

1. S. I. Auerbach
2. R. Baldock
3. R. E. Biggers
4. A. L. Boch
5. D. S. Billington
6. E. P. Blizard
7. C. J. Borkowski
8. G. E. Boyd
9–10. Clark E. Center (ORGDP)
11–12. D. D. Cowen
13. C. J. Collins
14. F. L. Culler
15. P. B. Dunaway
16. J. L. Fowler
17. J. H Frye, Jr.
18. R. F. Hibbs (Y-12)
19. A. S. Householder
20. J. S. Johnson
21. R. W. Johnson
22. W. H. Jordan
23. K. A. Kraus
24. M. T. Kelley
25. J. A. Lane
26–27. C. E. Larson
28. T. A. Lincoln
29. S. C. Lind
30. R. S. Livingston
31. K. Z. Morgan
32. J. P. Murray (K-25)
33. D. J. Nelson
34. M. L. Nelson
35. J. S. Olson
36. R. B. Parker
37. M. E. Ramsey
38. R. M. Rush
39. M. J. Skinner
40. J. A. Swartout
41. E. H. Taylor
42. A. M. Weinberg
43. G. C. Williams
44. H. I. Adler
45–54. N. G. Anderson
55. W. A. Arnold
56. R. H. Baum
57. M. A Bender
58. F. J. Bollum
59–60. C. L. Burger
61. S. F. Carson
62. E. H. Y. Chu
63. G. B. Cline
64. W. E Cohn
65. C. C Congdon
66. F. J. de Serres
67. D. G. Doherty
68. J. L. Fairley
69. W. D. Fisher
70–72. D. A. Fuccillo, Jr.
73. A. H. Haber
74. A. Hollaender
75. S. Karasaki
76. M. A. Kastenbaum
77. R. F. Kimball
78. S. P. Leibo
79. D. L. Lindsley, Jr.
80. T. Makinodan
81. P. Mazur
82. G. D. Novelli
83. T. T. Odell, Jr.
84. G. M. Padilla
85. A. P. Pfuderer
86. M. L. Randolph
87. W. L. Russell
88. R. B. Setlow
89. G. E. Stapleton
90. A. C. Upton
91. E. Volkin
92. R. C. von Borstel
93. S. Wolff
94. T. Yamada
95. E. F. Babelay
96. E. J. Barber
97. H. P. Barringer
98. J. C. Barton
99. A. S. Berman
100. H. A. Bernhardt
101. Barbara S. Bishop
102. H. D. Culpepper
103. J. T. Dalton
104–113. E. C. Evans
114. J. Farquharson

115. R. L. Farrar, Jr.
116. W. W. Harris
117–119. W. L. Harwell
120. E. T. Henson
121. A. P. Huber
122. G. R. Jamieson
123. E. C. Johnson
124. T. J. Lewis
125. E. F. Martin
126. J. R. Mahoney
127. L. L. McCauley
128. C. E. Nunley
129. P. R. Vanstrum
130. D. A. Waters
131. C. W. Weber
132. S. J. Wheatley
133. W. J. Wilcox, Jr.
134. E. Chargaff (consultant)
135. R. D. Hotchkiss (consultant)
136. Curt Stern (consultant)
137. M. M. Wintrobe (consultant)
138. P. C. Zamecnik (consultant)
139–140. Biology Library
141–143. Central Research Library
144. Reactor Division Library
145–146. ORNL – Y-12 Technical Library Document Reference Section
147–166. Laboratory Records Department
167. Laboratory Records, ORNL, R.C.
168. Laboratory Shift Supervisor

EXTERNAL DISTRIBUTION

169. R. W. McNamee, Union Carbide Corporation, New York
170. G. A. Andrews, ORINS
171. C. Baker, National Cancer Institute, Bethesda, Maryland
172. F. Baronowski, AEC Production Division, Washington, D.C.
173. N. F. Barr, Atomic Energy Commission, Washington, D.C.
174. N. Berlin, National Cancer Institute, Bethesda, Maryland
175. H. E. Bond, U.S. Naval Radiological Defense Laboratory, San Francisco, California
176. Myron Brakke, U.S. Department of Agriculture, Agriculture Research Service, Plant Physiol. Department, University of Nebraska, Lincoln 3, Nebraska
177. H. D. Bruner, Atomic Energy Commission, Washington, D.C.
178. W. R. Bryan, National Cancer Institute, Bethesda, Maryland
179. J. C. Bugher, Puerto Rico Nuclear Center, Rio Piedras, P.R.
180. W. W. Burr, Jr., Atomic Energy Commission, Washington, D.C.
181. R. S. Caldecott, Atomic Energy Commission, Washington, D.C.
182. R. M. Chanock, National Institute of Allergy and Infectious Diseases, Bethesda, Maryland
183. R. A. Charpie, Union Carbide Corporation, New York
184. M. A. Churchill, Chief, Stream Sanitation Staff, Edney Bldg., TVA, Chattanooga, Tennessee
185. W. D. Claus, Atomic Energy Commission, Washington, D.C.
186. Helen Coates, National Institute of Allergy and Infectious Diseases, Bethesda, Maryland
187. B. T. Cole, Department of Zoology, University of South Carolina, Columbia, S.C.
188. E. Dapper, U.S. Army Chemical Corps, Fort Detrick, Maryland
189. C. M. Davidson, Environmental Hygiene Branch, Edney Bldg., TVA, Chattanooga, Tennessee
190. W. W. Davis, Eli Lilly Co., Indianapolis, Indiana
191. O. M. Derryberry, Director of Health and Safety, Edney Bldg., TVA, Chattanooga, Tennessee
192. Harold S. Diehl, Sr. Vice President for Research in Medical Affairs, American Cancer Society, 521 W. 57th St., New York 19, New York
193. C. L. Dunham, Atomic Energy Commission, Washington, D.C.
194. K. M. Endicott, National Cancer Institute, Washington, D.C.
195. S. G. English, Assistant General Manager for Research and Development, AEC, Washington, D.C.
196. J. L. Fahey, National Cancer Institute, Bethesda, Maryland

197. E. Frei, National Cancer Institute, Bethesda, Maryland
198. F. E. Gartrell, Assistant Director of Health and Safety, Edney Bldg., TVA, Chattanooga, Tennessee
199. H. Bentley Glass, Johns Hopkins University, Baltimore, Maryland
200. H. N. Glassman, U.S. Army Chemical Corps, Fort Detrick, Maryland
201. E. Grabowski, AEC Production Division, Washington, D.C.
202. S. T. Grey, Food and Drug Administration, Washington, D.C.
203. N. S. Hall, University of Tennessee, Knoxville
204. John Harris, AEC Public Relations Division, ORO
205. Fred J. Hodges, University of Michigan, Medical Center, Ann Arbor
206. E. C. Horn, Department of Zoology, Duke University, Durham, N.C.
207. J. G. Horsfall, Connecticut Agricultural Experimental Station, New Haven
208. R. D. Housewright, U.S. Army Chemical Corps, Fort Detrick, Maryland
209. R. J. Huebner, National Cancer Institute, Bethesda, Maryland
210. J. S. Kirby-Smith, Atomic Energy Commission, Washington, D.C.
211. R. M. Kniseley, ORINS Medical Division
212. K. W. Kohn, National Cancer Institute, Bethesda, Maryland
213. P. Kotin, National Cancer Institute, Bethesda, Maryland
214. E. L. Kuff, National Cancer Institute, Bethesda, Maryland
215. W. T. Lammers, Davidson College, Davidson, S.C.
216. A. D. Langmuir, Chief, Epidemiology Branch, Communicable Disease Center, Atlanta, Georgia
217. R. E. Learmouth, National Cancer Institute, Bethesda, Maryland
218. J. L. Liverman, Atomic Energy Commission, Washington, D.C.
219. R. F. Loeb, College of Physicians and Surgeons, Columbia University, New York
220. W. H. Magruder, National Cancer Institute, Bethesda, Maryland
221. W. E. McMahon, Atomic Energy Commission, ORO
222. R. G. Meader, National Cancer Institute, Bethesda, Maryland
223. J. L. Melnick, Department of Virology and Epidemiology, Baylor University, College of Medicine, Houston, Texas
224. G. R. Mider, National Cancer Institute, Bethesda, Maryland
225. Carl V. Moore, Washington University, St. Louis, Missouri
226. P. T. Mora, National Cancer Institute, Bethesda, Maryland
227. J. E. Moynahan, National Institutes of Health, Bethesda, Maryland
228. M. A. Mufson, National Institute of Allergy and Infectious Diseases, Bethesda, Maryland
229. W. G. Pollard, ORINS
230. C. A. Price, Department of Plant Physiol., Rutgers·The State University, New Brunswick, N.J.
231. R. Quimby, National Aeronautics and Space Administration, Washington, D.C.
232. H. M. Roth, Research and Development Division, AEC, ORO
233. W. P. Rowe, National Institute of Allergy and Infectious Diseases, Bethesda, Maryland
234. P. S. Sarma, National Institute of Allergy and Infectious Diseases, Bethesda, Maryland
235. John Schacter, Union Carbide Corporation, New York
236. D. G. Sharp, University of North Carolina, Department of Biophysics, Chapel Hill
237. Byron T. Shaw, Administrator, Agricultural Research Service, U.S. Department of Agriculture, Washington, D.C.
238. C. S. Shoup, Atomic Energy Commission, Oak Ridge
239. R. G. Smith, Food and Drug Administration, Washington, D.C.
240. H. A. Sober, National Cancer Institute, Bethesda, Maryland
241. Sol Spiegleman, Department of Microbiology, University of Illinois, Urbana
242. W. M. Stanley, Virus Laboratory, University of California, Berkeley
243. S. R. Tipton, Department of Zoology, University of Tennessee, Knoxville
244. John Totter, Atomic Energy Commission, Washington, D.C.

245. Shields Warren, New England Deaconess Hospital, Boston, Massachusetts
246. A. G. Wedum, U.S. Army Chemical Corps, Fort Detrick, Maryland
247. J. White, National Cancer Institute, Bethesda, Maryland
248. H. G. Wood, Western Reserve University, Cleveland, Ohio
249. M. Zelle, Argonne National Laboratory, Argonne, Illinois
250–254. C. G. Zubrod, National Cancer Institute, Bethesda, Maryland
255. Atomic Energy Commission, Washington, D.C.
256. General Electric Company, Richland, Washington
257. New York Operations Office
258. AEC Patent Branch, Washington, D.C.
259. Division of Technical Information Extension, Oak Ridge
260. UCLA Medical Research Laboratory